

HYDRODYNAMIC ANALYSIS OF COMPLIANT JOURNAL BEARINGS

A Thesis

Submitted to the Graduate Faculty of the
Louisiana State University and
Agricultural and Mechanical College
in partial fulfillment of the
requirements for the degree of
Master of Science in Mechanical Engineering

in

The Department of Mechanical Engineering

by

Amith Hanumappa Reddy
B.Engr. in Mechanical Engineering
R.V.College of Engineering, Bangalore University, India, 1999
December 2005

“Education is the manifestation of the perfection already in man”

- *Swami Vivekananda (1863 – 1902), Sage & Great Monk.*

Acknowledgements

It gives me great pleasure to express my sincere gratitude to my major professor and research advisor Dr. Michael Khonsari who heads the “Center for Rotating Machinery” (CeRoM) facility at LSU, for giving me this wonderful opportunity to work under him. His constant academic and professional guidance has been the core to the success of this research. I am indebted for his valuable time spent in guidance, teaching and patience shown during all stages of this research.

I would like to thank my committee member Dr. Su-Seng Pang under whom I have taken courses and was also a Teaching Assistant for the Machine Design Lab which has helped me expand my skills practically. Also thankful to my committee member Dr. Yitshak Ram for the courses he taught me which has been really helpful in developing my mathematical and numerical techniques that was very important for this research.

I give my gratitude to my supervisor Dr. S. Ramamurthy at “National Aerospace Laboratories” under whom I was first exposed to the field of compliant journal bearings and also for his encouragement and support to pursue this field further.

I am very thankful to Dr. Cornelis Dehoop and Dr. Ramsay Smith from the School of Renewable Natural Resources at LSU for their constant support. It has been a great experience working under them and has helped me broaden my application of skills to various fields.

Also thankful to all my friends for being supportive and helpful at all times. My colleagues at the “CeRoM” facility in particular Zhengchun Peng for his assistance in helping me understand various concepts during the initial stages of the project. Dr. Joonyoung Jang for sharing his professional knowledge and valuable guidance at all stages of the project. Jianke Wang for all the fruitful discussions we had. I thank you all for your valuable time and effort spent in assisting me.

My grand parents, parents and all my family members for their constant encouragement and support all through out, I am indebted to all of you.

Finally I would like to thank “Louisiana Space Consortium” for supporting a part of this work under the “seed” research project category of Unsolicited Research Proposal.

Table of Contents

Acknowledgements.....	iii
List of Tables.....	vii
List of Figures.....	viii
Nomenclature.....	x
Abstract.....	xiii
Chapter	
1. Introduction and Literature Review	1
2. Mathematical Model	6
2.1 Derivation of Standard Reynolds Equation for Journal Bearings	
3. Journal Bearing Approximation Methods.....	11
3.1 Infinitely Long Approximation (ILA).....	11
3.1.1 Compressible Reynolds Equation in One Dimension.....	11
3.1.2 Numerical Procedure (ILA).....	13
3.1.3 Bearing Performance Parameters (ILA).....	16
3.2 Finite Analysis (FA).....	21
3.2.1 Compressible Reynolds Equation in Two Dimensions.....	21
3.2.2 Numerical Procedure (FA).....	23
3.2.3 Bearing Performance Parameters (FA).....	31
3.3 Modified Parabolic Approximation (MPA).....	39
3.3.1 Compressible Reynolds Equation with Modified Parabolic Approximation.....	39
3.3.2 Numerical Procedure (MPA).....	45
3.3.3 Bearing Performance Parameters (MPA).....	49
3.3.3.1 Rigid Journal Bearing.....	49
3.3.3.2 Compliant Journal Bearing.....	61
4. Conclusions.....	68
References.....	70
Appendix	
A Flow Chart for Numerical Relation between Rigid and Compliant Journal Bearings.....	72
B Flow Chart for Infinitely Long Approximation.....	73
C Flow Chart for Finite Approximation.....	75

D Flow Chart for Modified Parabolic Approximation.....	77
E Maple Program for Derivation of Modified Reynolds Equation.....	78
Vita.....	85

List of Tables

Table 1: Generation 1 Compliant Bearing Data (Peng, 2003).....	17
Table 2: Lubricant Properties (Air) (Peng, 2003).....	17
Table 3: Grid Refinement Study.....	31
Table 4: Finite Analysis Comparison with Experimental and Published Literature.....	33
Table 5: Study of Variation of θ_{sub} Along the Axial Direction	34
Table 6: Flow Rate Study Based on Different Load Capacities at 30,000 rpm.....	34

List of Figures

Fig 1	Schematic of a Compliant Journal Bearing.....	2
Fig 2	Schematic Configuration of Top and bump foils.....	2
Fig 3	Schematic of a Slider Bearing (Khonsari and Booser, 2001).....	7
Fig 4	Schematic of a Journal Bearing.....	9
Fig 5	Rigid Bearing and Compliant Bearing Mode of Function.....	14
Fig 6	Pressure Profiles for Rigid and Compliant Bearing at 30,000 rpm.....	18
Fig 7	Film Thickness Profiles for Rigid and Compliant Bearing at 30,000 rpm.....	19
Fig 8	Pressure Profiles for Rigid and Compliant Bearing at 45,000 rpm.....	19
Fig 9	Film Thickness Profiles for Rigid and Compliant Bearing at 45,000 rpm.....	20
Fig 10	Pressure Profile Comparison at Mid Section of Bearing at 30,000 rpm.....	32
Fig 11	Film Thickness Comparison at Mid Section of Bearing at 30,000 rpm.....	35
Fig 12	Three Dimensional Pressure Distributions for a Foil Bearing at 30,000 rpm (θ is reversed to indicate sub-ambient pressure).....	36
Fig 13	Three Dimensional Film Thickness Profile for a Foil Bearing at 30,000 rpm.....	37
Fig 14	Attitude Angle Comparison with Variation of Eccentricity Ratio.....	38
Fig 15	Load Carrying Capacity Comparison with Bearing Speeds.....	38
Fig 16	Pressure Profile Match by Varying the Parabolic Exponent Along the Circumferential Direction.....	49
Fig 17	Variation of Exponent along the Circumferential Direction.....	50
Fig 18	Pressure Profile Comparison between Finite and Modified Approximation at the Mid Section of the Bearing (Peak Pressure Match Case).....	51
Fig 19	Load Comparison between Finite and Modified Approximation with Fixed Eccentricity Ratios (Peak Pressure Match Case).....	52
Fig 20	Attitude Angle Comparison between Finite and Modified Approximation (Peak Pressure Match Case).....	53

Fig 21 Parametric Study of Parabolic Exponent (Peak Pressure Match, $L/D = 1$).....	54
Fig 22 Pressure Profile Comparison between Finite and Modified Approximation at Mid Section of Bearing (Load Imposed Condition).....	55
Fig 23 Load Comparison between Finite and Modified Approximation (Load Imposed Condition).....	56
Fig 24 Attitude Angle Comparison between Finite and Modified Approximation (Load Imposed Condition).....	57
Fig 25 Parametric Study of Parabolic Exponent (Load Imposed Condition, $L/D = 1$).....	58
Fig 26 Rigid Bearing Non-Dimensional Load Chart ($L/D = 1$).....	59
Fig 27 Rigid Bearing Parabolic Exponent Chart ($L/D = 1$).....	60
Fig 28 Pressure Profile Comparison between Finite and Modified Approximation at Mid Section of bearing at 30,000 rpm (Foil Bearing / Min Film Match).....	62
Fig 29 Film Thickness Profile Comparison between Finite and Modified Approximation at 30,000 rpm (Foil Bearing / Min Film Match).....	63
Fig 30 Load Comparison between Finite and Modified Approximation (Foil Bearing / Min Film Match).....	64
Fig 31 Attitude Angle Comparison (Foil Bearing / Min Film Match)	64
Fig 32 Three Dimensional Pressure Distribution for Foil Bearing at 30,000 rpm based on Modified Approach. (θ is reversed to indicate the sub-ambient pressure).....	65
Fig 33 Three Dimensional Pressure Distribution for Foil Bearing at 30,000 rpm based on Finite Analysis (θ is reversed to indicate the sub-ambient pressure).....	66
Fig 34 Parametric Study of Parabolic Exponent (Foil Bearing, $L/D = 1$).....	67

Nomenclature

e	eccentricity of shaft (m)
e_f	eccentricity of compliant bearing shaft (m)
e_r	eccentricity of rigid bearing shaft (m)
h	fluid film thickness (m)
\bar{h}	dimensionless fluid film thickness
\bar{h}_f	dimensionless compliant bearing film thickness
\bar{h}_r	dimensionless rigid bearing film thickness
h_{\min}	minimum fluid film thickness (m)
$\bar{h}_{\min f}$	compliant bearing dimensionless minimum fluid film thickness
$\bar{h}_{\min r}$	rigid bearing dimensionless minimum fluid film thickness
l	half bump length (m)
p	hydrodynamic pressure (Pa)
\bar{p}	dimensionless hydrodynamic pressure
\bar{p}_l	dimensionless hydrodynamic pressure at the mid-section of the bearing
p_a	ambient pressure (Pa)
s	bump pitch (m)
t	time
t_f	top foil thickness (m)
t_b	bump foil thickness (m)
u, v, w	velocity components

w_a, w_b	squeeze components
x, y, z	cartesian coordinates
C	radial clearance (m)
D	diameter of shaft (m)
E	modulus of elasticity (bump foil)
L	length of the bearing (m)
R	radius of shaft (m)
U_a, U_b	sliding velocity
W	load carrying capacity (N)
W_r	load carrying capacity for rigid bearing (N)
W_f	load carrying capacity for compliant bearing (N)
\bar{W}	dimensionless load
\bar{W}_x	dimensionless load component along line of centers
\bar{W}_z	dimensionless load component perpendicular to line of centers
α	compliance number of bump foils
α_r	under relaxation factor for pressure profiles
α_{rh}	under relaxation factor for the film thickness profiles
ε_f	eccentricity ratio for compliant bearing
ε_r	eccentricity ratio for rigid bearing
ρ	density of air (kg/m ³)
$\bar{\rho}$	dimensionless density of air

ρ_0	S.P.T density of air (kg/m^3)
μ	viscosity of fluid (air) (N.s/m^2)
$\bar{\mu}$	dimensionless fluid (air) viscosity
μ_0	ambient air viscosity (N.s/m^2)
ν	poissons ratio for bump foil
ω	angular speed for shaft (rpm)
Θ, θ	coordinate along the circumferential direction (direction of motion)
φ	attitude angle (degrees)
ϕ_f	attitude angle of compliant bearing
ϕ_r	attitude angle of rigid bearing
Λ	bearing or compressibility number
κ	parabolic exponent
κ_r	parabolic exponent for rigid bearing
κ_{rm}	mean parabolic exponent value for rigid bearing
κ_f	parabolic exponent for compliant bearing
$\chi_1, \chi_2, \chi_3, \chi_4$	constants
$\upsilon, \upsilon_1, \upsilon_2$	constants
τ, τ_1	constants
β, β_1, β_2	constants

Abstract

Compliant journal bearings are commonly used to support radial loads at extreme operating speeds and conditions where conventional bearings cannot operate. The journal and bearing system are supported by a thin lubricant film (gas) due to the hydrodynamic pressure distribution. To predict the bearing performance parameters, the compressible Reynolds equation is solved based on Infinitely Long Approximation (ILA), Finite Analysis (FA) and a new Modified Parabolic Approximation (MPA). The MPA method reduces the classical Reynolds equation to an ordinary differential equation. Appropriate equations and numerical solution are developed for treating a compressible Reynolds equation using MPA.

A series of parametric study is presented to validate the new method. This method can be extended to study the dynamic characteristics of a gas bearing considering the non-linearity of the equations which could further aid in design and understanding of newer generation of bearings.

Chapter 1. Introduction and Literature Review

Compliant journal bearings popularly known as foil bearings have gained significant attention in recent years because of their unique mode of operation and diversity of applications. These types of bearings have various advantages compared to the conventional rigid journal bearings in terms of higher load carrying capacity, lower power loss, better stability, and greater endurance. These bearings are self acting, and can operate with ambient air or any process gas as the lubricating fluid. The need for complex lubrication systems is eliminated, which result in significant weight reduction and lower maintenance. The most common lubricant used is air which is available abundantly and can operate at elevated temperatures whereas conventional oil-based lubricants fail since their viscosity drops exponentially with rise in temperature.

Air foil bearings are now being used in industries ranging from computer hard drives, spindles in textile industry (Rao et al., 1996), cryogenic turbo compressors, and high speed aerospace rotating machinery. In fact a successful test of a mesoscopic scale turbojet engine simulator has already been carried out with miniature air foil journal bearings (Salehi et al., 2004). These bearings are of importance in the aerospace industry with regards to reduction in weight as well as operating under extreme conditions.

Figure 1 represents the configuration of a first generation foil journal bearing (Dellacorte et al., 2000). It is comprised of an outer bearing sleeve or outer housing which houses the corrugated series of bumps on a thin foil strip and over the bump foil strip a thin smooth top foil sheet is laid. These foils are welded at one end (leading edge) and are free at the other (trailing edge). The series of bumps in the strip supports the top foil sheet and acts as a spring bed which makes the bearing compliant (Fig 2). The journal has an interference fit in the bearing with clearance being almost nil (Radil et al., 2002). The journal and the foils are in contact when the journal is

stationary and remain in contact until a critical lift-off speed is achieved, at which point the journal rides on a thin gas film developed due to the hydrodynamic pressure between the journal

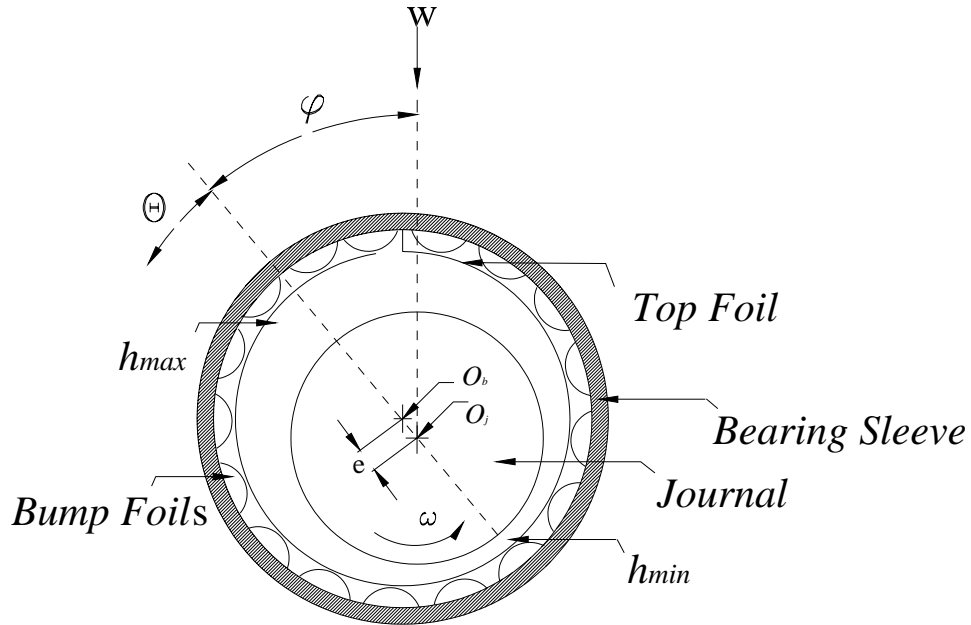


Figure 1: Schematic of Compliant Journal Bearing

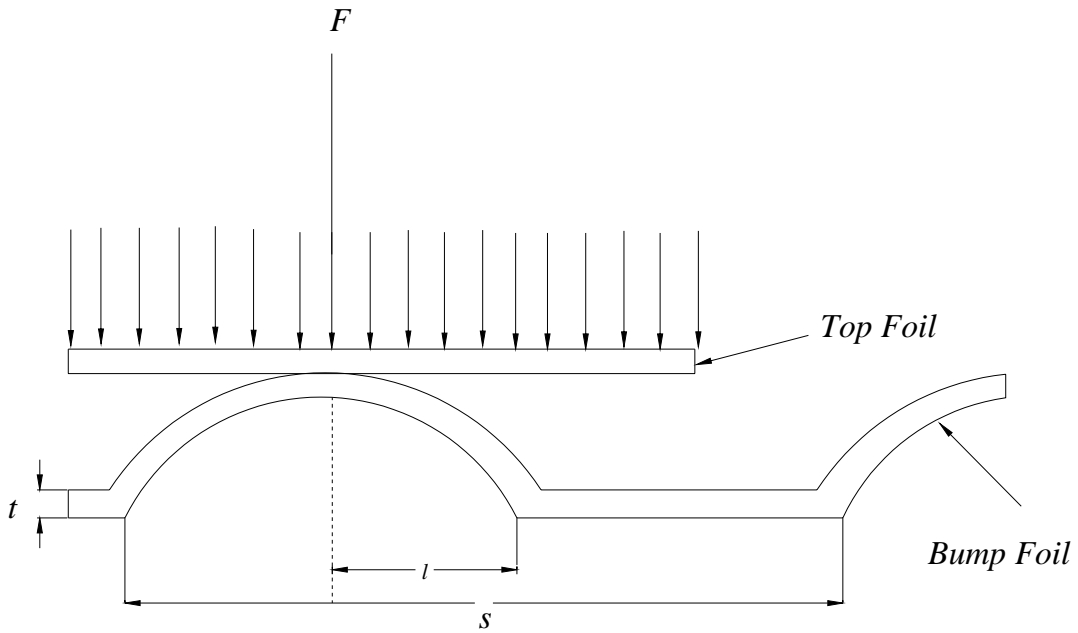


Figure 2: Schematic Configuration of Top and Bump Foils

and the bearing. Under the action of pressure, the top foil tends to deform, forcing it away from the shaft towards the bump strip which acts as a spring bed for the top foil sheet.

The hydrodynamic pressure developed varies with operating speed and has a significant influence on the deformation of the foils. Hence, the film thickness is function of hydrodynamic pressure and the elastic properties of the foils (Heshmat et al., 1983, Heshmat, 1994). An elasto-hydrodynamic analysis should account for the above parameters and also the compressibility of the lubricant. (Walowit et al., 1975, Gross et al., 1980, Hamrock, 1994, Khonsari and Booser, 2001, Peng and Khonsari, 2004).

The elastohydrodynamic analysis was reported for thrust type foil bearings using a coupled finite element and finite difference methods (Heshmat et al., 2000). In the case of compliant journal bearings the study of hydrodynamic behavior was reported by Heshmat et al., (1983) where the authors solved the Reynolds equation using the Newton-Raphson method and reported the effect of various structural, geometrical and operational variables on the bearing behavior. Also, estimation of load capacity for foil journal bearing was made using a “Rule of Thumb” by Dellacorte et al., (2000). This was based on the first principles and data available in the literature and it relates bearing load capacity to the bearing size and speed through an empirically-based, load-capacity coefficient. It reported that the “first generation” compliant support elements have a relatively low load-carrying capacity compared to the more advanced ones developed by Heshmat (1994) which achieved a breakthrough load-carrying capacity of 670,000 Pa at 59,700 rpm. This advanced design, which is referred to as the “third generation”, has unique compliant support elements where the elastic structural properties are modified with the use of multi-stage bumps and advanced solid lubricant coating. This design showed overall improvement of bearing performance at higher speeds, including a better load-carrying capacity.

The radial clearance in compliant journal bearings also represents a very important parameter whose effects lead to the overall performance of the bearing. Radil et al., (2002) reported a series of tests on two “third generation” type bearings with different radial clearances. They provided information on determining an optimum clearance for a bearing to perform well in terms of load-carrying capacity as well as for preventing bearing seizure due to thermal effects.

A steady state finite elastohydrodynamic analysis considering the compressibility of the lubricant and bearing compliance was reported (Peng and Khonsari, 2004). The authors reported the method of modeling and computational analysis by using an arithmetic mean pressure along the axial direction of the bearing. Reported analysis were in good agreement with the experimental analysis (Strom, 1987) for a range of operating speeds and different generation bearings. Also, by coupling the energy equations the analysis were further extended to thermohydrodynamic analysis to understand the thermal effects of the bearing at various operating speeds (Peng, 2003).

Various published literature (Ku et al., 1992, Heshmat et al., 1994) showed that compliant journal bearings are able to handle greater loads with improvements in the compliant support structures. Also, the use of advanced solid lubricants (Dellacorte et al., 2000) not only enhanced the operation of the bearings during the start up and shut down cycles but also provided frictional damping for the elastic structure.

A lot of work has also been reported on understanding the stiffness and damping characteristics of the bearing. By coupling the structural and fluid equations (Peng et al., 1993), a perturbation technique was used to obtain the linearized dynamic coefficients equations and a finite difference formulation was developed to solve for the four stiffness and four damping coefficients. Kim and San Andres (2005) used an exact advection model to solve the PDEs for

the zeroth and first order pressure fields to obtain the static and dynamic force characteristics of the “first generation” foil bearings.

Further extension of hydrodynamic analysis to transient cases is needed to better understand the dynamics of the foil bearings (Czolczynski, 1999).

The aim of this thesis was to come up with a simplified approach to predict the bearing performance parameters. First, the bearing performance parameters were evaluated using an infinitely long approximation and the results are compared to experiments reported (Strom, 1982). Next, we have formulated entirely new set of Reynolds equation using a modified parabolic approach along the axial direction where in the finite Reynolds equation is converted to an ODE which considers the compressibility effects. This method was first carried out for incompressible flows (Ettles and Shelly, 1970) and has been widely used to understand the dynamic characteristics of the bearing (Singhal and Khonsari, 2005, Singhal, 2004). The new set of equations were solved numerically and compared with numerical simulations using a finite approximation (Peng and Khonsari, 2004) for rigid bearings and compliant bearings. This method saves valuable computational time and can be further extended to transient analysis to determine the stiffness and damping characteristics of compliant journal bearings.

Chapter 2. Mathematical Model

2.1 Derivation of Standard Reynolds Equation for Journal Bearings

For any type of journal bearing systems the most accurate way of predicting the performance parameters is to solve for the lubricant flow equations obtained from the Navier-Stokes relationships. But the computational costs involved can be very high when variations in viscosity and flexibility of outer bearing sleeves are considered. Hence instead of the full solution, accepted approximate methods are obtained by solving for the lubricant flow using the two dimensional classical Reynolds equation. Reynolds equation reflects tremendous insight by Osborne Reynolds into fluid behavior in bearing lubricant films, and is responsible to giving birth to science of hydrodynamic lubrication (Khonsari and Booser 2001). Solution of the classical Reynolds equation enables one to determine the pressure distribution in a bearing with an arbitrary film shape. Once the pressure profile is evaluated the important bearing parameters such as the load-carrying capacity, friction force, flow rates etc., can be easily obtained.

The following assumptions are made in deriving the Reynolds Equation (Khonsari and Booser 2001).

1. Fluid is assumed Newtonian, with direct proportionality between shear stress and shearing velocity;
2. Inertia and body forces are assumed to be negligible compared to the viscous terms;
3. Variation of pressure across the film is assumed to be very small;
4. Flow is laminar; and
5. Curvature effects are negligible.

Figure 3, Indicates a three dimensional slider bearing configuration with a film gap of $h(x) = h(x, y)$. The top plate and bottom plate are considered to undergo a sliding motion U_a

and U_b . A normal squeeze motion may exist in the z direction. The squeeze components are denoted by w_a and w_b .

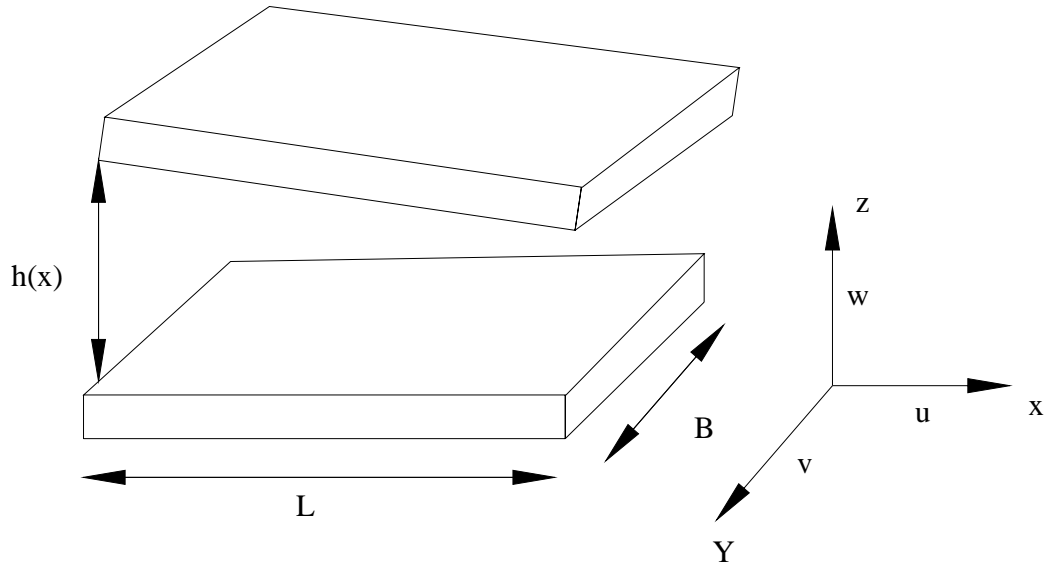


Figure 3: Schematic of Slider Bearing (Khonsari and Booser, 2001)

The X momentum equation is represented as follows:

$$\frac{\partial p}{\partial x} = \frac{\partial}{\partial z} \left(\mu \frac{\partial u}{\partial z} \right) \quad 2.1.1$$

The Y momentum equation is represented as follows:

$$\frac{\partial p}{\partial y} = \frac{\partial}{\partial z} \left(\mu \frac{\partial v}{\partial z} \right) \quad 2.1.2$$

The Z momentum equation is represented as follows:

$$\frac{\partial p}{\partial z} = 0 \quad \text{Variation of pressure across the film is considered to be very small.} \quad 2.1.3$$

Integrating equations 2.1.1 and 2.1.2 twice with the following boundary conditions:

$$\text{At } z = 0, \quad u = U_a, v = 0, w = w_a$$

$$\text{At } z = h, \quad u = U_b, v = 0, w = w_b \quad 2.1.4$$

$$u = \underbrace{\frac{1}{2\mu} \frac{\partial p}{\partial x} (z^2 - zh)}_{\text{Poiseuille flow Term}} + \underbrace{\left(1 - \frac{z}{h}\right) U_a + \frac{z}{h} U_b}_{\text{Couette Flow}} \quad 2.1.5$$

Equation 2.1.5 represents the velocity profile which is composed of the Poiseuille term due to the pressure gradient in the x direction and the Couette flow term due to the motion of the surfaces.

$$v = \frac{1}{2\mu} \frac{\partial p}{\partial y} (z^2 - zh) \quad 2.1.6$$

Equation 2.1.6 represents the flow velocity in the y direction. It represents the velocity profile of the fluid leaking out on the sides of the slider bearing.

Volumetric flow rates in the direction of sliding and leakage flow rates can be determined by integrating equations 2.1.5 and 2.1.6 across the gap respectively.

- **Conservation of Mass**

For compressible flows the general equation for conservation of mass is:

$$\frac{\partial \rho}{\partial t} + \frac{\partial(\rho u)}{\partial x} + \frac{\partial(\rho v)}{\partial y} + \frac{\partial(\rho w)}{\partial z} = 0 \quad 2.1.7$$

Integrating equation 2.1.7 across the film thickness yields:

$$\int_0^h \frac{\partial \rho}{\partial t} dz + \int_0^h \frac{\partial(\rho u)}{\partial x} dz + \int_0^h \frac{\partial(\rho v)}{\partial y} dz + \int_0^h \frac{\partial(\rho w)}{\partial z} dz = 0 \quad 2.1.8$$

The resulting equation is:

$$h \frac{\partial \rho}{\partial t} + \frac{\partial}{\partial x} \left(-\frac{\rho h^3}{12\mu} \frac{\partial p}{\partial x} \right) + \frac{1}{2} \frac{\partial}{\partial x} [\rho(U_a - U_b)h] - U_b \rho \frac{\partial h}{\partial x} + \frac{\partial}{\partial y} \left(-\frac{\rho h^3}{12\mu} \frac{\partial p}{\partial y} \right) + \rho(w_a - w_b) = 0 \quad 2.1.9$$

Rearranging:

$$\frac{\partial}{\partial x} \left(\frac{\rho h^3}{12\mu} \frac{\partial p}{\partial x} \right) + \frac{\partial}{\partial y} \left(\frac{\rho h^3}{12\mu} \frac{\partial p}{\partial y} \right) = \frac{1}{2} \frac{\partial}{\partial x} [\rho(U_a - U_b)h] - U_b \rho \frac{\partial h}{\partial x} + \rho(w_a - w_b) + h \frac{\partial \rho}{\partial t} \quad 2.1.10$$

Neglecting the stretch terms, density wedge and the local expansion terms equation 2.1.10 reduces to a simplified final Reynolds equation which is widely used for most applications.

$$\frac{\partial}{\partial x} \left(\frac{\rho h^3}{12\mu} \frac{\partial p}{\partial x} \right) + \frac{\partial}{\partial y} \left(\frac{\rho h^3}{12\mu} \frac{\partial p}{\partial y} \right) = \frac{1}{2} \rho(U_a - U_b) \frac{\partial h}{\partial x} + \rho(w_a - w_b) \quad 2.1.11$$

For a journal bearing configuration as represented in Figure 4, the bearing sleeve is fixed and the journal is rotating. Considering a case where film thickness varies with time and with the following conditions:

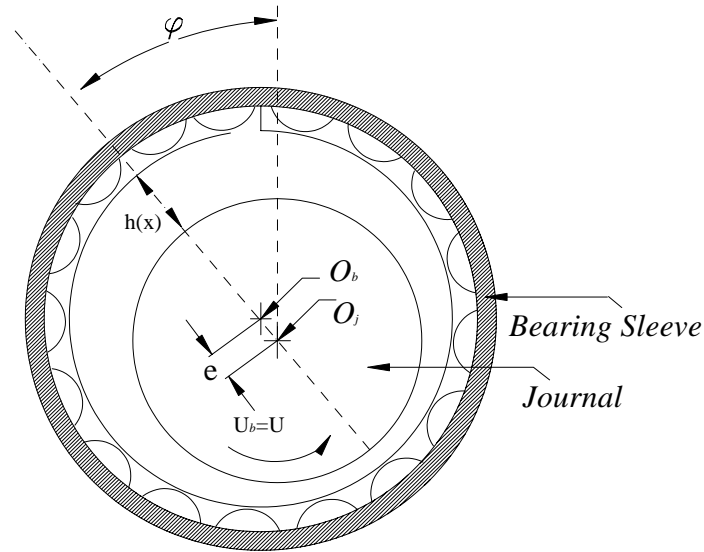


Figure 4: Schematic of a Journal Bearing

$$U_a = 0, w_a = 0 \text{ and } U_b = U \neq 0, w_b = w \neq 0 \quad 2.1.12$$

The final Reynolds equation is of the form:

$$\frac{\partial}{\partial x} \left(\frac{\rho h^3}{12\mu} \frac{\partial p}{\partial x} \right) + \frac{\partial}{\partial y} \left(\frac{\rho h^3}{12\mu} \frac{\partial p}{\partial y} \right) = \frac{1}{2} U \frac{\partial(\rho h)}{\partial x} + \frac{\partial(\rho h)}{\partial t} \quad 2.1.13$$

With this equation the bearings hydrodynamic pressure distribution can be obtained. It accounts for both the physical wedge and pressure generation capability due to normal approach of surfaces, in other words the squeeze action (Khonsari and Booser, 2001).

Chapter 3. Journal Bearing Approximation Methods

3.1 Infinitely Long Approximation (ILA)

3.1.1 Compressible Reynolds Equation in One Dimension

In this type of approximation the journal bearing length is considered to be infinitely long and the pressure along the axial direction is considered to be a constant. The Reynolds equation (2.1.13) is considered with the elimination of the axial terms and time variants.

$$\frac{\partial}{\partial x} \left(\frac{\rho h^3}{12\mu} \frac{\partial p}{\partial x} \right) = \frac{1}{2} U \frac{\partial(\rho h)}{\partial x} \quad 3.1.1.1$$

where x represents the circumferential direction of the bearing

In polar co-ordinates:

$$x = R\theta, U = R\omega \quad 3.1.1.2$$

$$\frac{\partial}{R\partial\theta} \left(\frac{\rho h^3}{12\mu R} \frac{\partial p}{\partial\theta} \right) = \frac{1}{2} R\omega \frac{\partial(\rho h)}{R\partial\theta} \quad 3.1.1.3$$

With ideal gas $\rho = \frac{P}{R_g T}$ it is modified as follows 3.1.1.4

$$\frac{\partial}{R\partial\theta} \left(\frac{ph^3}{R_g T 12\mu R} \frac{\partial p}{\partial\theta} \right) = \frac{1}{2} \frac{R\omega}{R_g T} \frac{\partial(ph)}{R\partial\theta} \quad 3.1.1.5$$

Further:

$$\frac{\partial}{\partial\theta} \left(\frac{ph^3}{12T\mu} \frac{\partial p}{\partial\theta} \right) = \frac{1}{2} \frac{R^2\omega}{T} \frac{\partial(ph)}{\partial\theta} \quad 3.1.1.6$$

Normalizing:

$$\frac{\partial}{\partial\theta} \left(\frac{\bar{p}\bar{h}^3}{12\bar{T}\bar{\mu}} \frac{\partial\bar{p}}{\partial\theta} \right) = \frac{\Lambda}{\bar{T}} \frac{\partial(\bar{p}\bar{h})}{\partial\theta} \quad 3.1.1.7$$

$$\text{where } \bar{p} = \frac{p}{p_a}, \bar{h} = \frac{h}{C}, \bar{\mu} = \frac{\mu}{\mu_0}, \bar{T} = \frac{T}{T_0} \quad \text{and} \quad 3.1.1.8$$

$$\Lambda = \frac{6\omega\mu_0}{p_a} \left(\frac{R}{C} \right)^2 \text{ represents the bearing number or the compressibility number} \quad 3.1.1.9$$

For a rigid gas bearing, the functional form of the film thickness is represented as:

$$h_r = C + e_r \cos \theta \quad 3.1.1.10$$

In dimensionless form it is represented as:

$$\bar{h}_r = 1 + \varepsilon_r \cos \theta \quad 3.1.1.11$$

$$\text{where } \bar{h}_r = \frac{h_r}{C}, \quad \varepsilon_r = \frac{e_r}{C}$$

But in case of a foil bearing since the bushing is compliant, the film thickness is a function of the pressure.

$$h_f = C + e_f \cos \theta + \alpha(p - 1) \quad 3.1.1.12$$

In dimensionless form (Radil et al., 2002) is represented as,

$$\bar{h}_f = 1 + \varepsilon_f \cos \theta + \alpha(\bar{p} - 1) \quad 3.1.1.13$$

$$\text{where } \bar{h}_f = \frac{h_f}{C}, \varepsilon_f = \frac{e_f}{C}, \bar{p} = \frac{p}{p_a}, \alpha = \frac{2p_a s}{CE} \left[\frac{l}{t} \right]^3 (1 - \nu^2) \quad 3.1.1.14$$

α represents the compliance number (Heshmat et al., 1983, Walowit et al., 1975).

From equation 3.1.1.13 the film thickness is not only a function of the eccentricity ratio as in the case of rigid bearings, but it is also the function of the hydrodynamic pressure which deform the top and lower bump foils. This is a unique feature with regards to the operation of the compliant journal bearings. With this feature, normally compliant journal bearings operate with eccentricity ratios that can be greater than one and still maintain a positive film thickness. This is due to the deformation of the top and bump foils by the developed hydrodynamic pressure which

creates a higher overall clearance compared to original clearance dimensions, when the bearing is not operating. Hence, the shaft moves towards the minimum film thickness as the foils deform.

3.1.2 Numerical Procedure (ILA)

Considering equation 3.1.1.7 it is expanded as follows:

$$\bar{p}\bar{h}^3\left(\frac{\partial^2\bar{p}}{\partial\theta^2}\right)+\bar{p}\frac{\partial\bar{p}}{\partial\theta}(3\bar{h}^2)\frac{\partial\bar{h}}{\partial\theta}+\bar{h}^3\left(\frac{\partial\bar{p}}{\partial\theta}\right)^2=\Lambda\left[\bar{p}\frac{\partial\bar{h}}{\partial\theta}+\bar{h}\frac{\partial\bar{p}}{\partial\theta}\right] \quad 3.1.2.1$$

Simplifying further:

$$\left(\frac{\partial^2\bar{p}}{\partial\theta^2}\right)+\left[\frac{3}{\bar{h}}\frac{\partial\bar{p}}{\partial\theta}\frac{\partial\bar{h}}{\partial\theta}\right]+\left[\frac{1}{\bar{p}}\left(\frac{\partial\bar{p}}{\partial\theta}\right)^2\right]=\frac{\Lambda}{\bar{p}\bar{h}^3}\left[\bar{p}\frac{\partial\bar{h}}{\partial\theta}+\bar{h}\frac{\partial\bar{p}}{\partial\theta}\right] \quad 3.1.2.2$$

Rearranging:

$$\left(\frac{\partial^2\bar{p}}{\partial\theta^2}\right)=-\frac{3}{\bar{h}}\left[\frac{\partial\bar{p}}{\partial\theta}\frac{\partial\bar{h}}{\partial\theta}\right]-\frac{1}{\bar{p}}\left[\left(\frac{\partial\bar{p}}{\partial\theta}\right)^2\right]+\frac{\Lambda}{\bar{p}\bar{h}^3}\left[\bar{p}\frac{\partial\bar{h}}{\partial\theta}+\bar{h}\frac{\partial\bar{p}}{\partial\theta}\right] \quad 3.1.2.3$$

The appropriate boundary conditions are:

$$\bar{p}=1 \quad \text{at} \quad \theta=0.$$

$$\bar{p}=1 \quad \text{at} \quad \theta=2\pi \quad 3.1.2.4$$

The above non-linear differential equation with appropriate boundary conditions is solved using the finite difference method (Ferziger et al., 2002, Gerald et al., 2002, Hunt et al., 2001).

$$\left(\frac{\bar{p}_{i+1}-2\bar{p}_i+\bar{p}_{i-1}}{\Delta\theta^2}\right)=-\frac{1}{\bar{p}_i}\left[\left(\frac{\partial\bar{p}}{\partial\theta}\right)_i^2\right]-\frac{3}{h_i}\left[\frac{\partial\bar{p}}{\partial\theta}\right]_i\left[\frac{\partial\bar{h}}{\partial\theta}\right]_i+\left[\frac{\Lambda}{\bar{p}_i\bar{h}_i^2}\frac{\partial\bar{p}}{\partial\theta}\right]_i+\left[\frac{\Lambda}{\bar{h}_i^3}\frac{\partial\bar{h}}{\partial\theta}\right]_i \quad 3.1.2.5$$

By assuming an initial guess value from solving the incompressible Reynolds equation for the dimensionless pressure \bar{p}_i . The above equation (3.1.2.5) is solved for pressure iteratively using the tridiagonal approximation method (Ferziger et al., 2002, Gerald et al., 2002, Patankar., 1980). Two hundred grid points were employed along the circumferential direction and under

relaxation was used to achieve convergence with rigid tolerances. The under-relaxation between successive iterations is given by the formula:

$$\bar{p}^{n+1} = \alpha_r \bar{p}^{n+1} + (1 - \alpha_r) \bar{p}^n \quad 3.1.2.6$$

where α_r is the under-relaxation factor and n is the iteration number, $\alpha_r = 0.99$ was typically used.

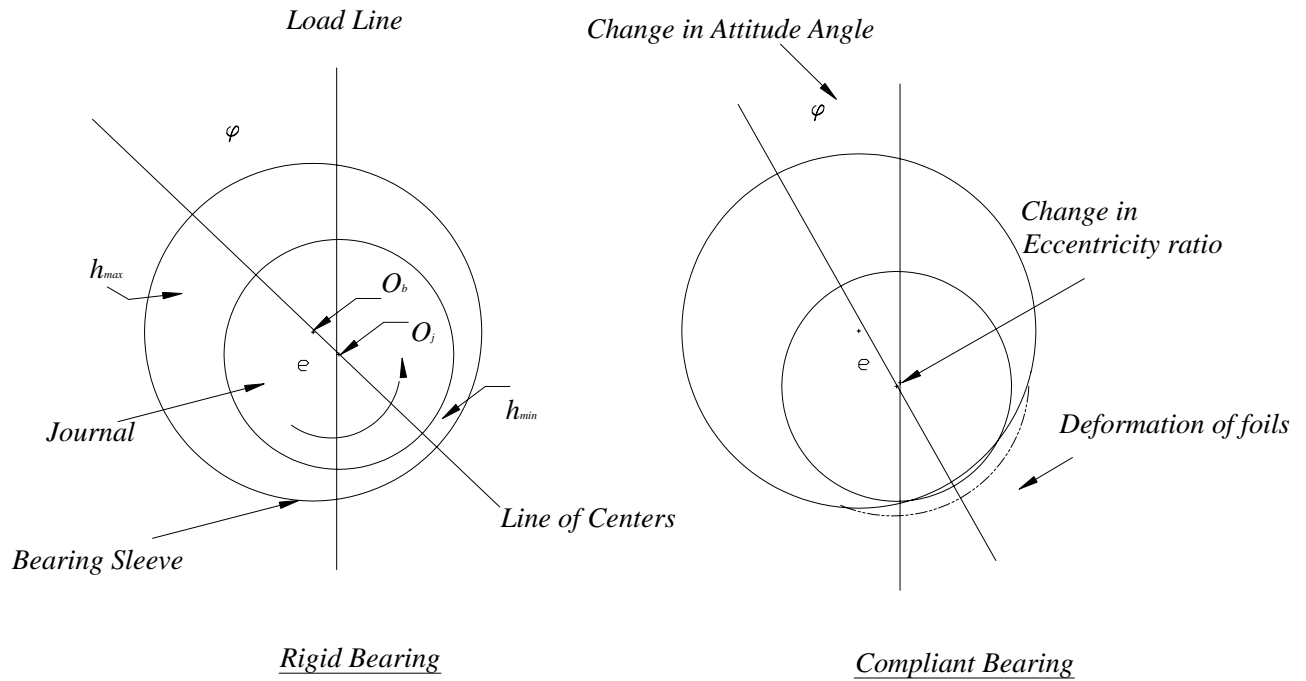


Figure 5: Rigid Bearing and Compliant Bearing Mode of Function.

The next part is to couple the hydrodynamic pressure and the foil structural compliance, which has a direct effect on the overall behavior of the fluid film profile. This is incorporated in an iterative scheme. Recalling equation (3.1.1.13), the film thickness \bar{h}_f is a function of the dimensionless pressure. As the top and bump foils deform due to the pressure, the shaft moves in the direction where there is maximum deformation (Fig. 5) and hence there is a significant

change in the eccentricity ratio ε_f and attitude angle ϕ_f which further changes the overall profile of the film thickness. This is not accounted for in the equation (3.1.1.13).

Hence to account for this the modified form of the film thickness equation is used (Peng and Khonsari, 2004):

$$\bar{h}_f = 1 + \varepsilon_f \cos(\theta - \Delta\varphi) + \alpha(\bar{p} - 1) \quad 3.1.2.7$$

$$\varepsilon_f = \varepsilon_r + \Delta\varepsilon \quad (\text{Peng and Khonsari, 2004}) \quad 3.1.2.8$$

where ε_f is determined by bisection method by assuming that the minimum film thickness $h_{\min r}$ in a rigid bearing and the corresponding minimum film thickness in a foil bearing $h_{\min f}$ is the same and that $\Delta\varphi$ represents the difference in the attitude angle for a rigid bearing ϕ_r and compliant bearing ϕ_f . The effect of the hydrodynamic pressure on the film thickness profile was determined iteratively by employing the method of under relaxation. The final film thickness is obtained as follows (Peng and Khonsari, 2004):

$$\bar{h}_f^{n+1} = 1 + \varepsilon_f^n \cos(\theta - \Delta\varphi^n) + \alpha(\bar{p}^n - 1) \quad 3.1.2.9$$

where n is the number of points used along the circumferential direction (two hundred).

The under-relaxation between successive iterations is given by the formula:

$$\bar{h}_f^{n+1} = \alpha_{rh} \bar{h}_f^{n+1} + (1 - \alpha_{rh}) \bar{h}_f^n \quad 3.1.2.10$$

where α_{rh} represents the under-relaxation factor for the fluid film. Typically α_{rh} varies from 0.7 to 0.95 depending on the eccentricity ratios and operating speeds.

- **Load Carrying Capacity**

Once the dimensionless pressure is calculated, the load-carrying capacity can then be calculated by integrating the positive pressure profile (Khonsari and Booser, 2001).

The x and z components are:

$$W_x = \int_0^{2\pi} LR(p-1)\cos\theta d\theta \quad W_z = \int_0^{2\pi} LR(p-1)\sin\theta d\theta \quad 3.1.2.11$$

In dimensionless form:

$$\bar{W}_x = \int_0^{2\pi} (\bar{p}-1)\cos\theta d\theta \quad \bar{W}_z = \int_0^{2\pi} (\bar{p}-1)\sin\theta d\theta \quad 3.1.2.12$$

$$\text{where } \bar{W}_{x,z} = \frac{W}{p_a RL}, \quad \bar{p} = \frac{p}{p_a} \Rightarrow p = \bar{p}p_a \quad 3.1.2.13$$

$$\bar{W}_f = \sqrt{\bar{W}_x^2 + \bar{W}_z^2}, \quad \text{also} \quad \bar{W}_f = \frac{W}{p_a RL} \quad 3.1.2.14$$

$$\text{The attitude angle is defined as:} \quad \tan\varphi = \frac{\bar{W}_z}{-\bar{W}_x} \quad 3.1.2.15$$

$$\text{Hence } W = \bar{W}_f p_a RL \text{ represents the load carrying capacity of the foil bearing.} \quad 3.1.2.16$$

Finally the Simpson's rule was employed for numerical integration to determine the load carrying capacity of the bearing.

3.1.3 Bearing Performance Parameters (ILA)

Figure 6 represents the pressure profile comparison between a rigid bearing and a first generation foil bearing whose properties are indicated in Table 1 (Peng, 2003). The operating speed is 30,000 rpm. The lubricant used is air whose properties are indicated in Table 2 (Peng, 2003). Note that the rigid bearing of equal dimensions and same lubricant properties and operating speeds are assumed for comparison. The pressure profile for the foil bearing is spread over a larger area compared to its rigid bearing counterpart resulting in a greater load carrying capacity.

Figure 7 represents the film thickness profile comparison between a rigid bearing and a compliant bearing. The overall film profile for a foil bearing spans over a greater area due to the deformation of the foils. The program converged with a minimum film thickness equivalent to $10\ \mu\text{m}$ ($h_{\min f}, h_{\min r}$) attitude angle of foil bearing $\phi_f = 36^\circ$ and that of rigid bearing $\phi_r = 42.3^\circ$ with a total load carrying capacity equivalent to 130 N. The results obtained are comparable with the set of experiments run (Strom, 1987).

Table 1: Generation 1 Compliant Bearing Data (Peng, 2003)

Radius of Shaft (R)	$19.05 \times 10^{-3}\ \text{m}$
Bearing Length (L)	$38.1 \times 10^{-3}\ \text{m}$
Nominal Radial Clearance (C)	$50 \times 10^{-6}\ \text{m}$
Top Foil Thickness (t_f)	$0.1016 \times 10^{-3}\ \text{m}$
Bump Foil Thickness (t_b)	$0.1016 \times 10^{-3}\ \text{m}$
Bump Pitch (s)	$4.572 \times 10^{-3}\ \text{m}$
Bump Length ($2l$)	$3.556 \times 10^{-3}\ \text{m}$
Bump Foil Youngs Modulus (E)	$200 \times 10^9\ \text{Pa}$
Bump Foil Poisson's Ratio (ν)	0.31

Table 2: Lubricant Properties (Air) (Peng, 2003)

Viscosity (μ)	$184.6 \times 10^{-7}\ \text{N.s/m}^2$
Density (ρ_0)	$1.1614\ \text{kg/m}^3$

Figures 8 and 9 present the pressure profile and film thickness profile comparison between a rigid bearing and first generation foil bearing run at 45,000 rpm respectively. The program converged with a minimum film thickness of $9.5\ \mu\text{m}$ ($h_{\min f}, h_{\min r}$). Attitude angle $\phi_f =$

30° and that of rigid bearing $\phi_r = 35^\circ$ with a total load carrying capacity of 210 N. These are comparable to experiments reported by Strom (1987).

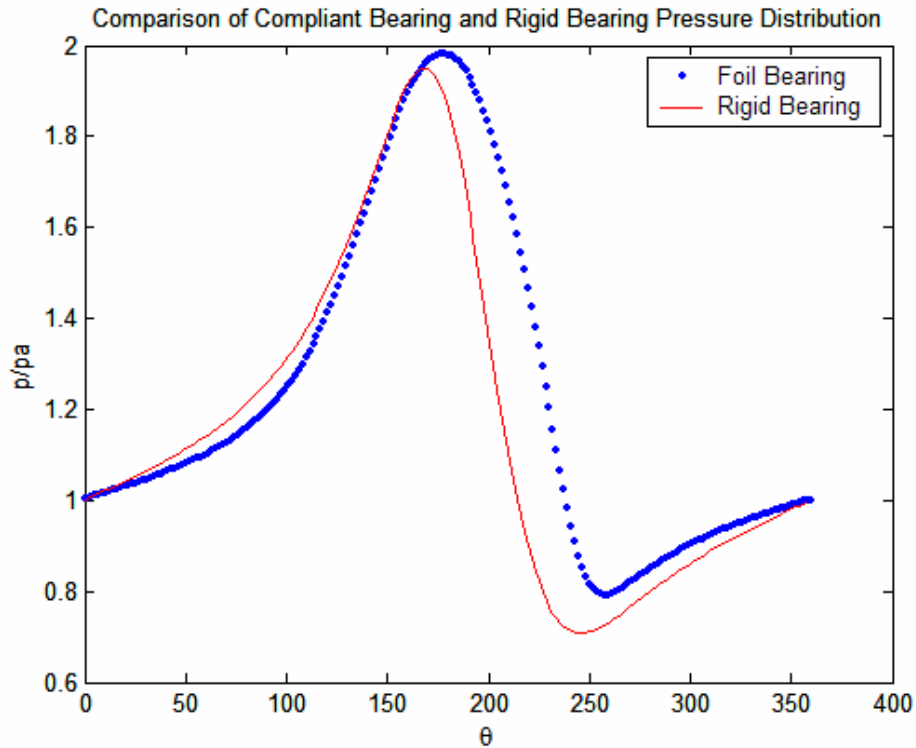


Figure 6: Pressure Profiles for Rigid and Compliant Bearing at 30,000 rpm.

Some unique features with regards to the operation of the foil bearings is to have eccentricity ratios greater than one. In the case of rigid bearings eccentricity equivalent to clearance will result in the contact between the journal and the bearing leading to seizure. But in the case of the foil bearings the clearance value changes depending on the operating speeds and design of the bump and top foils. The attitude angle in the case of foil bearings is less compared to its rigid bearing counterpart, which is thought to enhance the overall stability of operation (Peng and Khonsari, 2004). The numerical code developed was further tested to understand the performance parameters of the bearing at very high Λ (Peng and Khonsari, 2004). The maximum rpm which could be simulated was around 500,000. A numerical difficulty encountered was

waviness of the pressure at very high bearing numbers (Kawabata, 1987). The analysis trends indicated that the load carrying capacity flattens out after a certain rpm range.

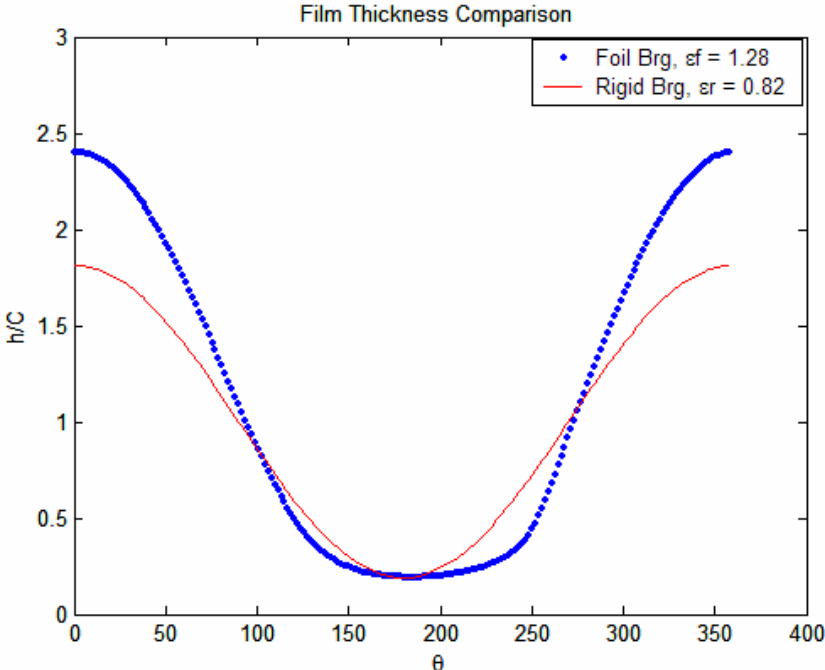


Figure 7: Film Thickness Profiles for Rigid and Compliant Bearing at 30,000 rpm.

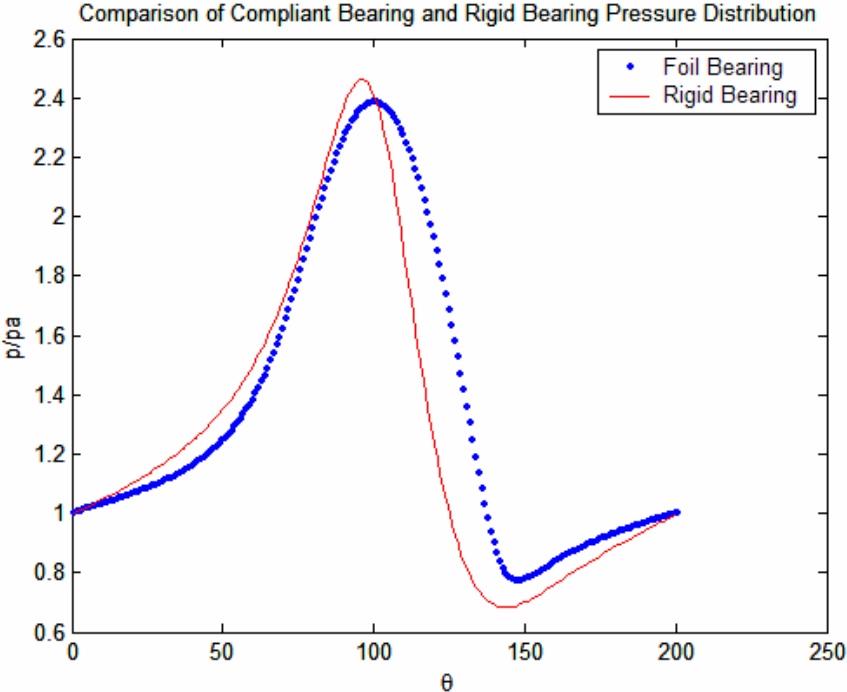


Figure 8: Pressure Profiles for Rigid and Compliant bearing at 45,000 rpm.

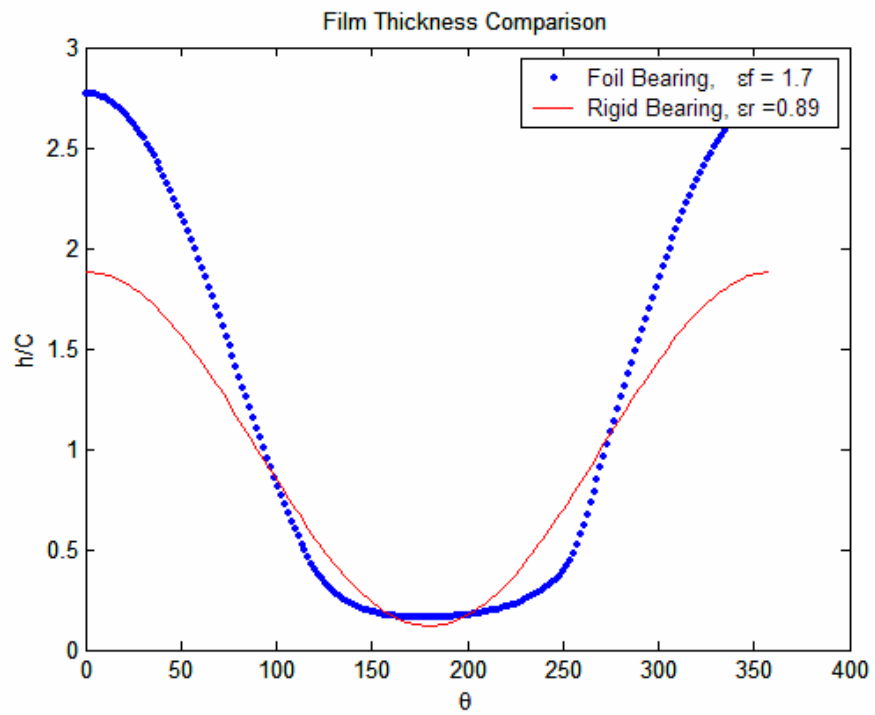


Figure 9: Film Thickness Profiles for Rigid and Compliant Bearing at 45,000 rpm.

3.2 Finite Analysis

3.2.1 Compressible Reynolds Equation in Two Dimensions

The standard Reynolds equation (2.1.13) is considered by neglecting the time variant. The solution to this equation is obtained by considering a bearing with finite length and other dimensions. This approximation represents the most accurate method to predict the performance parameters for any type of journal bearings.

$$\frac{\partial}{\partial x} \left(\frac{\rho h^3}{12\mu} \frac{\partial p}{\partial x} \right) + \frac{\partial}{\partial y} \left(\frac{\rho h^3}{12\mu} \frac{\partial p}{\partial y} \right) = \frac{1}{2} U \frac{\partial(\rho h)}{\partial x} \quad 3.2.1.1$$

In polar coordinates:

$$x = R\theta, U = R\omega \quad 3.2.1.2$$

$$\frac{\partial}{R\partial\theta} \left[\frac{\rho h^3}{12\mu} \frac{\partial p}{R\partial\theta} \right] + \frac{\partial}{\partial y} \left[\frac{\rho h^3}{12\mu} \frac{\partial p}{\partial y} \right] = \frac{1}{2} R\omega \frac{\partial}{R\partial\theta} (\rho h) \quad 3.2.1.3$$

For ideal gas:

$$\rho = \frac{p}{R_g T} \quad 3.2.1.4$$

Considering ideal gas the equation reduces to:

$$\frac{1}{R^2} \frac{\partial}{\partial\theta} \left[\frac{ph^3}{R_g T 12\mu} \frac{\partial p}{\partial\theta} \right] + \frac{\partial}{\partial y} \left[\frac{ph^3}{R_g T 12\mu} \frac{\partial p}{\partial y} \right] = \frac{1}{2} \frac{\omega}{R_g T} \frac{\partial}{\partial\theta} (ph) \quad 3.2.1.5$$

Multiply by R^2 and simplifying further.

$$\frac{\partial}{\partial\theta} \left[\frac{ph^3}{T 12\mu} \frac{\partial p}{\partial\theta} \right] + \frac{\partial}{\partial y} \left[\frac{ph^3}{T 12\mu} \frac{\partial p}{\partial y} \right] = \frac{\omega R^2}{2} \frac{\partial}{\partial\theta} \left(\frac{ph}{T} \right) \quad 3.2.1.6$$

Normalizing the above equation with:

$$\bar{y} = \frac{y}{L/2}, \bar{p} = \frac{p}{p_a}, \bar{h} = \frac{h}{C}, \bar{\mu} = \frac{\mu}{\mu_0}, \bar{T} = \frac{T}{T_0} \quad 3.2.1.7$$

$$\frac{\partial}{\partial \theta} \left[\frac{\bar{p} p_a \bar{h}^3 C^3}{12 \bar{\mu} \mu_0 \bar{T} T_0} \frac{\partial}{\partial \theta} (p p_a) \right] + R^2 \frac{\partial}{\partial \bar{y}} \frac{L}{2} \left[\frac{\bar{p} p_a \bar{h}^3 C^3}{12 \bar{\mu} \mu_0 \bar{T} T_0} \frac{\partial}{\partial \bar{y}} \left(\frac{L}{2} \right) (p p_a) \right] = \frac{\omega R^2}{2} \frac{\partial}{\partial \theta} \left(\frac{\bar{p} p_a \bar{h} C}{T T_0} \right) \quad 3.2.1.8$$

Simplifying further:

$$\left[\frac{p_a^2 C^3}{12 \mu_0} \left[\frac{\partial}{\partial \theta} \left[\frac{\bar{p} p_a \bar{h}^3 C^3}{12 \bar{\mu} \mu_0 \bar{T}} \frac{\partial}{\partial \theta} (p p_a) \right] + R^2 \frac{\partial}{\partial \bar{y}} \frac{L}{2} \left[\frac{\bar{p} p_a \bar{h}^3 C^3}{12 \bar{\mu} \mu_0 \bar{T}} \frac{\partial}{\partial \bar{y}} \left(\frac{L}{2} \right) (p p_a) \right] \right] \right] = \frac{\omega R^2}{2} \frac{\partial}{\partial \theta} \left(\frac{\bar{p} p_a \bar{h} C}{\bar{T}} \right) \quad 3.2.1.9$$

Assuming an isothermal and isoviscous case where $\bar{T} = 1$ and $\bar{\mu} = 1$.

The equation (3.2.1.9) reduces to:

$$\frac{\partial}{\partial \theta} \left(\bar{p} \bar{h}^3 \frac{\partial \bar{p}}{\partial \theta} \right) + \left(\frac{D}{L} \right)^2 \frac{\partial}{\partial \bar{y}} \left(\bar{p} \bar{h}^3 \frac{\partial \bar{p}}{\partial \bar{y}} \right) = \Lambda \frac{\partial}{\partial \theta} (\bar{p} \bar{h}) \quad 3.2.1.10$$

where $\Lambda = \frac{6 \omega \mu_0}{p_a} \left(\frac{R}{C} \right)^2$ represents the compressibility number or the bearing number.

Equation 3.2.1.10 represents the standard compressible Reynolds equation in two dimensions.

For a rigid gas bearing, functional form of the film thickness is represented as:

$$h_r = C + e_r \cos \theta \quad 3.2.1.11$$

In dimensionless form it is represented as:

$$\bar{h}_r = 1 + \varepsilon_r \cos \theta \quad 3.2.1.12$$

where $\bar{h}_r = \frac{h_r}{C}$ and $\varepsilon_r = \frac{e_r}{C}$

But in case of a foil bearing since the bushing is compliant, the film thickness is a function of the pressure.

Hence:

$$h_f = C + e_f \cos \theta + \alpha(p - 1) \quad 3.2.1.13$$

In dimensionless form (3.2.1.13) is represented as,

$$\bar{h}_f = 1 + \varepsilon_f \cos \theta + \alpha(\bar{p} - 1) \quad 3.2.1.14$$

$$\text{where } \bar{h}_f = \frac{h_f}{C}, \varepsilon_f = \frac{e_f}{C}, \bar{p} = \frac{p}{p_a}, \alpha = \frac{2p_a s}{CE} \left[\frac{l}{t} \right]^3 (1 - \nu^2) \quad 3.2.1.15$$

α represents the compliance number (Heshmat et al., 1983, Walowit et al., 1975)

From equation (3.2.1.14) the film thickness is not only a function of the eccentricity ratio as in the case of rigid bearings but it is also a function of the hydrodynamic pressure which deform the top and lower bump foils. This is a unique feature with regards to the operation of the compliant journal bearings. With this feature normally compliant journal bearings operate with eccentricity ratios being greater than one and still maintain a positive film thickness. This is due to the deformation of the top and bump foils by the developed hydrodynamic pressure which creates a higher overall clearance when compared to original clearance dimensions when the bearing is not operating. Hence the shaft moves towards the minimum film thickness as the foils deform.

3.2.2 Numerical Procedure (FA)

Equation 3.2.1.10 is a non-linear equation and hence a numerical solution of the pressure must be obtained.

$$\underbrace{\frac{\partial}{\partial \theta} \left(\bar{p} \bar{h}^3 \frac{\partial \bar{p}}{\partial \theta} \right)}_A + \underbrace{\left(\frac{D}{L} \right)^2 \frac{\partial}{\partial y} \left(\bar{p} \bar{h}^3 \frac{\partial \bar{p}}{\partial y} \right)}_B = \underbrace{\Lambda \frac{\partial}{\partial \theta} (\bar{p} \bar{h})}_C$$

It is expanded as follows:

$$A = \frac{\partial}{\partial \theta} \left(\bar{p} \bar{h}^3 \frac{\partial \bar{p}}{\partial \theta} \right) = \left(\bar{p} \bar{h}^3 \left(\frac{\partial^2 \bar{p}}{\partial \theta^2} \right) + \bar{p} \frac{\partial \bar{p}}{\partial \theta} (3\bar{h}^2) \frac{\partial \bar{h}}{\partial \theta} + \bar{h}^3 \left(\frac{\partial \bar{p}}{\partial \theta} \right)^2 \right) \quad 3.2.1.16$$

$$B = \frac{\partial}{\partial y} \left(\bar{p} \bar{h}^3 \frac{\partial \bar{p}}{\partial y} \right) \left(\frac{D}{L} \right)^2 = \left(\bar{p} \bar{h}^3 \frac{\partial}{\partial y} \left(\frac{\partial \bar{p}}{\partial y} \right) + \bar{p} \frac{\partial \bar{p}}{\partial y} \frac{\partial}{\partial y} (\bar{h}^3) + \bar{h}^3 \frac{\partial \bar{p}}{\partial y} \frac{\partial}{\partial y} (\bar{p}) \right) \left(\frac{D}{L} \right)^2 \quad 3.2.1.17$$

$$C = \Lambda \frac{\partial}{\partial \theta} (\bar{p} \bar{h}) = \Lambda \left(\bar{p} \frac{\partial \bar{h}}{\partial \theta} + \bar{h} \frac{\partial \bar{p}}{\partial \theta} \right) \quad 3.2.1.18$$

Combining the above equations as A+B=C

$$\begin{aligned} & \left(\bar{p} \bar{h}^3 \left(\frac{\partial^2 \bar{p}}{\partial \theta^2} \right) + \bar{p} \frac{\partial \bar{p}}{\partial \theta} (3\bar{h}^2) \frac{\partial \bar{h}}{\partial \theta} + \bar{h}^3 \left(\frac{\partial \bar{p}}{\partial \theta} \right)^2 \right) + \left(\bar{p} \bar{h}^3 \left(\frac{\partial \bar{p}}{\partial y} \right)^2 + \bar{p} \frac{\partial \bar{p}}{\partial y} (3\bar{h}^2) \frac{\partial \bar{h}}{\partial y} + \bar{h}^3 \left(\frac{\partial \bar{p}}{\partial y} \right)^2 \right) \left(\frac{D}{L} \right)^2 \\ & = \Lambda \left(\bar{p} \frac{\partial \bar{h}}{\partial \theta} + \bar{h} \frac{\partial \bar{p}}{\partial \theta} \right) \end{aligned} \quad 3.2.1.19$$

Simplifying further:

$$\left(\frac{\partial^2 \bar{p}}{\partial \theta^2} \right) + \left(\frac{D}{L} \right)^2 \left(\frac{\partial \bar{p}}{\partial y} \right)^2 + \left[\frac{3}{\bar{h}} \frac{\partial \bar{p}}{\partial \theta} \frac{\partial \bar{h}}{\partial \theta} + \left(\frac{D}{L} \right)^2 \frac{3}{\bar{h}} \frac{\partial \bar{p}}{\partial y} \frac{\partial \bar{h}}{\partial y} \right] + \left[\frac{1}{\bar{p}} \left(\frac{\partial \bar{p}}{\partial \theta} \right)^2 + \left(\frac{D}{L} \right)^2 \frac{1}{\bar{p}} \left(\frac{\partial \bar{p}}{\partial y} \right)^2 \right] = \frac{\Lambda}{\bar{p} \bar{h}^3} \left[\bar{p} \frac{\partial \bar{h}}{\partial \theta} + \bar{h} \frac{\partial \bar{p}}{\partial \theta} \right] \quad 3.2.1.20$$

Rearranging terms

$$\underbrace{\left[\left(\frac{\partial^2 \bar{p}}{\partial \theta^2} \right) + \left(\frac{D}{L} \right)^2 \left(\frac{\partial \bar{p}}{\partial y} \right)^2 \right]}_{L.H.S} = \underbrace{-\frac{3}{\bar{h}} \left[\frac{\partial \bar{p}}{\partial \theta} \frac{\partial \bar{h}}{\partial \theta} + \left(\frac{D}{L} \right)^2 \frac{\partial \bar{p}}{\partial y} \frac{\partial \bar{h}}{\partial y} \right] - \frac{1}{\bar{p}} \left[\left(\frac{\partial \bar{p}}{\partial \theta} \right)^2 + \left(\frac{D}{L} \right)^2 \left(\frac{\partial \bar{p}}{\partial y} \right)^2 \right]}_{R.H.S} + \left[\frac{\Lambda}{\bar{h}^3} \frac{\partial \bar{h}}{\partial \theta} + \frac{\Lambda}{\bar{p} \bar{h}^2} \frac{\partial \bar{p}}{\partial \theta} \right] \quad 3.2.1.21$$

Equation 3.2.1.21 represents the similar form of Poissons equation but the R.H.S of the equation is the non-linear function of the hydrodynamic pressure. This equation is normally solved by the Liebmann method or the successive over relaxation method ‘‘S.O.R’’ (Gerald et al., 2002). Finite Difference approximations of L.H.S and R.H.S are:

$$\text{L.H.S} = \left(\frac{\bar{p}_{i+1,j} - 2\bar{p}_{i,j} + \bar{p}_{i-1,j}}{\Delta\theta^2} \right) + \left(\frac{D}{L} \right)^2 \left(\frac{\bar{p}_{i+1,j} - 2\bar{p}_{i,j} + \bar{p}_{i-1,j}}{\Delta y^2} \right) \quad 3.2.1.22$$

R.H.S=

$$-\frac{1}{\bar{p}_{i,j}} \left[\left(\frac{\partial \bar{p}}{\partial \theta} \right)_i^2 + \left(\frac{D}{L} \right)^2 \left(\left(\frac{\partial \bar{p}}{\partial y} \right)_j^2 \right) \right] - \frac{3}{\bar{h}} \left(\frac{\partial \bar{p}}{\partial \theta} \right)_i \left(\frac{\partial \bar{h}}{\partial \theta} \right)_i + \left(\frac{D}{L} \right)^2 \frac{\partial \bar{p}}{\partial y} \left(\frac{\partial \bar{h}}{\partial y} \right)_j + \frac{\Lambda}{\bar{p}_{i,j} \bar{h}_{i,j}^2} \frac{\partial \bar{p}}{\partial \theta} \Big|_i + \frac{\Lambda}{\bar{h}_{i,j}^3} \frac{\partial \bar{h}}{\partial \theta} \Big|_i \quad 3.2.1.23$$

Consider RHS to be = $f(i, j)$

$$f(i, j) = -\frac{1}{\bar{p}_{i,j}} \left[\left(\frac{\partial \bar{p}}{\partial \theta} \right)_i^2 + \left(\frac{D}{L} \right)^2 \left(\left(\frac{\partial \bar{p}}{\partial y} \right)_j^2 \right) \right] - \frac{3}{\bar{h}} \left(\frac{\partial \bar{p}}{\partial \theta} \right)_i \left(\frac{\partial \bar{h}}{\partial \theta} \right)_i + \left(\frac{D}{L} \right)^2 \frac{\partial \bar{p}}{\partial y} \left(\frac{\partial \bar{h}}{\partial y} \right)_j + \frac{\Lambda}{\bar{p}_{i,j} \bar{h}_{i,j}^2} \frac{\partial \bar{p}}{\partial \theta} \Big|_i + \frac{\Lambda}{\bar{h}_{i,j}^3} \frac{\partial \bar{h}}{\partial \theta} \Big|_i \quad 3.2.1.24$$

Simplifying L.H.S and R.H.S and considering the method of S.O.R

$$\bar{p}^{n+1}_{i,j} = \bar{p}^n_{i,j} + \omega \left[\frac{\left(\frac{L}{D} \right)^2 \Delta y^2 (\bar{p}_{i+1,j}, \bar{p}_{i-1,j}) + \Delta \theta^2 (\bar{p}_{i,j+1}, \bar{p}_{i,j-1}) - 2\bar{p}_{i,j} \left(\left(\frac{L}{D} \right)^2 \Delta y^2 + \Delta \theta^2 \right) - \Delta \theta^2 \Delta y^2 \left(\frac{L}{D} \right)^2 f(i, j)}{2 \left(\left(\frac{L}{D} \right)^2 \Delta y^2 + \Delta \theta^2 \right)} \right] \quad 3.2.1.25$$

The solution begins by evaluating the R.H.S of the equation 3.2.1.25 by an initial guess pressure $\bar{p}^n_{i,j}$ by solving for an incompressible bearing with an assumed rigid bearing eccentricity ratio ε_r and an initial guess for the film thickness $\bar{h}_{i,j}$. This is done iteratively until a convergence of the pressure is achieved for a given film thickness. Convergence is achieved when the relative error between two successive iterations fall below a specified value. One hundred finite difference grid points along the circumferential direction and twenty grid points

along the axial direction were chosen based on the grid refinement study and available literature (Peng and Khonsari, 2004).

The next part is to couple the hydrodynamic pressure and the foil structural compliance which has a direct effect on the overall behavior of the fluid film profile. This is incorporated in an iterative scheme. Recalling equation (3.1.1.13), the film thickness \bar{h}_f is a function of dimensionless pressure. As the top and bump foils deform due to the pressure, the shaft moves in the direction where the deformation is maximum (Fig 5) and there is a significant change in the eccentricity ratio ε_f and attitude angle ϕ_f , which further changes the overall profile of the film thickness. This is not accounted for in the equation (3.1.1.13). Hence, to account for this the modified form of the film thickness equation is (Peng and Khonsari, 2004):

$$\bar{h}_{f,i,j} = 1 + \varepsilon_f \cos(\theta - \Delta\varphi) + \alpha(\bar{p}_{i,j} - 1) \quad 3.2.1.26$$

$$\varepsilon_f = \varepsilon_r + \Delta\varepsilon \quad (\text{Peng and Khonsari, 2004}) \quad 3.2.1.27$$

where ε_f is determined by bisection method by assuming that the minimum film thickness $h_{\min r}$ in a rigid bearing and the corresponding minimum film thickness in a foil bearing $h_{\min f}$ are same and that $\Delta\varphi$ represents the difference in the attitude angle for a rigid bearing ϕ_r and compliant bearing ϕ_f . The effect of the hydrodynamic pressure on the film thickness profile was obtained by employing the method of under-relaxation. The final film thickness is obtained in an iterative scheme as follows (Peng and Khonsari, 2004):

$$\bar{h}_{f,i,j}^{n+1} = 1 + \varepsilon_f^n \cos(\theta - \Delta\varphi^n) + \alpha(\bar{p}_{i,j}^n - 1) \quad 3.2.1.28$$

where n is the number of points used along the circumferential direction (one hundred).

The under-relaxation between successive iterations is given by the formula:

$$\bar{h}_{f,i,j}^{n+1} = \alpha_{rh} \bar{h}_{f,i,j}^{n+1} + (1 - \alpha_{rh}) \bar{h}_{f,i,j}^n \quad 3.2.1.29$$

where α_{rh} represents the under-relaxation factor for the fluid film. Typically α_{rh} varies from 0.3 to 0.5 depending on the eccentricity ratios and operating speeds.

- **Load Carrying Capacity**

Once the dimensionless pressure profile is obtained, the load-carrying capacity can then be calculated (Khonsari and Booser, 2001).

The x and z components are:

$$W_x = \int_{-y}^y \int_0^{2\pi} LR(p-1) \cos \theta d\theta dy \quad W_z = \int_{-y}^y \int_0^{2\pi} LR(p-1) \sin \theta d\theta dy \quad 3.2.1.30$$

In dimensionless form:

$$\bar{W}_x = \int_{-y}^y \int_0^{2\pi} (\bar{p}-1) \cos \theta d\theta dy \quad \bar{W}_z = \int_{-y}^y \int_0^{2\pi} (\bar{p}-1) \sin \theta d\theta dy \quad 3.2.1.31$$

$$\text{where } \bar{W}_{x,z} = \frac{W}{p_a RL}, \quad \bar{p} = \frac{p}{p_a} \Rightarrow p = \bar{p} p_a \quad 3.2.1.32$$

$$\bar{W}_f = \sqrt{\bar{W}_x^2 + \bar{W}_z^2}, \quad \text{also} \quad \bar{W}_f = \frac{W}{p_a RL} \quad 3.2.1.33$$

$$\text{The attitude angle is represented as: } \tan \varphi = \frac{\bar{W}_z}{-\bar{W}_x} \quad 3.2.1.34$$

$$W = \bar{W}_f p_a RL \quad 3.2.1.35$$

Equation 3.2.1.35 represents the load-carrying capacity of the foil bearing.

Finally the Simpson's rule was employed for numerical integration to determine the load-carrying capacity of the bearing.

- **Flow rate formulation**

As the shaft rotates, leakage flow exits the bearing from both sides. This flow must be made up by the suction of air into the bearing to account for proper operation. Normally in the case of oil lubricated bearings the supply feed hole is located at the midsection of the bearing. But in the case of compliant journal bearings, there does not exist any supply feed hole.

The axial volumetric flow exiting the bearing is represented by following equation (Khonsari and Booser, 2001).

$$Q_y = 2 \int_0^{\theta_{sub}} R \frac{h^3}{12\mu} \frac{dp}{dy} \Big|_{y=L/2} d\theta \quad 3.2.1.36$$

θ_{sub} Represents the point at which the pressure becomes sub ambient

Normalizing equation 3.2.1.36:

$$\bar{p} = \frac{p}{p_a}, \bar{h} = \frac{h}{C}, \bar{\mu} = \frac{\mu}{\mu_0}, \bar{y} = \frac{y}{L/2} \quad 3.2.1.37$$

Equation 3.2.1.36 becomes:

$$Q_y = 2 \int_0^{\theta_{sub}} R \frac{h^3 C^3}{12\bar{\mu}\mu_0} \frac{d\bar{p}p_a}{d\bar{y}L/2} \Big|_{\bar{y}=L/2} d\theta \quad 3.2.1.38$$

Simplifying:

$$Q_y = \frac{RC^3 P_a}{\mu_0 L/2} 2 \int_0^{\theta_{sub}} \frac{\bar{h}^3}{12\bar{\mu}} \frac{d\bar{p}}{d\bar{y}} \Big|_{\bar{y}=L/2} d\theta \quad 3.2.1.39$$

Equation 3.2.1.39 yields:

$$\bar{Q}_y = 2 \int_0^{\theta_{sub}} \frac{\bar{h}^3}{12\bar{\mu}} \frac{d\bar{p}}{d\bar{y}} \Big|_{\bar{y}=L/2} d\theta \quad 3.2.1.40$$

$$\text{where } \bar{Q}_y = \frac{Q_y}{Q_{ref}}, Q_{ref} = \frac{RC^3 P_a}{\mu_0 L/2} \quad 3.2.1.41$$

The leakage in the bearing is contributed by the positive pressure profile developed in the bearing. The pressure gradient along the axial direction varies from high at the mid-section to low towards both the ends of the bearing.

$$\text{Hence } \bar{Q}_{Leak} = 2 \int_0^{\theta_{sub}} \frac{\bar{h}^3}{12\bar{\mu}} \frac{d\bar{p}}{d\bar{y}} \Big|_{\bar{y}=\frac{L}{2}} d\theta \quad 3.2.1.42$$

Since the bearing does not have any feed holes at the mid plane, the leaked air has to be compensated for the continuous flow of lubricant. The suction occurs due to the negative profile developed in the pressure profiles. The flow is due to the pressure gradient from ambient at the ends of the bearing which is high to the mid section of the bearing where the pressure is sub ambient.

$$\text{Hence } \bar{Q}_{Suct} = -2 \int_{\theta_{sub}}^{2\pi} \frac{\bar{h}^3}{12\bar{\mu}} \frac{d\bar{p}}{d\bar{y}} \Big|_{\bar{y}=\frac{L}{2}} d\theta \quad 3.2.1.43$$

To show a mass conservation for the bearing the leakage flow and suction flow rates must be equal. The occurrences of θ_{sub} , which represent the sub-ambient pressure, varies along the axial direction. Hence an average value for the sub-ambient pressure θ_{sub_avg} is obtained to calculate the leakage and suction rates.

$$\bar{Q}_{Leak} = 2 \int_0^{\theta_{sub_avg}} \frac{\bar{h}^3}{12\bar{\mu}} \frac{d\bar{p}}{d\bar{y}} \Big|_{\bar{y}=\frac{L}{2}} d\theta \quad 3.2.1.44$$

$$\bar{Q}_{Suct} = -2 \int_{\theta_{sub_avg}}^{2\pi} \frac{\bar{h}^3}{12\bar{\mu}} \frac{d\bar{p}}{d\bar{y}} \Big|_{\bar{y}=\frac{L}{2}} d\theta \quad 3.2.1.45$$

Recirculation of lubricant:

$$Q_{rec} = 2 \int_0^{\frac{L}{2}} \underbrace{\int_0^{h_{sub_avg}} u \Big|_{\theta=\theta_{sub_avg}} dz}_{q_x} dy \quad 3.2.1.46$$

$$\text{Where } q_x = \frac{Uh}{2} - \frac{h^3}{12\mu} \frac{dp}{dx} \quad (\text{Khonsari and Booser, 2001}) \quad 3.2.1.47$$

$$x = R\theta \quad 3.2.1.48$$

Substituting for x, q_x

$$Q_{rec} = 2 \int_0^{\frac{L}{2}} \left(\frac{h_{sub_avg} U}{2} - \frac{h_{sub_avg}^3}{12\mu} \frac{\partial p}{R\partial\theta} \Big|_{\theta=\theta_{sub_avg}} \right) dy \quad 3.2.1.49$$

Simplifying:

$$Q_{rec} = U \int_0^{\frac{L}{2}} h_{sub_avg} dy + 2 \int_0^{\frac{L}{2}} - \frac{h_{sub_avg}^3}{12\mu} \frac{\partial p}{R\partial\theta} \Big|_{\theta=\theta_{sub_avg}} dy \quad 3.2.1.50$$

Normalizing:

$$\bar{p} = \frac{p}{p_a}, \bar{h} = \frac{h}{C}, \bar{\mu} = \frac{\mu}{\mu_0}, \bar{y} = \frac{y}{L/2}$$

Finally:

$$\bar{Q}_{rec} = \frac{\mu_0 U L^2}{4 p_a R C^2} \int_0^{L/2} \bar{h}_{sub_avg} d\bar{y} - \frac{1}{6 \bar{\mu}_{sub_avg}} \left(\frac{L}{D} \right)^2 \int_0^{L/2} \bar{h}_{sub_avg}^3 \frac{\partial \bar{p}}{\partial \theta} \Big|_{\theta=\theta_{sub_avg}} d\bar{y} \quad 3.2.1.51$$

$$\text{where } U = R\omega, \bar{Q}_{rec} = \frac{Q_{rec}}{Q_{ref}}, Q_{ref} = \frac{RC^3 P_a}{\mu_0 L/2} \quad 3.2.1.52$$

3.2.3 Bearing Performance Parameters (FA)

An accurate grid refinement study was carried out to determine the appropriate grid size. Based on the tabulated results as indicated in Table 3, 100 grid points along the circumferential direction and 20 grid points along the axial direction were chosen to run all the simulations. Grid sizes higher than this would increase computational time without much variation on the overall results.

Table 3: Grid Refinement Study

No of Grid points							
θ	\bar{y}	ε_r	ε_f	W_r	W_f	ϕ_r	ϕ_f
Case 1							
50	10	0.3	0.3231	11.8044	11.9443	68.4325	68.3021
100	20	0.3	0.3261	13.615	13.665	70.3127	70.2733
120	20	0.3	0.3279	13.818	13.8722	70.4771	70.3979
Case2							
50	10	0.7	0.8727	69.0906	72.1681	41.8896	39.6024
100	20	0.7	0.8759	71.2918	73.3726	42.6598	39.9248
120	20	0.7	0.8767	71.4898	73.5969	42.7529	40.8498

Figure 10 represent the pressure profile comparison between a rigid bearing and first generation foil bearing whose properties are indicated in Table 1 (Peng, 2003). The operating speed is 30,000 rpm. The lubricant used is air whose properties are indicated in Table 2 (Peng, 2003). Note that the rigid bearing of equal dimensions and same lubricant properties and operating speeds are assumed for comparison.

The pressure profile for the foil bearing is spread over a larger area compared to its rigid bearing counterpart resulting in a greater load carrying capacity. Figure 11 represents the film

thickness profile comparison between a rigid bearing and compliant bearing. The overall film profile for a foil bearing spans over a greater area due to the deformation of the foils. The program converged to minimum film thickness equivalent to $11\ \mu\text{m}$ ($h_{\min f}, h_{\min r}$) based on the load imposed condition. Attitude angle $\phi_f = 39^\circ$ and that of rigid bearing $\phi_r = 45.47^\circ$ with a total load carrying capacity $W = 127\ \text{N}$. These results are in agreement with experimental results reported by Strom (1987) and prediction by Peng and Khonsari, (2004) as indicated in Table 4.

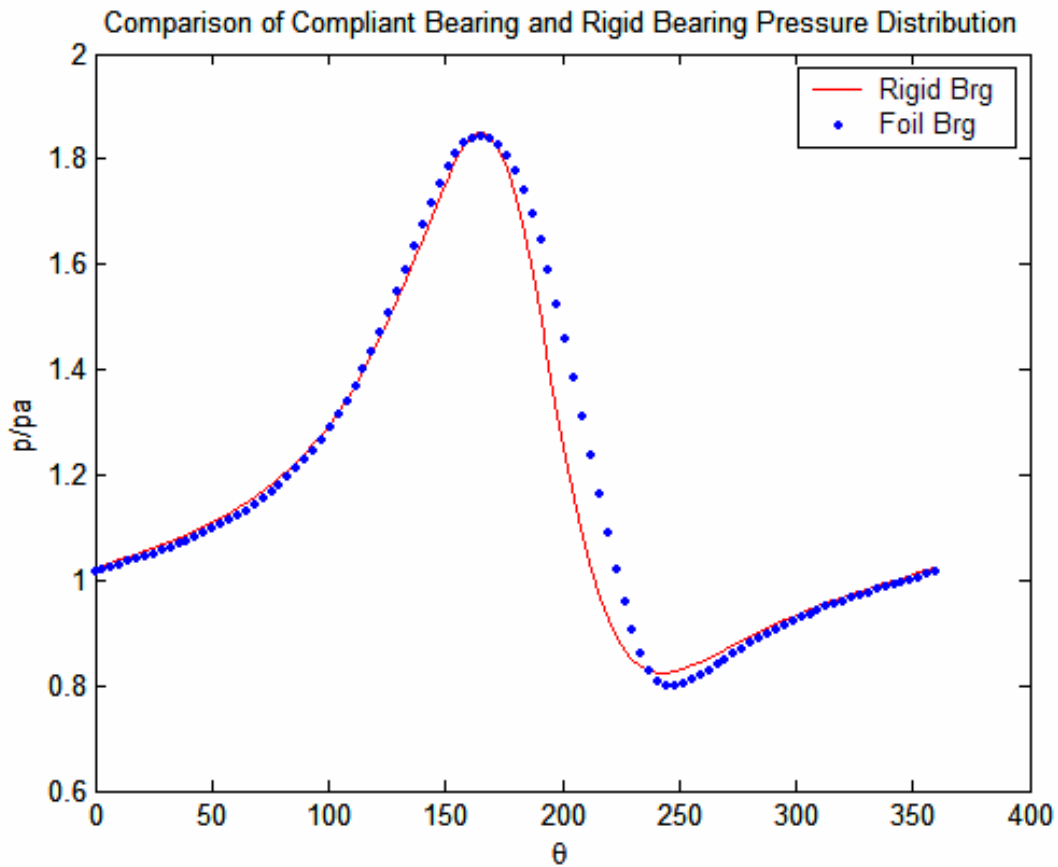


Figure 10: Pressure Profile Comparison at Mid Section of Bearing at 30,000 rpm

The first generation type foil bearings is based on a bump layer foil sheet which is uniform in design and construction unlike the other generation designs which incorporate staggered bumps. Some also have split ends which account for tailoring the stiffness along the

axial direction of the bearing. Hence, in the current simulations for the first generation foil bearings, the film thickness is not a function in the axial direction, more over the variation is negligible. Consequently, the arithmetic mean pressure in the axial direction is used to calculate the deformation of the top foils (Peng and Khonsari, 2004). Therefore, half of the geometry of the bearing along the axial direction was treated as the bearing is symmetric about its ends.

Figures 12 and 13 represent the three dimensional plot of the hydrodynamic pressure distribution and film thickness profiles for the compliant journal bearing running at 30,000 rpm, respectively. The hydrodynamic pressure developed along the axial direction has a parabolic profile wherein the pressure is maximum at the mid-section or at the center of the bearing and the pressure becomes ambient at the ends of the bearing. The circumferential direction is reversed to show the sub ambient pressure. In general, the variation of film thickness is also parabolic along the axial direction, but the variation is negligible and can be assumed to be a constant as indicated in figure 13.

Table 4: Finite Analysis Comparison with Experimental and Published Literature

	RPM	Load (N)	$h_{\min f}$	ε_f
Exp (Strom,1987)	30,000	130	-	-
(Peng ,2004)	30,000	130	10.5	1.12
Current Analysis	30,000	127	11	1.05

Unlike the oil lubricated bearings in which there exists a supply feed hole for constant supply of leaked lubricant, for compliant journal bearings there does not exist a supply feed hole. Hence the leaked lubricant which is air has to be replenished for proper functionality of the

bearing. This is accomplished due to the sub-ambient pressure developed which results in suction of air to replace the leaked air and mixes with the recirculating lubricant.

Table 5: Study of Variation of θ_{sub} Along the Axial Direction

\bar{y}	2	4	6	8	10	12	14	16	18	20
θ_{sub}	194.4	198	198	201.6	201.6	201.6	201.6	205.2	205.2	205.2

The leakage flow and suction flow of the bearing at different operating loading conditions were predicted to ensure and prove the conservation of mass holds. Table 5 presents the circumferential co-ordinate θ_{sub} along the axial direction where the pressure reaches sub-ambient. To predict accurate values of the leakage flow and suction flow involved in a bearing an average value θ_{sub_avg} was obtained. Finally, the flow rates of the bearing were calculated at different loading conditions and the equality between the flow rates is indicated in Table 6.

Table 6: Flow Rate Study Based on Different Load Capacities, 30,000 rpm

Load (N)	ε_f	$Q_{suction} \text{ m}^3/\text{min}$	$Q_{leak} \text{ m}^3/\text{min}$	$Q_{recirc} \text{ m}^3/\text{min}$
11.3	0.3229	0.0013	0.0019	0.0026
71.3	0.8759	0.0083	0.0086	0.0014

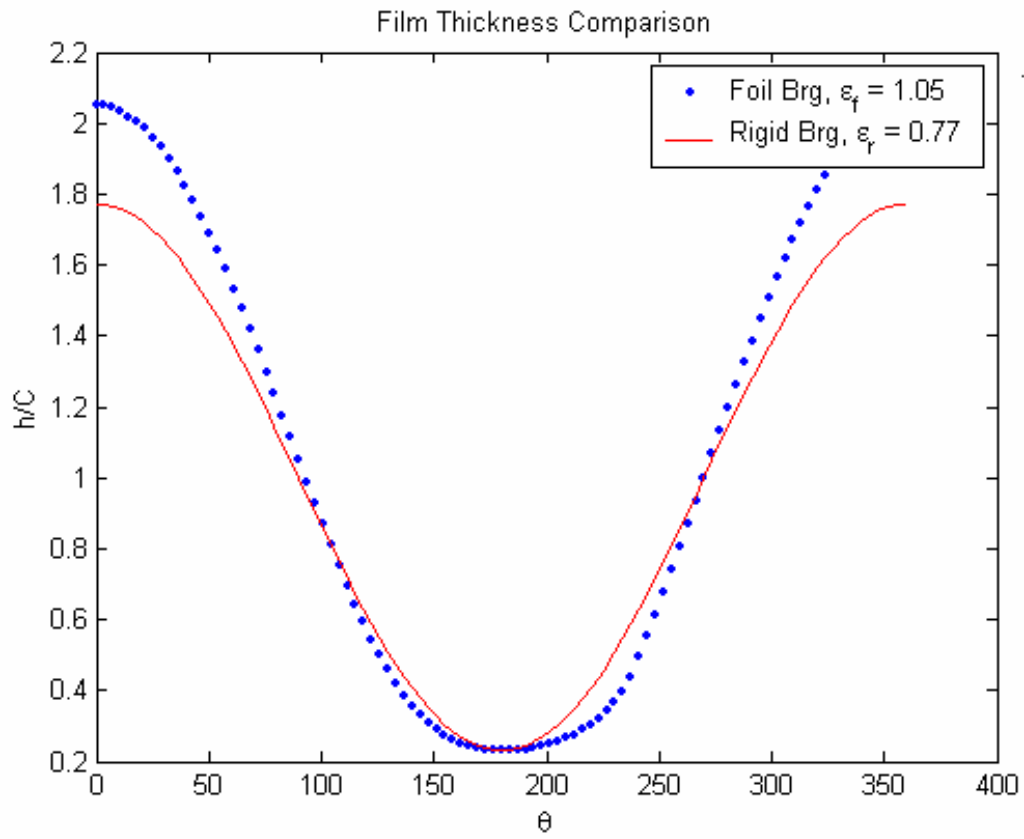
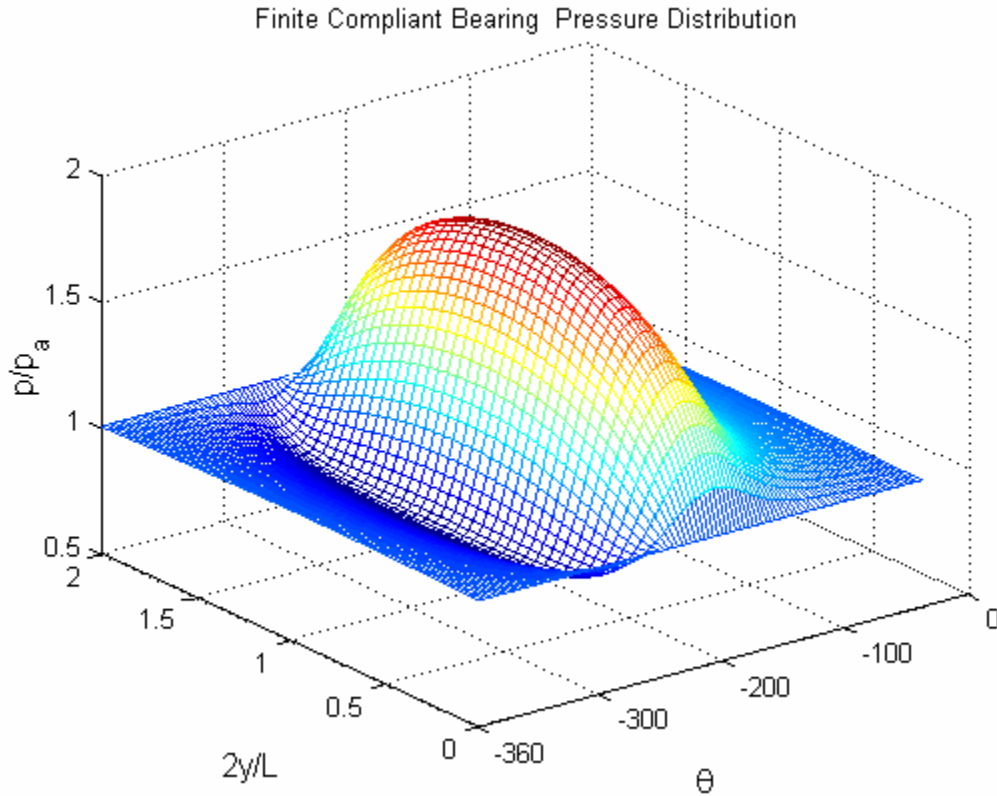


Figure 11: Film Thickness Comparison at Mid Section of Bearing at 30,000 rpm.



**Figure 12: Three Dimensional Pressure Distribution for a Foil Bearing at 30,000 rpm
(θ is reversed to indicate the sub-ambient pressure)**

Another important parameter is the bearing attitude angle. In general a lower attitude angle is known to contribute for better bearing stability. Figure 14 compares the attitude angle between a rigid bearing and a compliant journal bearing. From this plot, we can clearly see that the attitude angle for a compliant journal bearing is less at a given eccentricity compared to rigid journal bearing of similar dimension and operating conditions.

Also, the load-carrying capacity of compliant journal bearings achieve a higher value at higher operating speeds when compared to rigid bearings with similar operating conditions and dimensions as indicated in Figure 15. Extensive studies on the limiting load carrying capacity for compliant journal bearings at higher bearing numbers are reported by Peng and Khonsari, (2004).

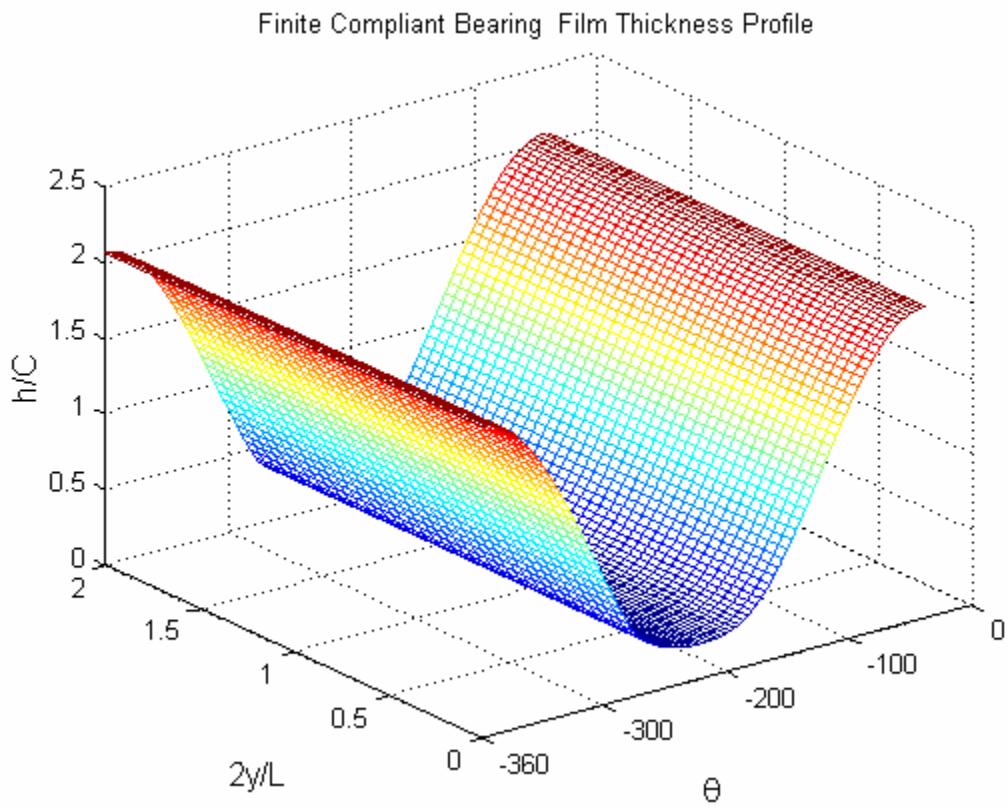


Figure 13: Three dimensional Film Thickness Profile for a Foil Bearing at 30,000 rpm

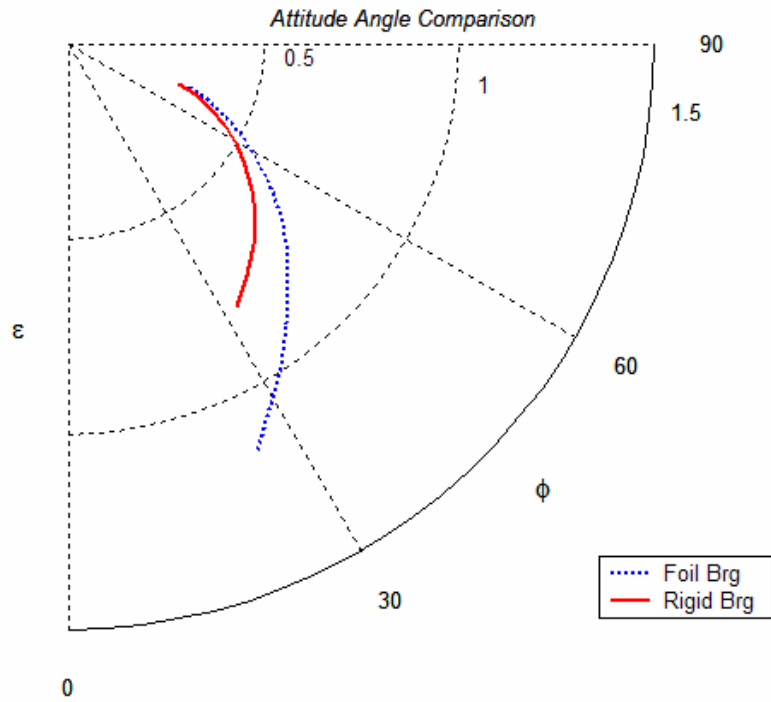


Figure 14: Attitude Angle Comparison with Variation of Eccentricity Ratio

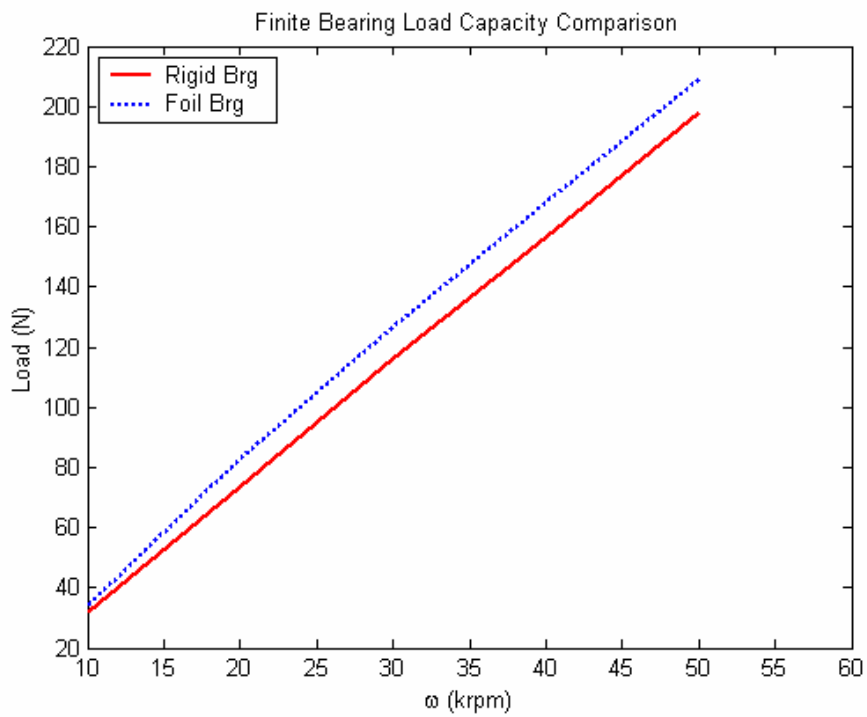


Figure 15: Load Carrying Capacity Comparison with Bearing Speeds

3.3 Modified Parabolic Approximation (MPA)

3.3.1 Compressible Reynolds Equation with Modified Parabolic Approximation

The finite Reynolds equation 3.2.1.10 can be tedious to solve for applications involving dynamic applications. The situation may be particularly complex in the case of foil bearings when the pressure distribution and the compliant structure must be accounted for.

In general, in journal bearings the pressure distribution along the axial direction is parabolic. This can be seen from the finite simulation results presented in the last chapter (Fig. 12). Hence, by making reasonable assumptions for the pressure distribution along the axial length of the bearing, it would be possible to convert the non-linear partial differential equation to an ordinary differential equation. This method could result in savings in computational time. This type of approach was successfully implemented for incompressible flows (Ettles and Shelly, 1970). But there are no reports currently available for cases considering fluid compressibility. Hence, using a similar method to Ettles and Shelly (1970), we formulate a new set of equations and also propose a numerical methodology to solve the formulated equations. The results are validated using the finite bearings simulations.

Consider the Finite Reynolds equation in polar coordinates (3.2.1.6).

$$\frac{\partial}{\partial \theta} \left[\frac{ph^3}{T12\mu} \frac{\partial p}{\partial \theta} \right] + \frac{\partial}{\partial y} \left[\frac{ph^3}{T12\mu} \frac{\partial p}{\partial y} \right] = \frac{\omega R^2}{2} \frac{\partial}{\partial \theta} \left(\frac{ph}{T} \right)$$

Normalizing the above equation.

$$\bar{y} = \frac{y}{L/2}, \bar{p} = \frac{p - p_a}{p_a}, \bar{h} = \frac{h}{C}, \bar{\mu} = \frac{\mu}{\mu_0}, \bar{T} = \frac{T}{T_0} \quad 3.3.1.1$$

$$\frac{\partial}{\partial \theta} \left[\frac{(\bar{p}p_a + p_a)\bar{h}^3 C^3}{12\bar{\mu}\mu_0\bar{T}T_0} \frac{\partial}{\partial \theta} (\bar{p}p_a + p_a) \right] + R^2 \frac{\partial}{\partial \bar{y}} \left[\frac{(\bar{p}p_a + p_a)\bar{h}^3 C^3}{12\bar{\mu}\mu_0\bar{T}T_0} \frac{\partial}{\partial \bar{y}} \left(\frac{L}{2} \right) (\bar{p}p_a + p_a) \right] = \frac{\omega R^2}{2} \frac{\partial}{\partial \theta} \left(\frac{(\bar{p}p_a + p_a)\bar{h}C}{\bar{T}T_0} \right)$$

3.3.1.2

Simplifying yields:

$$\left[\frac{p_a^2 C^3}{12\mu_0} \right] \left[\frac{\partial}{\partial \theta} \left[\frac{(\bar{p}\bar{h}^3 + \bar{h}^3)}{\bar{\mu}\bar{T}} \frac{\partial \bar{p}}{\partial \theta} \right] + R^2 \frac{\partial}{\partial y} \frac{L}{2} \left[\frac{(\bar{p}\bar{h}^3 + \bar{h}^3)}{\bar{\mu}\bar{T}} \frac{\partial \bar{p}}{\partial y} \left(\frac{L}{2} \right) \right] \right] = \frac{\omega R^2 p_a}{2\bar{T}} \left[\frac{\partial(\bar{p}\bar{h})}{\partial \theta} + \frac{\partial \bar{h}}{\partial \theta} \right]$$

3.3.1.3

Assuming an Isothermal and isoviscous case where $\bar{T} = 1$, $\bar{\mu} = 1$

Equation Reduces to

$$\frac{\partial}{\partial \theta} \left[(\bar{p}\bar{h}^3 + \bar{h}^3) \left(\frac{\partial \bar{p}}{\partial \theta} \right) \right] + \left(\frac{D}{L} \right)^2 \frac{\partial}{\partial y} \left[(\bar{p}\bar{h}^3 + \bar{h}^3) \left(\frac{\partial \bar{p}}{\partial y} \right) \right] = \Lambda \left[\frac{\partial(\bar{p}\bar{h})}{\partial \theta} + \frac{\partial \bar{h}}{\partial \theta} \right] \quad 3.3.1.4$$

where $\Lambda = \frac{6\omega\mu_0}{p_a} \left(\frac{R}{C} \right)^2$ represents the compressibility number or the bearing number.

Substituting $\bar{p}(\theta, y) = \bar{p}_l(1 - \bar{y}^\kappa)$ in equation 3.3.1.4 3.3.1.5

$$\frac{\partial}{\partial \theta} \left[(\bar{p}_l(1 - \bar{y}^\kappa)\bar{h}^3 + \bar{h}^3) \left(\frac{\partial \bar{p}_l(1 - \bar{y}^\kappa)}{\partial \theta} \right) \right] + \left(\frac{D}{L} \right)^2 \frac{\partial}{\partial y} \left[(\bar{p}_l(1 - \bar{y}^\kappa)\bar{h}^3 + \bar{h}^3) \left(\frac{\partial \bar{p}_l(1 - \bar{y}^\kappa)}{\partial y} \right) \right] = \Lambda \left[\frac{\partial(\bar{p}_l(1 - \bar{y}^\kappa)\bar{h})}{\partial \theta} + \frac{\partial \bar{h}}{\partial \theta} \right]$$

3.3.1.6

Simplifying yields:

$$\begin{aligned} & \frac{\partial}{\partial \theta} \left[\left(\left(\frac{\partial \bar{p}_l(1 - \bar{y}^\kappa)}{\partial \theta} \right) \bar{p}_l(1 - \bar{y}^\kappa)\bar{h}^3 + \left(\frac{\partial \bar{p}_l(1 - \bar{y}^\kappa)}{\partial \theta} \right) \bar{h}^3 \right) \right] + \left(\frac{D}{L} \right)^2 \frac{\partial}{\partial y} \left[\left(\frac{\partial \bar{p}_l(1 - \bar{y}^\kappa)}{\partial y} \right) \bar{p}_l(1 - \bar{y}^\kappa)\bar{h}^3 + \left(\frac{\partial \bar{p}_l(1 - \bar{y}^\kappa)}{\partial y} \right) \bar{h}^3 \right] \\ & = \Lambda \left[\frac{\partial(\bar{p}_l\bar{h})}{\partial \theta} (1 - \bar{y}^\kappa) + \frac{\partial \bar{h}}{\partial \theta} \right] \end{aligned}$$

3.3.1.7

Equation 3.3.1.7 has to be integrated twice along the axial direction with appropriate boundary conditions. The film thickness is considered to be constant along the axial direction as the variation is negligible.

Integrate 3.3.1.7 once along axial direction (\bar{y})

$$\begin{aligned} & \frac{\partial}{\partial \theta} \left[\left(\left(\frac{\partial \bar{p}_l}{\partial \theta} \right) \bar{p}_l \bar{v} \bar{h}^3 + \left(\frac{\partial \bar{p}_l}{\partial \theta} \right) \tau \bar{h}^3 \right) \right] + \left(\frac{D}{L} \right)^2 \left[\left(\frac{\partial (1 - \bar{y}^\kappa)}{\partial \bar{y}} \right) (1 - \bar{y}^\kappa) \bar{p}_l^2 \bar{h}^3 + \left(\frac{\partial (1 - \bar{y}^\kappa)}{\partial \bar{y}} \right) \bar{p}_l \bar{h}^3 \right] \\ & = \Lambda \left[\frac{\partial (\bar{p}_l \bar{h})}{\partial \theta} \tau + \frac{\partial \bar{h}}{\partial \theta} \bar{y} \right] + C1 \end{aligned} \quad 3.3.1.8$$

where

$$v = \frac{y + 3y\kappa + 2y\kappa^2 + y^{(1+2\kappa)} + y^{(1+2\kappa)}\kappa - 2y^{(1+\kappa)} - 4y^{(1+\kappa)}\kappa}{(1+2\kappa)(1+\kappa)} \quad 3.3.1.9$$

$$\tau = y - \frac{y^{(1+\kappa)}}{(1+\kappa)} \quad 3.3.1.10$$

Integrating 3.3.1.8 again along the axial direction (\bar{y}) yields:

$$\begin{aligned} & \frac{\partial}{\partial \theta} \left[\left(\left(\frac{\partial \bar{p}_l}{\partial \theta} \right) \bar{p}_l v_1 \bar{h}^3 + \left(\frac{\partial \bar{p}_l}{\partial \theta} \right) \tau_1 \bar{h}^3 \right) \right] + \left(\frac{D}{L} \right)^2 \left[\bar{p}_l^2 \bar{h}^3 \left(-\bar{y}^\kappa + \frac{1}{2} \bar{y}^{2\kappa} \right) + (1 - \bar{y}^\kappa) \bar{p}_l \bar{h}^3 \right] \\ & = \Lambda \left[\frac{\partial (\bar{p}_l \bar{h})}{\partial \theta} \tau_1 + \frac{\partial \bar{h}}{\partial \theta} \frac{\bar{y}^2}{2} \right] + C1 \bar{y} + C2 \end{aligned} \quad 3.3.1.11$$

where

$$v_1 = \frac{1(2y^2\kappa^3 + 7y^2\kappa^2 + \kappa y^{2+2\kappa}) + 7y^2\kappa - 8\kappa y^{(2+\kappa)} + 2y^2 + 2y^{(2+2\kappa)} - 4y^{(2+\kappa)}}{2(1+2\kappa)(1+2\kappa)(1+\kappa)} \quad 3.3.1.12$$

$$\tau_1 = \frac{y^2}{2} - \frac{y^{(2+\kappa)}}{(1+\kappa)(2+\kappa)} \quad 3.3.1.13$$

The constants C_1 and C_2 are evaluated with the following boundary conditions:

$$\bar{y} = 0, \quad \bar{p} = \bar{p}_l \quad 3.3.1.14$$

$$\bar{y} = 1, \quad \bar{p} = 0 \quad 3.3.1.15$$

where $\bar{p} = \bar{p}_l (1 - \bar{y}^\kappa)$.

Using 3.3.1.14

$$C_2 = \left(\frac{D}{L}\right)^2 [\bar{p}l\bar{h}^3] \quad 3.3.1.16$$

Using 3.3.1.15

$$\frac{\partial}{\partial\theta} \left[\left(\left(\frac{\partial\bar{p}_l}{\partial\theta} \right) \bar{p}_l \psi_1 \bar{h}^3 + \left(\frac{\partial\bar{p}_l}{\partial\theta} \right) \beta_1 \bar{h}^3 \right) \right] - \left(\frac{D}{L} \right)^2 \left[\frac{\bar{p}_l^2 \bar{h}^3}{2} \right] = \Lambda \left[\frac{\partial(\bar{p}_l \bar{h})}{\partial\theta} \beta_1 + \frac{\partial\bar{h}}{\partial\theta} \frac{1}{2} \right] + C1 + \left(\frac{D}{L} \right)^2 [\bar{p}_l \bar{h}^3] \quad 3.3.1.17$$

where

$$\psi_1 = \frac{1(2\kappa^3 + 7\kappa^2)}{2(2 + \kappa)(1 + 2\kappa)(1 + \kappa)} \quad 3.3.1.18$$

$$\beta_1 = \frac{1\kappa(3 + \kappa)}{2(1 + \kappa)(2 + \kappa)} \quad 3.3.1.19$$

Finally

$$C_1 = \frac{\partial}{\partial\theta} \left[\left(\left(\frac{\partial\bar{p}_l}{\partial\theta} \right) \bar{p}_l \psi_1 \bar{h}^3 + \left(\frac{\partial\bar{p}_l}{\partial\theta} \right) \beta_1 \bar{h}^3 \right) \right] - \left(\frac{D}{L} \right)^2 \left[\frac{\bar{p}_l^2 \bar{h}^3}{2} + \bar{p}l\bar{h}^3 \right] - \Lambda \left[\frac{\partial(\bar{p}_l \bar{h})}{\partial\theta} \beta_1 + \frac{\partial\bar{h}}{\partial\theta} \frac{1}{2} \right] \quad 3.3.1.20$$

Substituting the constants in 3.3.1.11

$$\begin{aligned}
& \frac{\partial}{\partial \theta} \left[\left(\left(\frac{\partial \bar{p}_l}{\partial \theta} \right) \bar{p}_l \nu_1 \bar{h}^3 + \left(\frac{\partial \bar{p}_l}{\partial \theta} \right) \tau_1 \bar{h}^3 \right) \right] + \left(\frac{D}{L} \right)^2 \left[\bar{p}_l^2 \bar{h}^3 \left(-\bar{y}^\kappa + \frac{1}{2} \bar{y}^{2\kappa} \right) + (1 - \bar{y}^\kappa) \bar{p}_l \bar{h}^3 \right] = \Lambda \left[\frac{\partial(\bar{p}_l \bar{h})}{\partial \theta} \tau_1 + \frac{\partial \bar{h}}{\partial \theta} \frac{\bar{y}^2}{2} \right] \\
& + \bar{y} \left[\frac{\partial}{\partial \theta} \left[\left(\left(\frac{\partial \bar{p}_l}{\partial \theta} \right) \bar{p}_l \psi_1 \bar{h}^3 + \left(\frac{\partial \bar{p}_l}{\partial \theta} \right) \beta_1 \bar{h}^3 \right) \right] - \left(\frac{D}{L} \right)^2 \left[\frac{\bar{p}_l^2 \bar{h}^3}{2} + \bar{p}_l \bar{h}^3 \right] - \Lambda \left[\frac{\partial(\bar{p}_l \bar{h})}{\partial \theta} \beta_1 + \frac{\partial \bar{h}}{\partial \theta} \frac{1}{2} \right] \right] \\
& + \left(\frac{D}{L} \right)^2 \left[\bar{p}_l \bar{h}^3 \right]
\end{aligned}$$

3.3.1.21

Rearranging the terms and simplifying:

$$\begin{aligned}
& \frac{\partial}{\partial \theta} \left[\left(\left(\frac{\partial \bar{p}_l}{\partial \theta} \right) \bar{p}_l \bar{h}^3 [\nu_1 - \bar{y} \psi_1] + \left(\frac{\partial \bar{p}_l}{\partial \theta} \right) \bar{h}^3 [\tau_1 - \bar{y} \beta_1] \right) \right] \\
& + \left(\frac{D}{L} \right)^2 \left[\bar{h}^3 \left[\bar{p}_l^2 \left(-\bar{y}^\kappa + \frac{1}{2} \bar{y}^{2\kappa} \right) + \bar{p}_l (1 - \bar{y}^\kappa) + \frac{\bar{y} \bar{p}_l^2}{2} + \bar{y} \bar{p}_l - \bar{p}_l \right] \right] = \Lambda \left[\frac{\partial(\bar{p}_l \bar{h})}{\partial \theta} [\tau_1 - \bar{y} \beta_1] + \frac{\partial \bar{h}}{\partial \theta} \left[\frac{\bar{y}^2}{2} - \frac{\bar{y}}{2} \right] \right]
\end{aligned}$$

3.3.1.21

$$\begin{aligned}
& \frac{\partial}{\partial \theta} \left[\left(\left(\frac{\partial \bar{p}_l}{\partial \theta} \right) \bar{p}_l \bar{h}^3 [\nu_1 - \bar{y} \psi_1] + \left(\frac{\partial \bar{p}_l}{\partial \theta} \right) \bar{h}^3 [\tau_1 - \bar{y} \beta_1] \right) \right] + \left(\frac{D}{L} \right)^2 \left[\bar{h}^3 \left[\bar{p}_l^2 \left(-\bar{y}^\kappa + \frac{1}{2} \bar{y}^{2\kappa} + \frac{\bar{y}}{2} \right) + \bar{p}_l ((1 - \bar{y}^\kappa) + \bar{y} - 1) \right] \right] \\
& = \Lambda \left[\frac{\partial(\bar{p}_l \bar{h})}{\partial \theta} [\tau_1 - \bar{y} \beta_1] + \frac{\partial \bar{h}}{\partial \theta} \left[\frac{\bar{y}^2}{2} - \frac{\bar{y}}{2} \right] \right]
\end{aligned}$$

3.3.1.22

Equation 3.3.1.22 is again integrated along the axial direction \bar{y} from 0 to 1.

$$\begin{aligned}
& \frac{\partial}{\partial \theta} \left[\left(\left(\frac{\partial \bar{p}_l}{\partial \theta} \right) \bar{p}_l \bar{h}^3 \left[\nu_2 - \frac{\bar{y}^2 \psi_1}{2} \right]_0^1 + \left(\frac{\partial \bar{p}_l}{\partial \theta} \right) \bar{h}^3 \left[\tau_2 - \frac{\bar{y}^2 \beta_1}{2} \right]_0^1 \right) \right] \\
& + \left(\frac{D}{L} \right)^2 \left[\bar{h}^3 \left[\bar{p}_l^2 \left[\frac{-\bar{y}^{\kappa+1}}{\kappa+1} + \frac{\bar{y}^{2\kappa+1}}{2(2\kappa+1)} + \frac{\bar{y}^2}{4} \right]_0^1 + \bar{p}_l \left[\left(\tau + \frac{\bar{y}^2}{2} - \bar{y} \right) \right]_0^1 \right] \right] = \Lambda \left[\frac{\partial(\bar{p}_l \bar{h})}{\partial \theta} \left[\tau_2 - \frac{\bar{y}^2 \beta_1}{2} \right]_0^1 + \frac{\partial \bar{h}}{\partial \theta} \left[\frac{\bar{y}^3}{6} - \frac{\bar{y}^2}{4} \right]_0^1 \right]
\end{aligned}$$

3.3.1.23

where

$$\begin{aligned}
v_2 = & \frac{1}{6(2+\kappa)(1+2\kappa)(1+\kappa)(3+2\kappa)(3+\kappa)} (1(95y^3\kappa^3 + 32y^3\kappa^4 + 4y^3\kappa^5 + 130y^3\kappa^2 \\
& + 15\kappa y^{(3+2\kappa)} + 3\kappa^2 y^{(3+2\kappa)} + 81y^3\kappa - 96\kappa y^{(3+\kappa)} - 48\kappa^2 y^{(3+\kappa)} + 18y^3 + 18y^{(3+2\kappa)} \\
& - 36y^{(3+\kappa)}))
\end{aligned}
\tag{3.3.1.24}$$

Evaluating the limits of integrals and rearranging further yields:

$$\begin{aligned}
\frac{\partial}{\partial \theta} \left[\left(\left(\frac{\partial \bar{p}_l}{\partial \theta} \right) \bar{p}_l \bar{h}^3 \left[\psi_2 - \frac{\psi_1}{2} \right] + \left(\frac{\partial \bar{p}_l}{\partial \theta} \right) \bar{h}^3 \left[\beta_2 - \frac{\beta_1}{2} \right] \right) \right] + \left(\frac{D}{L} \right)^2 \left[\bar{h}^3 \left[\bar{p}_l^2 \left[\frac{-1}{\kappa+1} + \frac{1}{2(2\kappa+1)} + \frac{1}{4} \right] + \bar{p}_l \left[\beta - \frac{1}{2} \right] \right] \right] \\
= \Lambda \left[\frac{\partial(\bar{p}_l \bar{h})}{\partial \theta} \left[\beta_2 - \frac{\beta_1}{2} \right] - \frac{\partial \bar{h}}{\partial \theta} \frac{1}{12} \right]
\end{aligned}
\tag{3.3.1.25}$$

where

$$\psi_2 = \frac{1\kappa^2(95\kappa + 32\kappa^2 + 4\kappa^3 + 85)}{6(2+\kappa)(1+2\kappa)(1+\kappa)(3+2\kappa)(3+\kappa)}
\tag{3.3.1.26}$$

$$\beta = \frac{\kappa}{1+\kappa}
\tag{3.3.1.27}$$

$$\beta_2 = \frac{1\kappa(11+6\kappa+\kappa^2)}{6(1+\kappa)(2+\kappa)(3+\kappa)}
\tag{3.3.1.28}$$

Finally:

$$\frac{d}{d\theta} \left[\left(\left(\frac{d\bar{p}_l}{d\theta} \right) \bar{p}_l \bar{h}^3 \chi_1 + \left(\frac{d\bar{p}_l}{d\theta} \right) \bar{h}^3 \chi_2 \right) \right] + \left(\frac{D}{L} \right)^2 \left[\bar{h}^3 \left[\bar{p}_l^2 \chi_3 + \bar{p}_l \chi_4 \right] \right] = \Lambda \left[\frac{d(\bar{p}_l \bar{h})}{d\theta} \chi_2 - \frac{d\bar{h}}{d\theta} \frac{1}{12} \right]
\tag{3.3.1.29}$$

where

$$\chi_1 = -\frac{1(2\kappa^2 + 15\kappa + 19)\kappa^2}{12(3+\kappa)(3+2\kappa)(1+\kappa)(2+\kappa)}
\tag{3.3.1.30}$$

$$\chi_2 = -\frac{1(\kappa+5)\kappa}{12(3+\kappa)(2+\kappa)} \quad 3.3.1.31$$

$$\chi_3 = \frac{1(-3\kappa-1+2\kappa^2)}{4(1+\kappa)(2\kappa+1)} \quad 3.3.1.32$$

$$\chi_4 = \frac{1(\kappa-1)}{2(1+\kappa)} \quad 3.3.1.33$$

This represents the final modified parabolic form of the finite Reynolds equation which is an ordinary differential equation.

3.3.2 Numerical Procedure (MPA)

Considering equation 3.3.1.29 it is expanded as follows:

$$\begin{aligned} & \left[\bar{p}_l \bar{h}^3 \frac{d^2 \bar{p}_l}{d\theta^2} \chi_1 \right] + \left[3 \bar{p}_l \bar{h}^2 \frac{d\bar{h}}{d\theta} \frac{d\bar{p}_l}{d\theta} \chi_1 \right] + \left[\bar{h}^3 \left(\frac{d\bar{p}_l}{d\theta} \right)^2 \chi_1 \right] + \left[3 \bar{h}^2 \frac{d\bar{h}}{d\theta} \frac{d\bar{p}_l}{d\theta} \chi_2 \right] + \left[\bar{h}^3 \frac{d^2 \bar{p}_l}{d\theta^2} \chi_2 \right] + \left(\frac{D}{L} \right)^2 (\bar{h}^3 \bar{p}^2 l \chi_3) \\ & + \left(\frac{D}{L} \right)^2 [\bar{h}^3 \bar{p}_l \chi_4] = \Lambda \left[\bar{h} \frac{d\bar{p}_l}{d\theta} \chi_2 \right] + \Lambda \left[\bar{p}_l \frac{d\bar{h}}{d\theta} \chi_2 \right] - \Lambda \left[\frac{d\bar{h}}{d\theta} \left(\frac{1}{12} \right) \right] \end{aligned} \quad 3.3.2.1$$

Divide by \bar{h}^3

$$\begin{aligned} & \left[\bar{p}_l \frac{d^2 \bar{p}_l}{d\theta^2} \chi_1 \right] + \left[3 \bar{p}_l \frac{1}{\bar{h}} \frac{d\bar{h}}{d\theta} \frac{d\bar{p}_l}{d\theta} \chi_1 \right] + \left[\left(\frac{d\bar{p}_l}{d\theta} \right)^2 \chi_1 \right] + \left[\frac{3}{\bar{h}} \frac{d\bar{h}}{d\theta} \frac{d\bar{p}_l}{d\theta} \chi_2 \right] + \left[\frac{d^2 \bar{p}_l}{d\theta^2} \chi_2 \right] \\ & + \left(\frac{D}{L} \right)^2 (\bar{p}^2 l \chi_3) + \left(\frac{D}{L} \right)^2 [\bar{p}_l \chi_4] = \Lambda \left[\frac{1}{\bar{h}^2} \frac{d\bar{p}_l}{d\theta} \chi_2 \right] + \Lambda \left[\frac{\bar{p}_l}{\bar{h}^3} \frac{d\bar{h}}{d\theta} \chi_2 \right] - \Lambda \left[\frac{1}{\bar{h}^3} \frac{d\bar{h}}{d\theta} \left(\frac{1}{12} \right) \right] \end{aligned} \quad 3.3.2.2$$

Equation 3.3.2.2 will be solved iteratively by using tridiagonal approximation method (Ferziger et al., 2002, Gerald et al., 2002, Patankar, 1980) with all the non-linear terms on to the RHS and the linear terms to the LHS as follows:

$$\begin{aligned}
& \underbrace{\frac{3}{\bar{h}} \frac{d\bar{h}}{d\theta} \frac{d\bar{p}_l}{d\theta} \chi_2 + \frac{d^2 \bar{p}_l}{d\theta^2} \chi_2 + \left(\frac{D}{L}\right)^2 [\bar{p}_l \chi_4] - \Lambda \left[\frac{1}{\bar{h}^2} \frac{d\bar{p}_l}{d\theta} \chi_2 \right] - \Lambda \left[\frac{\bar{p}_l}{\bar{h}^3} \frac{d\bar{h}}{d\theta} \chi_2 \right]}_{L.H.S} \\
& = - \underbrace{\left[\bar{p}_l \frac{d^2 \bar{p}_l}{d\theta^2} \chi_1 \right] - \left[3 \bar{p}_l \frac{1}{\bar{h}} \frac{d\bar{h}}{d\theta} \frac{d\bar{p}_l}{d\theta} \chi_1 \right] - \left[\left(\frac{d\bar{p}_l}{d\theta} \right)^2 \chi_1 \right] - \left(\frac{D}{L} \right)^2 (\bar{p}^2 l \chi_3) - \Lambda \left[\frac{1}{\bar{h}^3} \frac{d\bar{h}}{d\theta} \left(\frac{1}{12} \right) \right]}_{R.H.S}
\end{aligned}$$

3.3.2.3

Expanding:

$$\begin{aligned}
& \left[\frac{3}{\bar{h}} \frac{d\bar{h}}{d\theta} \chi_2 \left(\frac{\bar{p}l^{n+1}_{i+1} - \bar{p}l^{n+1}_{i-1}}{2d\theta} \right) \right] + \left[\chi_2 \left(\frac{\bar{p}l^{n+1}_{i+1} - 2\bar{p}l^{n+1}_i + \bar{p}l^{n+1}_{i-1}}{d\theta^2} \right) \right] + \left(\frac{D}{L} \right)^2 [\bar{p}_i^{n+1} \chi_4] \\
& - \Lambda \left[\frac{1}{\bar{h}^2} \left(\frac{\bar{p}l^{n+1}_{i+1} - \bar{p}l^{n+1}_{i-1}}{2d\theta} \right) \chi_2 \right] - \Lambda \left[\frac{\bar{p}l_i^{n+1}}{\bar{h}^3} \frac{d\bar{h}}{d\theta} \chi_2 \right] = - \left[\bar{p}l^n \chi_1 \left(\frac{d^2 \bar{p}_l}{d\theta^2} \right) \right] - \left[\frac{3 \bar{p}l_i^n}{\bar{h}_i} \frac{d\bar{h}}{d\theta} \frac{d\bar{p}_l}{d\theta} \chi_1 \right] \\
& - \left[\left(\frac{d\bar{p}_l}{d\theta} \right)^2 \chi_1 \right] - \left(\frac{D}{L} \right)^2 (\bar{p}^2 l_i \chi_3) - \Lambda \left[\frac{1}{\bar{h}^3} \frac{d\bar{h}}{d\theta} \left(\frac{1}{12} \right) \right]
\end{aligned}$$

3.3.2.4

Setting up in tridiagonal form:

$$\begin{aligned}
& \bar{p}l^{n+1}_{i+1} \left[\frac{3}{\bar{h}_i} \frac{d\bar{h}}{d\theta} \chi_2 - \frac{\Lambda}{\bar{h}_i^2} \chi_2 + \frac{\chi_2}{2d\theta} + \frac{\chi_2}{d\theta^2} \right] + \bar{p}l^{n+1}_i \left[\frac{-2(\chi_2)}{d\theta^2} + \left(\frac{D}{L} \right)^2 [\chi_4] - \Lambda \left[\frac{1}{\bar{h}_i^3} \frac{d\bar{h}}{d\theta} \chi_2 \right] \right] + \\
& \bar{p}l^{n+1}_{i-1} \left[\frac{-3}{\bar{h}_i} \frac{d\bar{h}}{d\theta} \chi_2 + \frac{\Lambda}{\bar{h}_i^2} \chi_2 + \frac{\chi_2}{2d\theta} + \frac{\chi_2}{d\theta^2} \right] = - \left[\bar{p}l^n \chi_1 \frac{d^2 \bar{p}_l}{d\theta^2} \right] - \left[\frac{3 \bar{p}l_i^n}{\bar{h}_i} \frac{d\bar{h}}{d\theta} \frac{d\bar{p}_l}{d\theta} \chi_1 \right] - \left[\left(\frac{d\bar{p}_l}{d\theta} \right)^2 \chi_1 \right] \\
& - \left(\frac{D}{L} \right)^2 (\bar{p}^2 l_i \chi_3) - \Lambda \left[\frac{1}{\bar{h}_i^3} \frac{d\bar{h}}{d\theta} \left(\frac{1}{12} \right) \right]
\end{aligned}$$

3.3.2.5

The solution begins by evaluating the R.H.S of the equation 3.3.2.5 by an initial mid section guess pressure $\bar{p}l^n$, by solving for an incompressible bearing with an assumed rigid

bearing eccentricity ratio ε_r and an initial guess for the film thickness \bar{h}_i and parabolic exponent κ . This is done iteratively until the pressure converge for a given film thickness and parabolic exponent. Convergence is assumed when the relative error between two successive iterations fall below a specified value. One hundred finite difference grid points along the circumferential direction is used.

The pressure obtained in this fashion represents the pressure at the mid section of the bearing. This pressure is substituted in $\bar{p}(\theta, y) = \bar{p}_l(1 - \bar{y}^\kappa)$ to determine the pressure distribution along the axial length of the bearing. Thus the final pressure \bar{p} represents the pressure along the circumferential and axial direction of the bearing. The mid- section pressure profile \bar{p}_l can be controlled by the variation of the parabolic exponent κ , which in turn changes the entire pressure distribution for the bearing. A series of parametric study to characterize the behavior of the exponent was simulated. This is explained in detail in the next section.

The next part is to couple the hydrodynamic pressure and the foil structural compliance which has a direct effect on the overall behavior of the fluid film profile. This is incorporated in an iterative scheme. Recalling equation (3.1.1.13), the film thickness \bar{h}_f is a function of dimensionless pressure. As the top and bump foils deform due to the pressure, the shaft moves in the direction where there is maximum deformation (Fig 5) and hence there is a significant change in the eccentricity ratio ε_f and attitude angle ϕ_f which further changes the overall profile of the film thickness. This is not accounted for in the equation (3.1.1.13). To account for this the modified form of the film thickness equation is:

$$\bar{h}_{f_i} = 1 + \varepsilon_f \cos(\theta - \Delta\varphi) + \alpha(\bar{p}_l) \quad 3.3.2.6$$

$$\varepsilon_f = \varepsilon_r + \Delta\varepsilon \quad (\text{Peng and Khonsari, 2004}) \quad 3.3.2.7$$

where ε_f is determined by bisection method by assuming the minimum film thickness $h_{\min r}$ in a rigid bearing and the corresponding minimum film thickness in a foil bearing $h_{\min f}$ are identical and $\Delta\varphi$ represents the difference in attitude angle for a rigid bearing ϕ_r and compliant bearing ϕ_f . The effect of the hydrodynamic pressure on the film thickness profile was obtained by employing the method of under relaxation. It was very important to have a good initial profile for the pressure as this has a direct effect on the fluid film geometry. The final film thickness is obtained in an iterative scheme as follows:

$$\bar{h}_{f_i}^{n+1} = 1 + \varepsilon_f^n \cos(\theta - \Delta\varphi^n) + \alpha(\bar{p}l_i^n) \quad 3.3.2.8$$

The under-relaxation between successive iterations is given by the formula:

$$\bar{h}_{f_i}^{n+1} = \alpha_{rh} \bar{h}_{f_i}^{n+1} + (1 - \alpha_{rh}) \bar{h}_{f_i}^n \quad 3.3.2.9$$

where α_{rh} represents the under-relaxation factor for the fluid film and n represents the iteration number. Typically α_{rh} varies from 0.5 – 0.8 based on the eccentricity ratios and operating speeds.

- **Load Carrying Capacity**

The x and z components:

$$W_x = \int_{-y}^y \int_0^{2\pi} LR(p) \cos \theta d\theta dy \quad W_z = \int_{-y}^y \int_0^{2\pi} LR(p) \sin \theta d\theta dy \quad 3.3.2.10$$

In dimensionless form:

$$\bar{W}_x = \int_{-y}^y \int_0^{2\pi} (\bar{p}) \cos \theta d\theta dy \quad \bar{W}_z = \int_{-y}^y \int_0^{2\pi} (\bar{p}) \sin \theta d\theta dy \quad 3.3.2.11$$

$$\text{where } \bar{W}_{x,z} = \frac{W}{p_a RL}, \quad \bar{p} = \frac{p - p_a}{p_a} \Rightarrow p = \bar{p}p_a + p_a \quad 3.3.2.12$$

$$\bar{W}_f = \sqrt{\bar{W}_x^2 + \bar{W}_z^2}, \quad \text{also} \quad \bar{W}_f = \frac{W}{p_a RL}$$

The attitude angle is represented as: $\tan \varphi = \frac{\bar{W}_z}{-\bar{W}_x}$ 3.3.2.13

$$W = \bar{W}_f p_a RL$$
 3.3.2.14

Equation 3.3.2.14 represents the load-carrying capacity of the bearing.

3.3.3 Bearing Performance Parameters (MPA)

3.3.3.1 Rigid Journal Bearing

To understand the behavior of the parabolic exponent κ , first a series of simulations were run using a full Reynolds equation (finite analysis) at different eccentricity ratio and the bearing

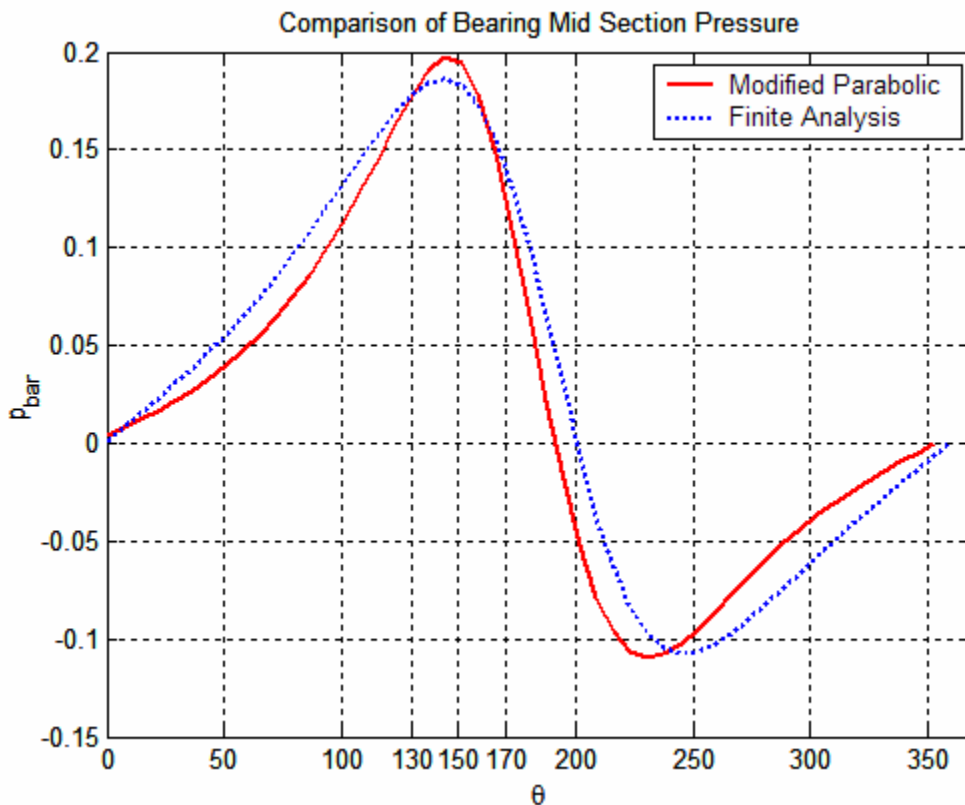


Figure 16: Pressure Profile Match by Varying the Parabolic Exponent Along the Circumferential Direction

performance parameters were obtained. Next, using the modified approach and with a guess value for parabolic exponent κ_r , simulations were run for a given eccentricity ratio and the bearing performance parameters were compared with the solutions obtained from the finite approximation.

Figure 16 represents the bearing mid-section pressure profile comparison between finite analysis and the new modified parabolic approximation for a bearing running at 30,000 rpm and at an eccentricity ratio $\varepsilon_r=0.5$. The pressure profile obtained through the modified approach is in good agreement with the one obtained from finite analysis along the circumferential direction. Further the exponent value κ_r was varied such that the pressure profile matches at various chosen sections along the circumferential direction for the bearing running at 30,000 rpm and at an eccentricity ratio $\varepsilon_r=0.5$. Figure 17 represents this understanding for two types of eccentricity ratios, from which it can be seen that the parabolic exponent κ_r reaches a higher value for the peak pressure.

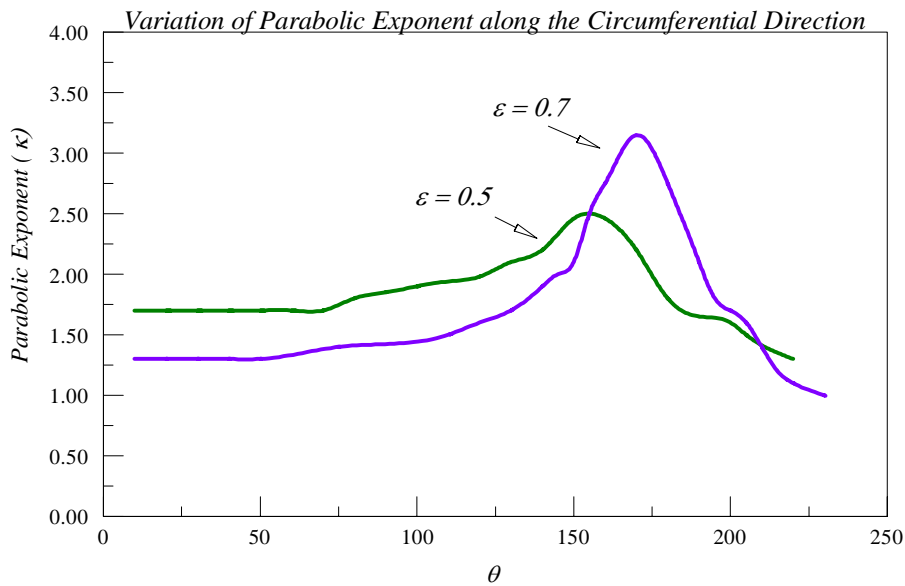


Figure 17: Variation of Exponent along the Circumferential Direction

The main goal was to obtain the bearing performance parameters using the current method and compare the results with the finite approximation. Hence, we further investigate different cases to evaluate the performance parameters.

- **Case 1: Peak Pressure Match Condition. (Trial Investigation Case)**

In this case the peak pressure from the finite analysis for a given eccentricity is considered and modified simulations for the same eccentricity are run by varying the parabolic exponent κ_r to match the peak pressure of the profile obtained through the modified approach. The program converged once the pressure profile \bar{p}_l at the peak was matched with the peak obtained by finite analysis. This pressure represents the pressure at the mid-section of the bearing and is substituted in equation $\bar{p}(\theta, y) = \bar{p}_l (1 - \bar{y}^{\kappa_r})$ to obtain the pressure distribution for the complete bearing which represents the pressure along the circumferential direction as well as the axial direction.

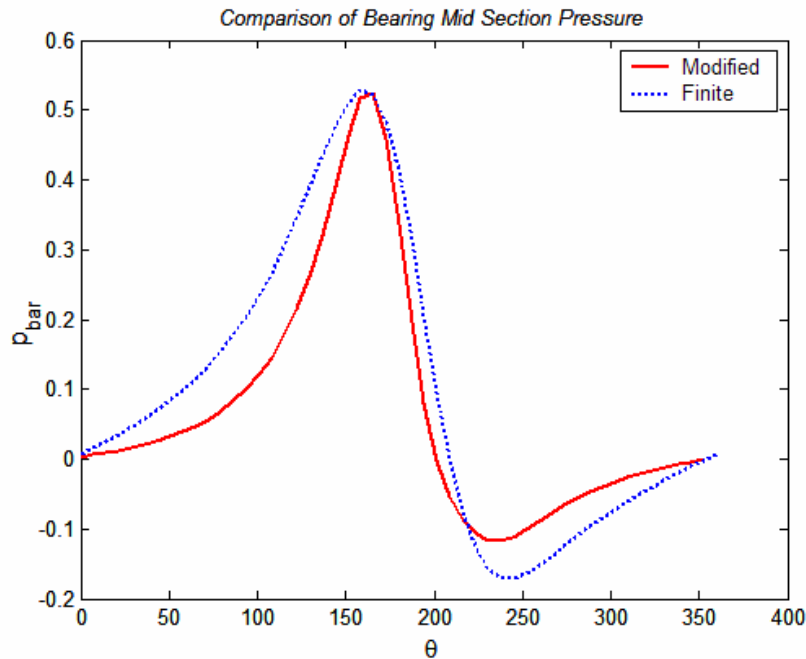


Figure 18: Pressure Profile comparison between Finite and Modified Approximation at the Mid Section of the Bearing. (Peak Pressure Match Case)

Figure 18 represents a case where the bearing is running at 30,000 rpm and at an eccentricity ratio $\varepsilon_r = 0.7$. To match the finite approximation peak pressure, the parabolic exponent was obtained by bisection method at value of 3.5. Further the bearing performance parameters which included the load-carrying capacity (Fig 19) and attitude angle (Fig 20) were obtained. A range of eccentricities were run to determine the behavior of the parabolic exponent κ_r (Fig 21).

It was interesting to see that with lower eccentricity ratios, the bearing performance parameters were comparable with the finite approximations, but at higher eccentricity ratios the deviation in the performance parameters was significant. The pressure profile at the mid section seemed to grow thinner at higher eccentricity ratios which resulted in variation of the bearing

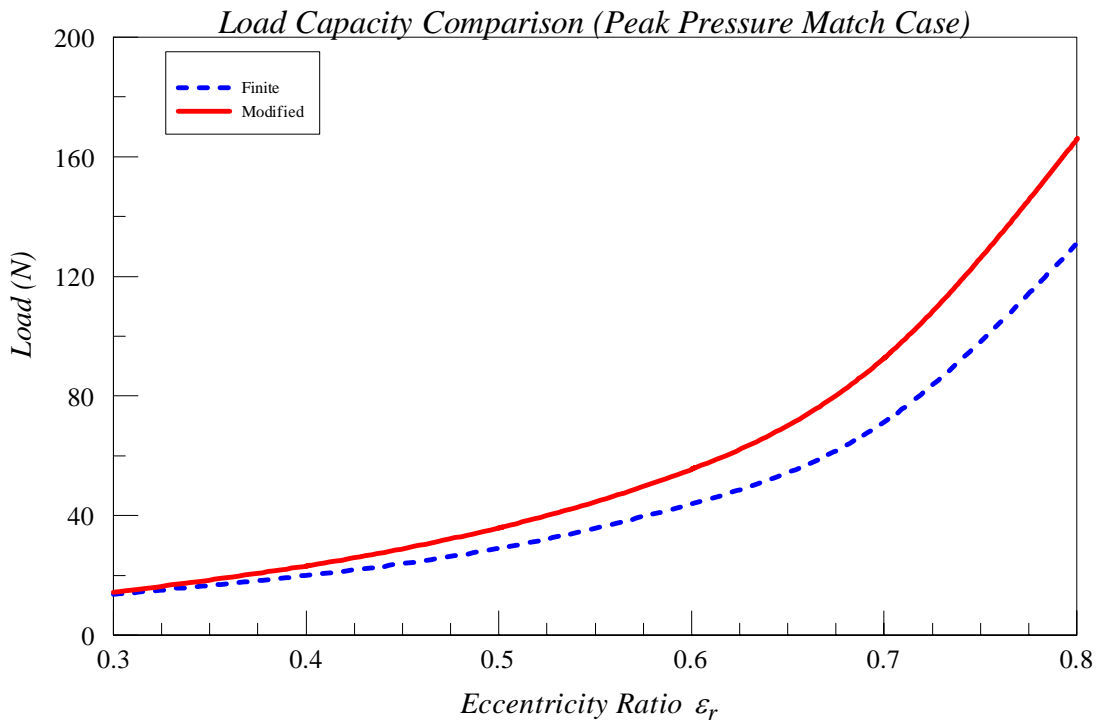


Figure 19: Load Comparison between Finite and Modified Approximation with Fixed Eccentricity Ratios. (Peak Pressure Match Case)

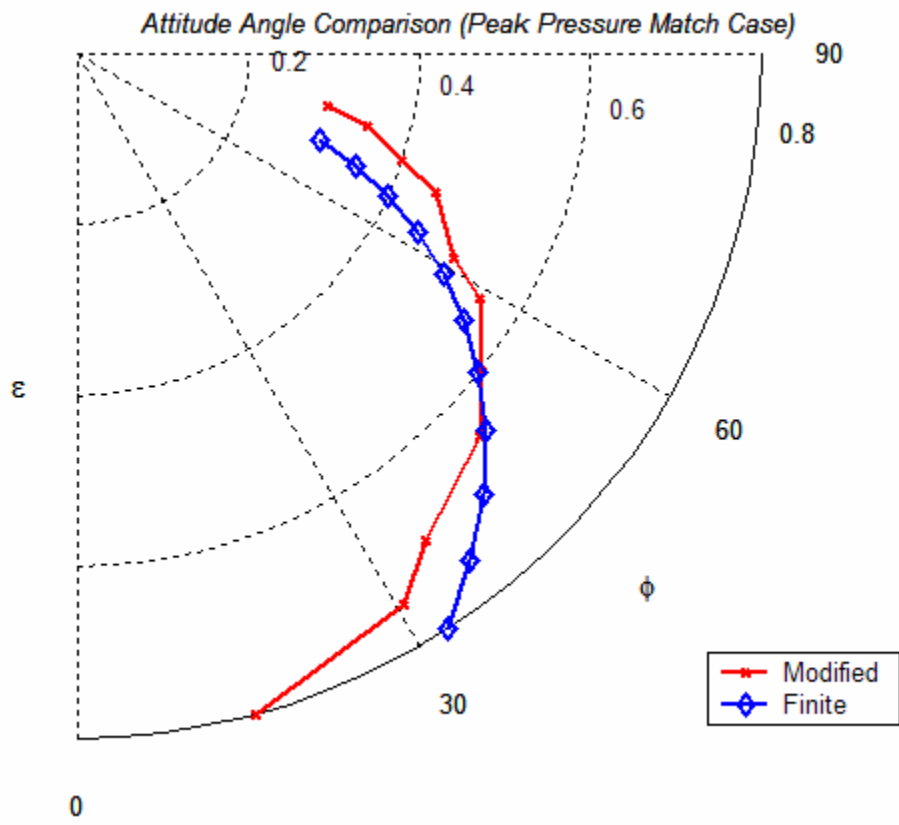


Figure 20: Attitude Angle Comparison between Finite and Modified Approximation (Peak Pressure Match Case)

performance parameters. Also the value of the parabolic exponent increases as the eccentricity ratios reach higher values (Fig 21).

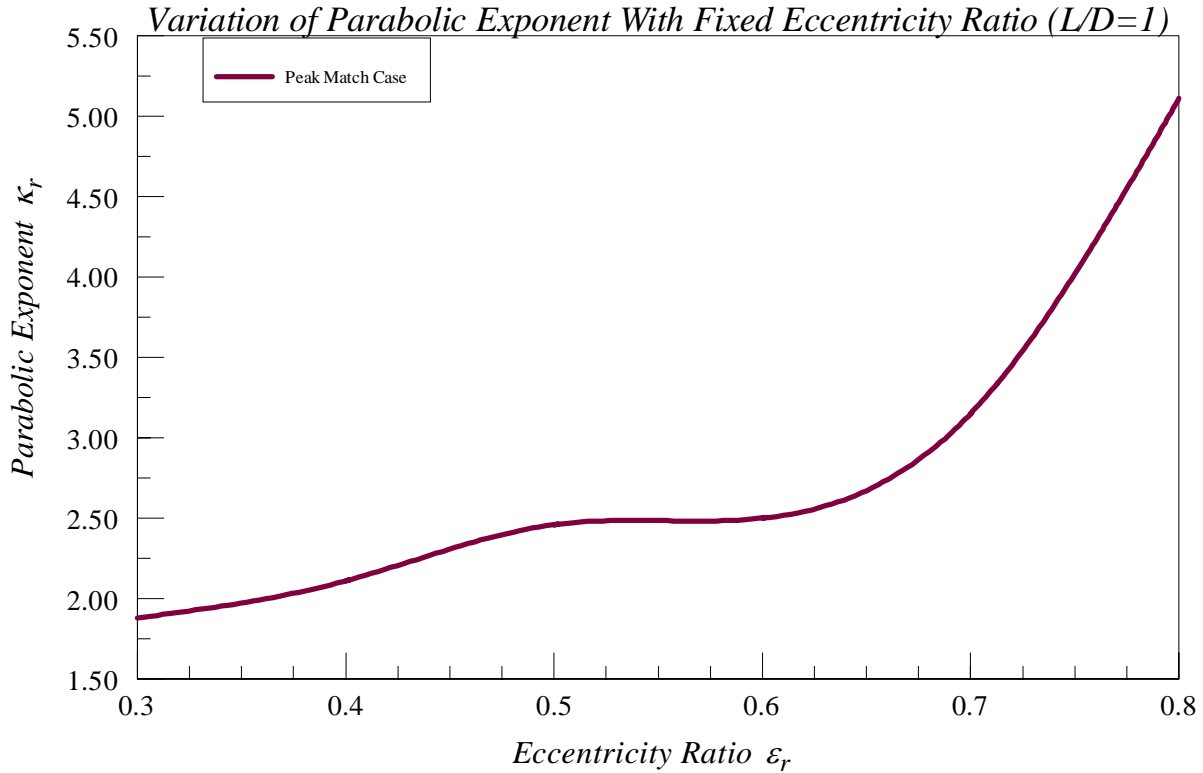


Figure 21: Parametric Study of Parabolic Exponent. (Peak Pressure Match, L/D =1)

The peak pressure match is considered as an investigation process to better understand the behavior of the parabolic exponent κ_r . Based on the final performance parameters, it clearly indicates the deviations are high when compared with finite analysis results.

- **Case 2: Load Imposed condition**

Instead of matching the peak pressure from the finite solution at a given eccentricity, the final load-carrying capacity was considered as the main target to match from the modified simulations run. The variable parabolic exponent κ_r was obtained iteratively when the final

load-carrying capacity was matched with the corresponding load-carrying capacity from the finite solution.

First the bearing mid-section pressure \bar{p}_l for a given eccentricity was obtained by assuming a guess value for the parabolic exponent κ_r . Then, the pressure profile \bar{p}_l was substituted in eqn $\bar{p}(\theta, y) = \bar{p}_l (1 - \bar{y}^{\kappa_r})$ to obtain the pressure distribution along the circumferential and axial direction of the bearing. This profile was numerically integrated using Simpson's rule to obtain the final load-carrying capacity. As mentioned earlier, the entire process was solved iteratively to target the final load-carrying capacity and finally the

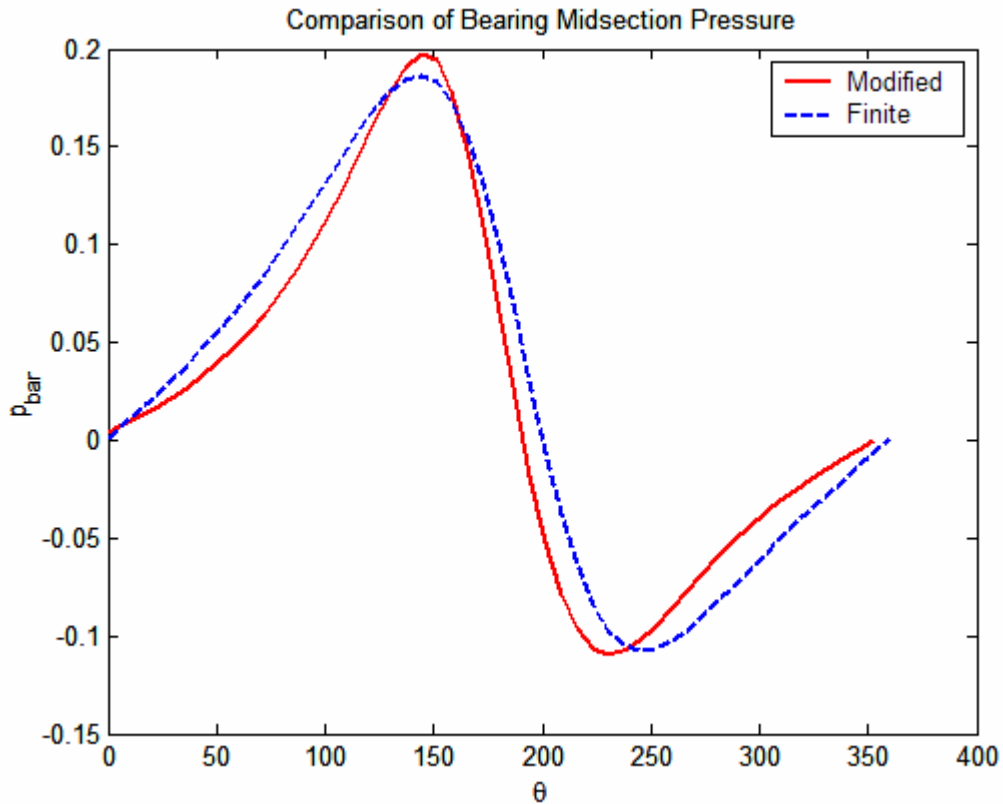


Figure 22: Pressure Profile Comparison between Finite and Modified Approximation at Mid Section of Bearing. (Load Imposed Condition)

modified parabolic exponent κ_r was obtained. Figure 22 represents the comparison of the pressure profile \bar{p}_l at the mid-section of the bearing between the finite analysis and modified approximation running at 30,000 rpm with an eccentricity ratio $\varepsilon_r = 0.5$.

The modified parabolic exponent κ_r was obtained when the load-carrying capacity (Fig 23) between the two methods matched. A series of simulations were run and comparisons at range of loads obtained at different eccentricity ratios were made to study the behavior of the parabolic exponent κ_r (Fig 25). The attitude angle comparison (Fig 24) revealed a comparable agreement for range of load conditions imposed.

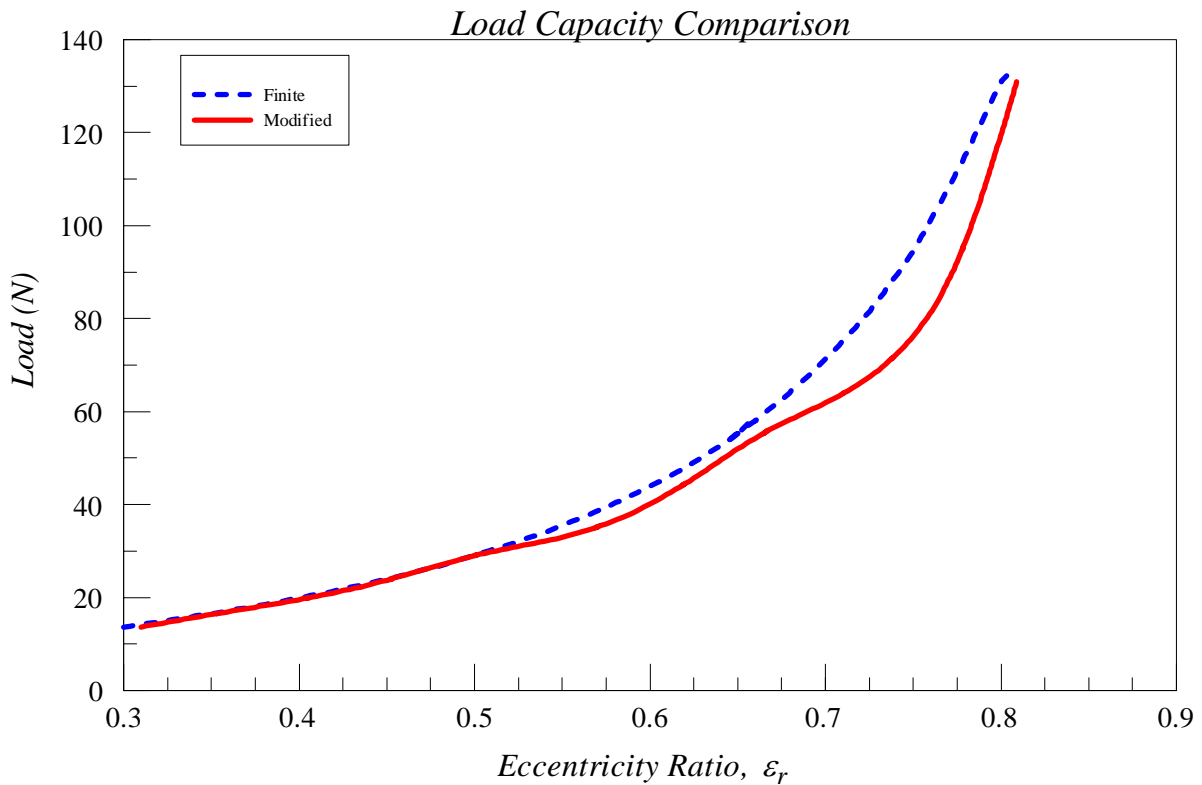


Figure 23: Load Comparison between Finite and Modified Approximation (Load Imposed Condition)

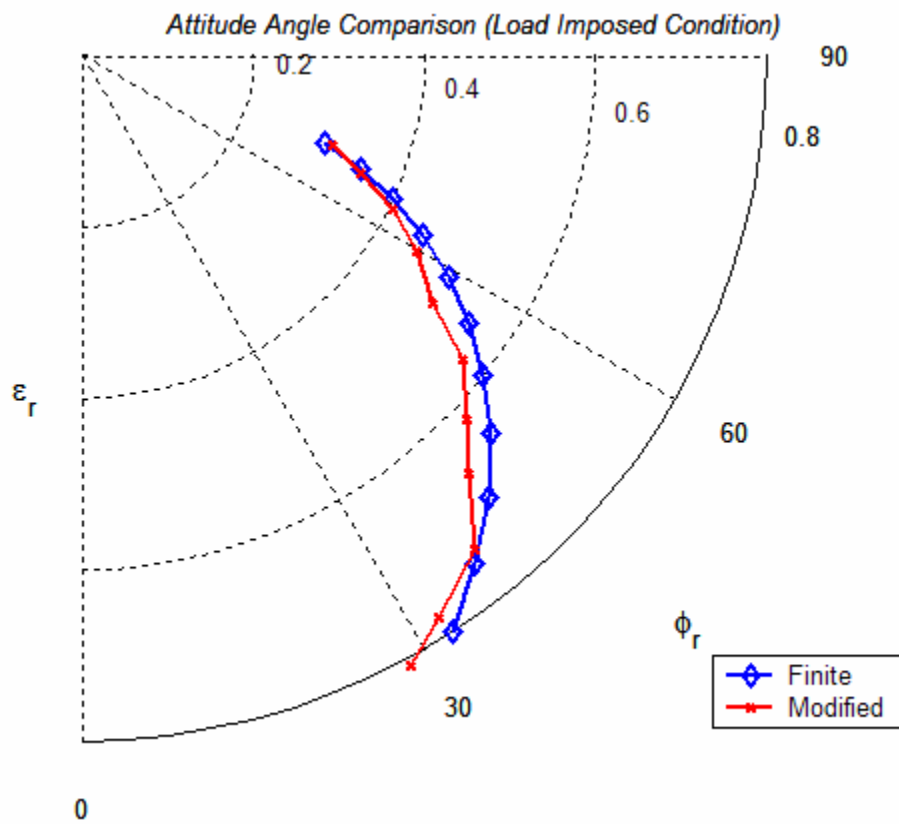


Figure 24: Attitude Angle Comparison between Finite and Modified Approximation (Load Imposed Condition)

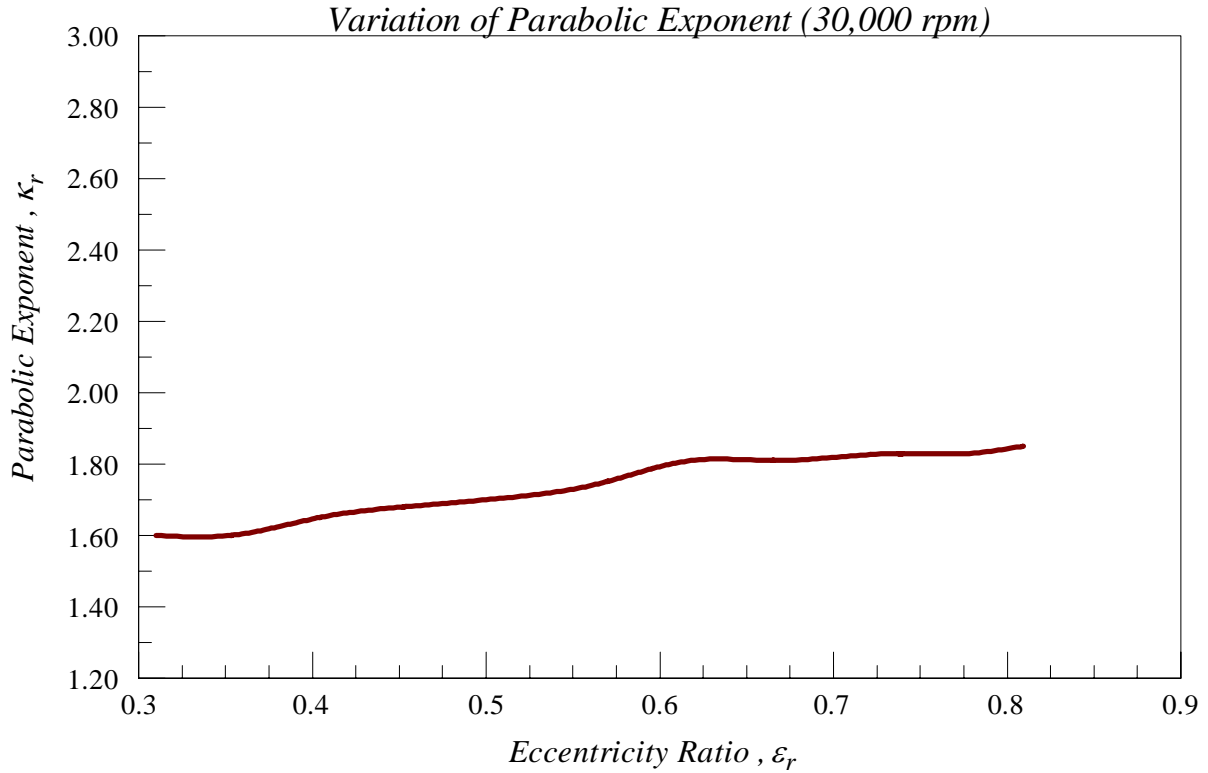


Figure 25: Parametric Study of Parabolic Exponent (Load Imposed Condition, L/D=1)

- **Generalization for rigid bearing based on load imposed condition**

Considering the equation 3.3.1.29:

$$\frac{d}{d\theta} \left[\left(\left(\frac{d\bar{p}_l}{d\theta} \right) \bar{p}_l \bar{h}^3 \chi_1 + \left(\frac{d\bar{p}_l}{d\theta} \right) \bar{h}^3 \chi_2 \right) \right] + \left(\frac{D}{L} \right)^2 \left[\bar{h}^3 \left[\bar{p}^2 \chi_3 + \bar{p}_l \chi_4 \right] \right] = \Lambda \left[\frac{d(\bar{p}_l \bar{h})}{d\theta} \chi_2 - \frac{d\bar{h}}{d\theta} \frac{1}{12} \right]$$

The key non-dimensional parameters are as follows:

1. Bearing Length to Diameter ratio , $\frac{L}{D}$ 3.3.3.1.1

2. Eccentricity ratio , ϵ_r 3.3.3.1.2

3. Bearing Number , $\Lambda = \frac{6\omega\mu_0}{p_a} \left(\frac{R}{C} \right)^2$ 3.3.3.1.3

Based on these key non-dimensional parameters the non-dimensional load capacity \bar{W} and parabolic exponent kappa κ_r can be obtained.

A series of simulations were run initially based on the finite analysis to obtain the bearing performance parameters for various range of operating speeds (10,000, 20,000 and 30,000 rpm) and eccentricity ratios by fixing the bearing length to diameter ratio (L/D) to one. With similar conditions using the modified parabolic approach simulations were run to match the load-carrying capacity obtained by the finite analysis. The end result was based on developing a set of charts based on the simulations run (Fig 26) which indicates non-dimensional load \bar{W} versus the eccentricity ratio ε_r at various bearing numbers Λ . Figure 27 represents the average value of the parabolic exponent obtained for various speeds. With these charts for a given bearing number and non-dimensional load, the appropriate parabolic exponent can be obtained for a suitable eccentricity ratio.

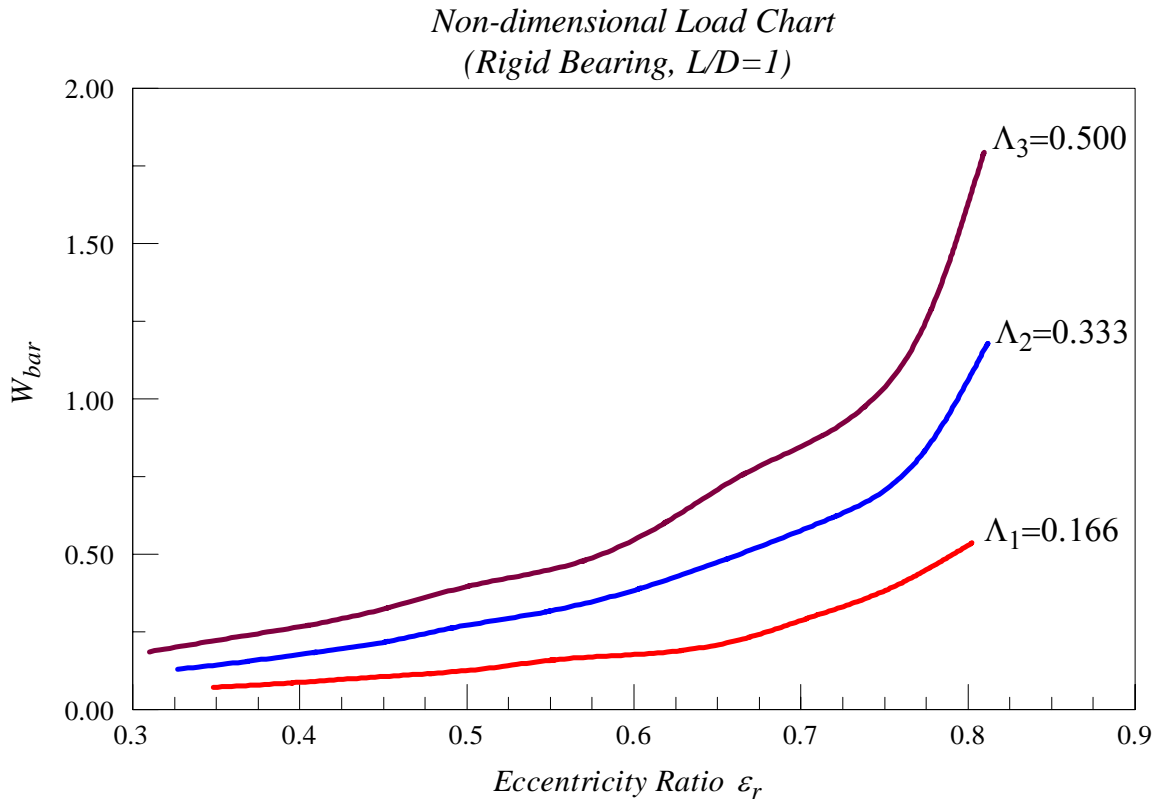


Figure 26: Rigid Bearing Non-Dimensional Load Chart ($L/D=1$)

*Parabolic Exponent Chart
(Rigid Bearing, L/D=1)*

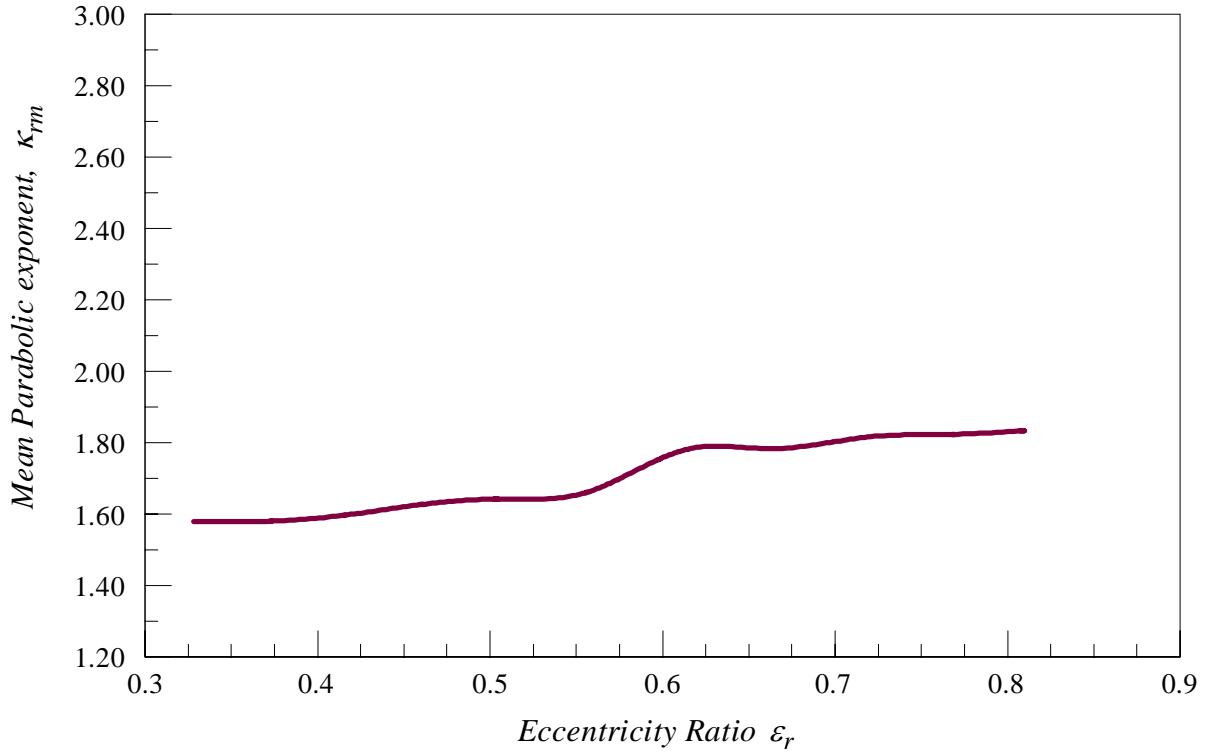


Figure 27: Rigid Bearing Parabolic Exponent Chart (L/D=1)

- **Example to use the rigid bearing non-dimensional charts (Fig 26 and Fig 27)**

To predict the performance parameters for a given non-dimensional load $\bar{W}=0.5$ and bearing number $\Lambda = 0.5$ requires a three step process as indicated below:

1. Using Figure 26 for the given conditions i.e. $\bar{W}=0.5$ and $\Lambda=0.5$, determine the eccentricity ratio. The result is : $\epsilon_r = 0.58$.
2. Using Figure 27 for a eccentricity ratio of $\epsilon_r = 0.58$, determine the mean parabolic exponent. The result is : $\kappa_{fm} = 1.7$

3. The eccentricity ratio ε_r , mean parabolic exponent κ_{m} along with the given non-dimensional bearing number Λ should be substituted in equation 3.3.1.29 and solved numerically to obtain the pressure profiles and other bearing parameters.

3.3.3.2 Compliant Journal Bearing

The application of the MPA method to obtain the solution for compliant journal bearings has to be carefully considered since the hydrodynamic pressure developed interacts with the fluid film thickness. Hence, certain important assumptions were made in obtaining the solution for compliant journal bearings.

Assumptions:

- The minimum film thickness value obtained for a given eccentricity ratio for a rigid gas bearing $\bar{h}_{\min r}$ is used as a final convergence target to obtain the final solution for compliant journal bearings. In other words the program converges when $\bar{h}_{\min f} = \bar{h}_{\min r}$.
- The final solution obtained through the MPA method will be based on matching the minimum film thickness and appropriate load-capacity values obtained by Finite Analysis.

To understand the behavior of the parabolic exponent κ_f for compliant journal bearings, a series of simulations was run using the full Reynolds equation (Finite Analysis) at different eccentricity ratios and the bearing performance parameters were obtained. Using the modified approach and with a guess value for parabolic exponent κ_f , simulations were run to match the minimum film thickness and were compared with the solutions obtained from the finite analysis.

Figures 28 and 29 represents the pressure profile comparison and film thickness profile respectively between the finite analysis and modified approximation at the mid-section of the

bearing running at 30,000 rpm with an eccentricity ratio $\epsilon_r = 0.7$. These profiles were obtained by varying the eccentricity ratio using the bisection method to match the minimum film thickness value at the given eccentricity ratio obtained by finite analysis. The program converged when the

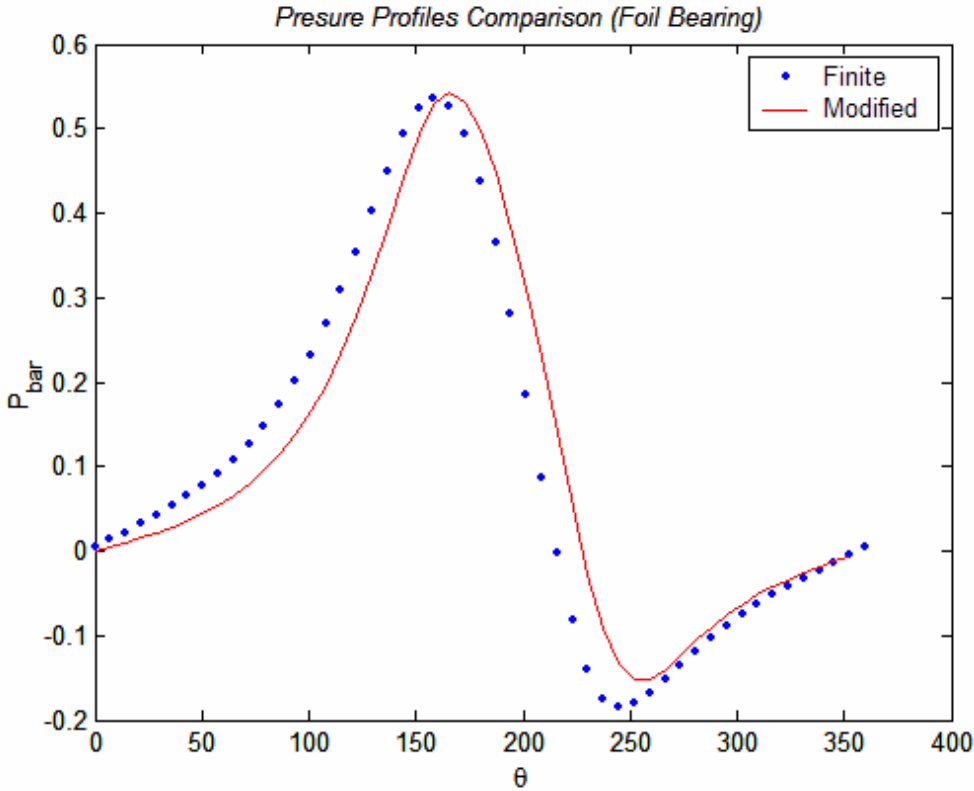


Figure 28: Pressure Profile Comparison between Finite and Modified Approximation at Mid Section of bearing at 30,000 rpm. (Foil Bearing / Min Film Match)

minimum film thickness of the bearing matched with the minimum film thickness obtained by finite analysis.

Figure 30 represents the load comparison between the finite and the modified approximation for a range of eccentricity ratios. Since the main condition here was based on matching the minimum film, the load capacity varies slightly at higher eccentricity ratios. The attitude angles comparisons can be seen from figure 31, indicates acceptable values over a range of eccentricity ratios. Figures 32 and 33 represent the three dimensional plot obtained by

modified approach and finite approach for a bearing running at 30,000 rpm and eccentricity ratio $\varepsilon_r=0.7$. Finally the variation of the parabolic exponent κ_f for a range of eccentricities is indicated in figure 34. The exponent κ_f reaches a higher value as the eccentricity ratios increase. The analysis carried out for compliant journal bearings was only for a certain operating speed of 30,000 rpm and a range of eccentricity ratios for a fixed bearing length to diameter ratio equivalent to one. Further study has to be carried out based on different bearing numbers and length to diameter ratios to generalize the parabolic exponent κ_f based on the key non-dimensional operating parameters.

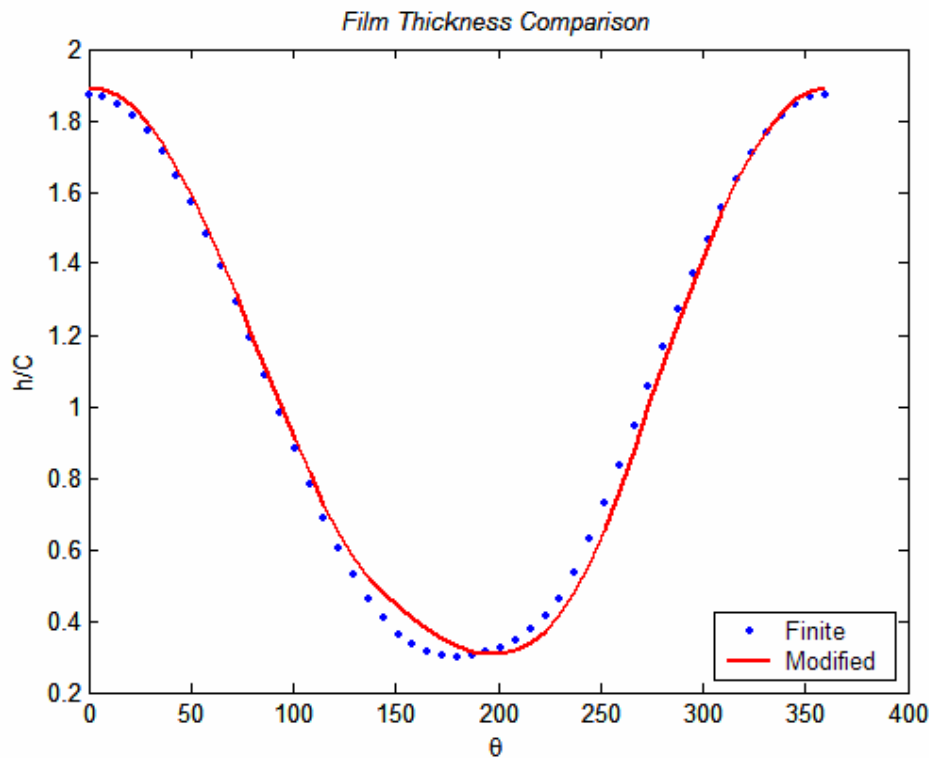


Figure 29: Film Thickness Profile Comparison between Finite & Modified Approximation at 30,000 rpm. (Foil Bearing / Min Film Match)

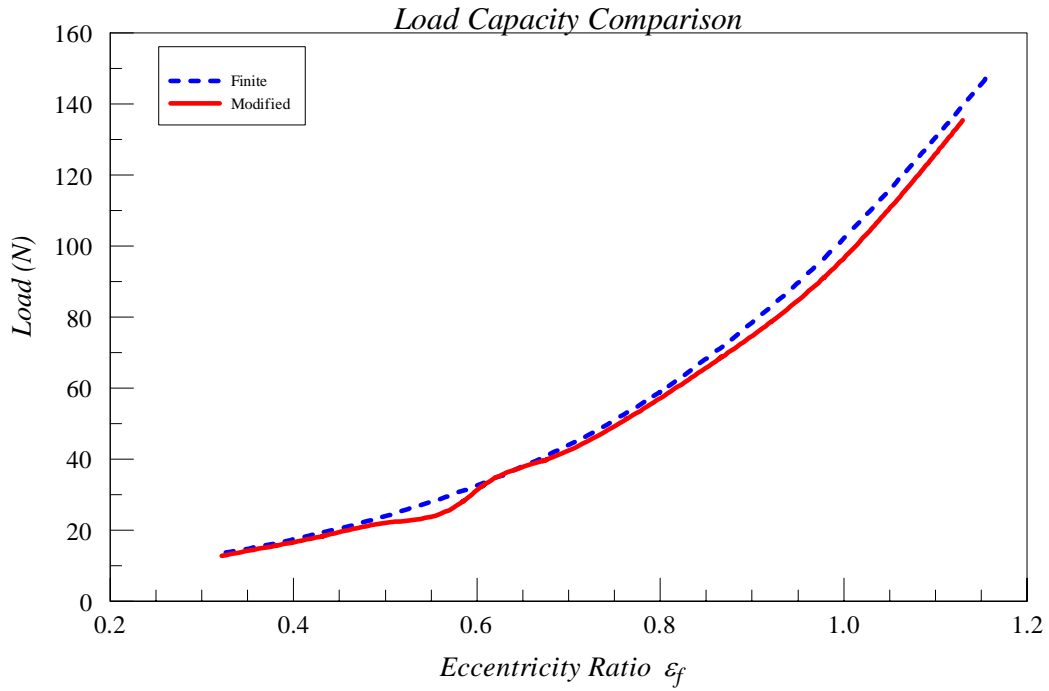


Figure 30: Load Comparison between Finite and Modified Approximation (Foil Bearing / Min Film Match)

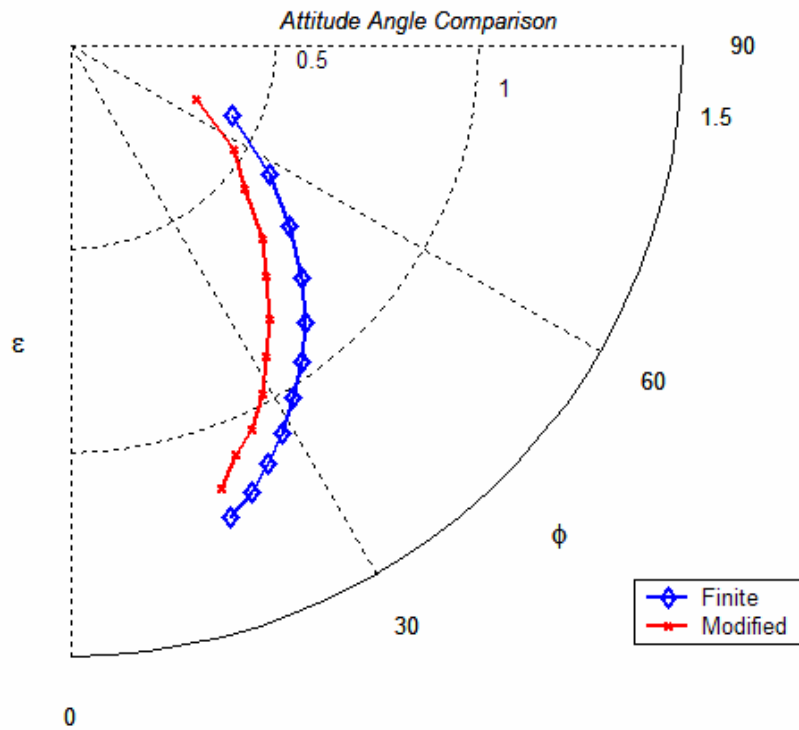


Figure 31: Attitude Angle Comparison (Foil Bearing / Min Film Match)

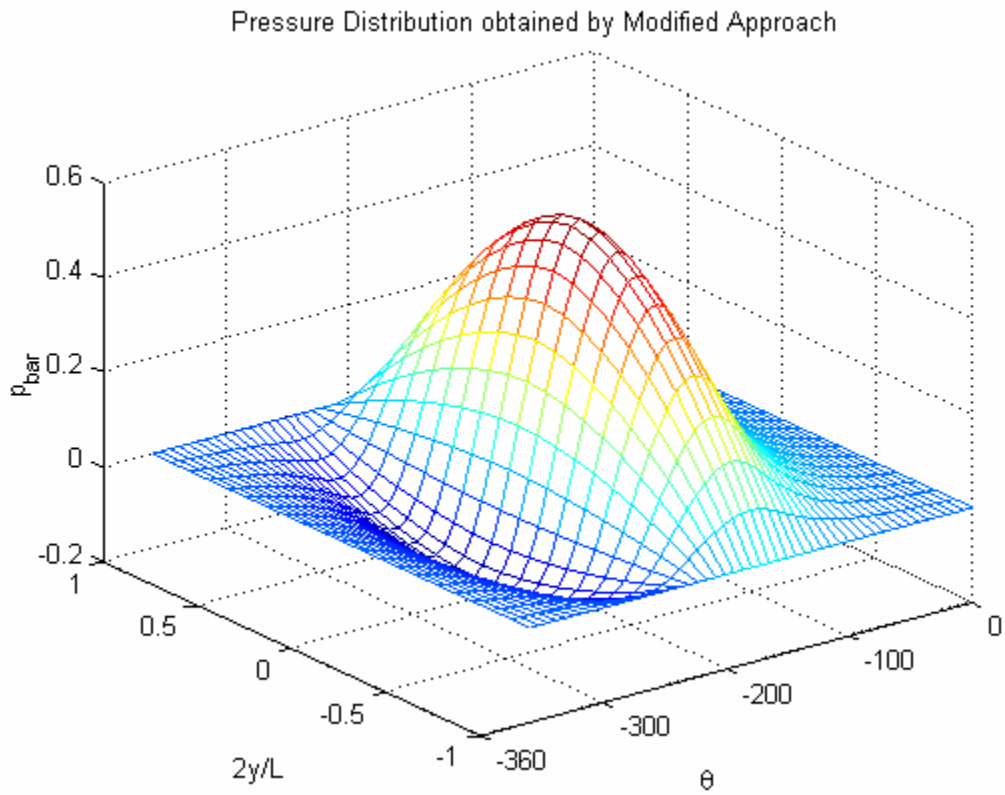


Figure 32: Three Dimensional Pressure Distribution for Foil Bearing at 30,000 rpm based on Modified Approach. (θ is reversed to indicate the sub-ambient pressure)

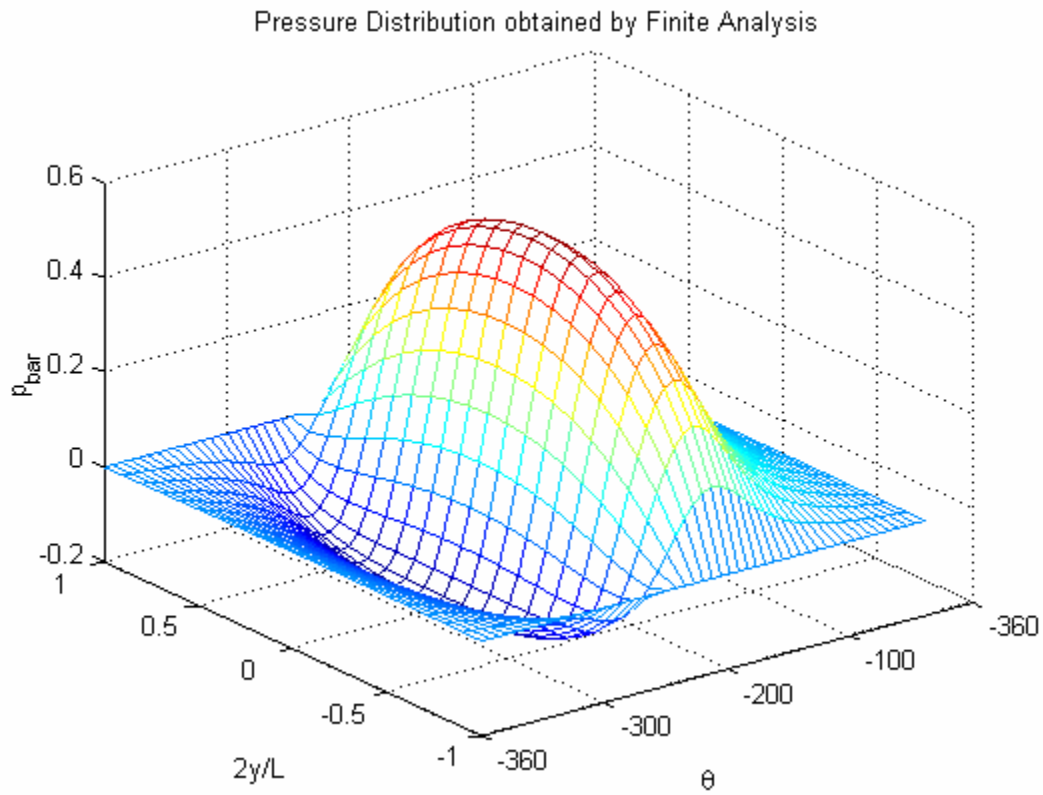


Figure 33: Three Dimensional Pressure Distribution for Foil Bearing at 30,000 rpm based on Finite Analysis. (θ is reversed to indicate the sub-ambient pressure)

*Variation of Parabolic Exponent
(Compliant Bearing)*

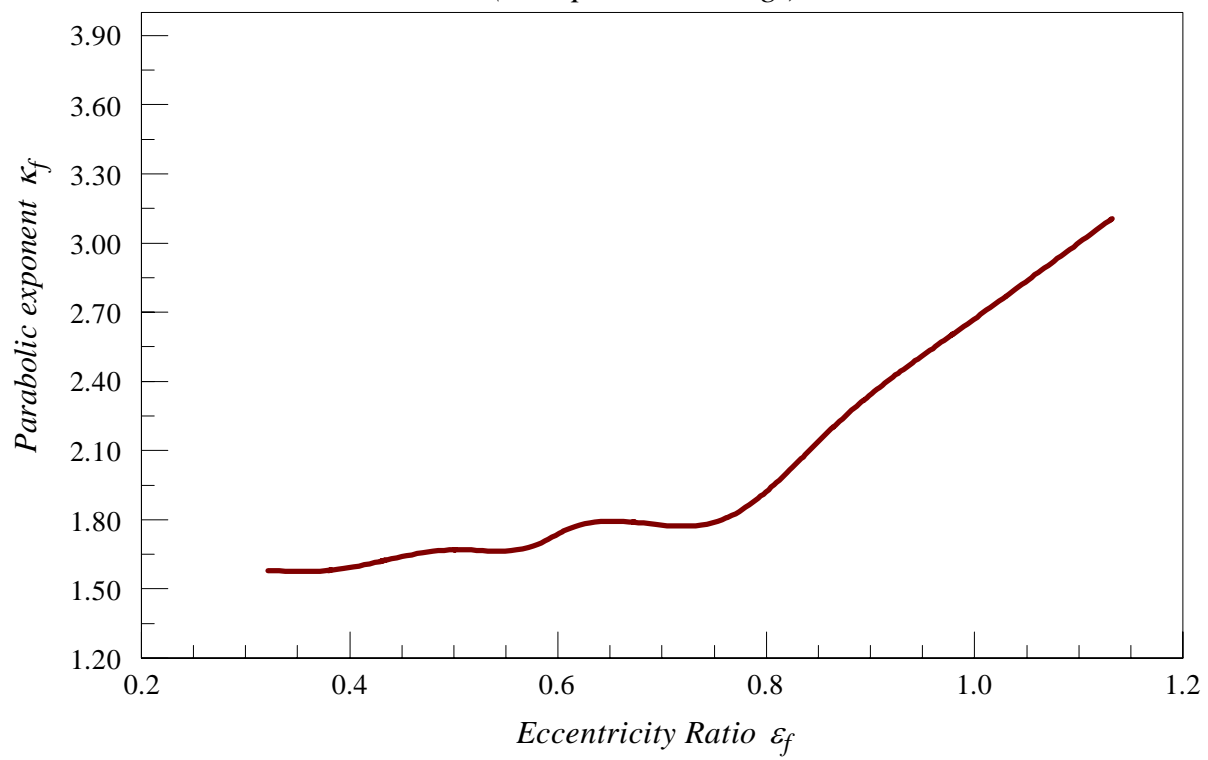


Figure 34: Parametric Study of Parabolic Exponent (Foil Bearing / Min Film Match Case)

Chapter 4. Conclusions

The current needs of the aerospace rotating machinery, energy efficient turbines and other vital rotating machinery are pushing the envelope of the existing knowledge in design and development, of particular importance are bearings that operate at exceedingly high speeds and temperature. To this end, compliant journal bearings are known to play a crucial role in providing these requirements. Hence, it is very important to understand their fundamental operating characteristics and limitations to assist designers and manufacturers.

This thesis presents a mathematical model for compliant journal bearings based on “Classical Reynolds” equation (Khonsari and Booser, 2001). This non-linear equation is solved numerically first by infinitely long approximation to understand and predict the bearing performance parameters. The results obtained based on this approximation are in agreement with experimental results of Strom, 1987.

A finite analysis based on the methodology developed by Peng and Khonsari, 2004 is used to predict the bearing performance parameters. The results obtained based on finite analysis are in agreement with experimental results of Strom, 1987 and predicted results by Peng and Khonsari, (2004).

Based on an assumption regarding the pressure, along the axial direction the Classical Reynolds equation (a partial differential equation) is converted to an Ordinary Differential Equation. The new sets of equations are much simpler to solve numerically using the Modified Parabolic Approximation proposed in this thesis to predict the bearing performance parameters for rigid journal bearings and compliant journal bearings. The results obtained are in agreement with the finite analysis.

A set of non-dimensional charts for rigid journal bearing is proposed based on the key non-dimensional parameters which are the bearing length to diameter ratio, eccentricity ratio and bearing number. These charts provide the non-dimensional load obtained at various bearing numbers and a range of eccentricity ratios with the corresponding exponent needed for the MPA analysis. The utility of this approach is for computing the dynamic characteristics of compliant gas bearing which requires significant computational time and programming effort.

References

- Czolczynski, K., 1999, *Rotordynamics of Gas-Lubricated Journal Bearing Systems*, Mechanical engineering series, Springer.
- DellaCorte, C., Lukaszewicz, V., Valco, M. J., Radil, K. C., and Heshmat, H., 2000, "Performance and Durability of High Temperature Foil Air Bearings for Oil-Free Turbomachinery", *STLE, Tribology Transactions.*, 43, pp.774-780.
- Dellacorte, C. and Valco, M.J., 2000, "Load Capacity Estimation of Foil Air Bearings for Oil-Free Turbo machinery Applications", NASA/TM-2000-209782. ARL-TR-2334.
- Ettles, C., and Shelly, P., 1970, "A tractable solution for medium length Journal Bearings", *Wear*, 16. pp 221-228.
- Ferziger, J.H., Peric, M., 2002, *Computational Methods for Fluid Dynamics*, 3rd edition, Springer.
- Gerald, C. F., Wheatley, P. O., 2002, *Applied Numerical Analysis*, 6th Edition, Pearson Education Asia.
- Gross, W.A., Matsch, L.A., Castelli, V., Eshel, A., Vohr, J.H., Wildmann, M., *Fluid Film Lubrication*, 1980, John Wiley & Sons Inc.
- Hamrock, B.J, *Fundamentals of Fluid Film Lubrication*, 1994, McGraw-Hill series in mechanical engineering.
- Heshmat, H., Walowit, J. A., Pinkus, O., 1983, "Analysis of Gas Lubricated Foil Journal Bearings", *Journal of Lubrication Technology*, 105, pg 647-655.
- Heshmat, H. and Ku, C.-P. R., 1994, "Structural Damping of Self Acting Compliant Foil Journal Bearings", *ASME J. Tribol.*, 116, pp. 76-82.
- Heshmat, H., 1994, "Advancements in the performance of Aerodynamic foil journal bearings: High Speed and load capability", *Journal of Tribology*, 116, pp287-295.
- Hunt, B.R., Lipsman, R., Rosenberg, J., Coombes, K., Osborn, J., Stuck, G., *A guide to Matlab*, Cambridge University Press.
- Kawabata, N., 1987, "Numerical Analysis of Reynolds Equation for Gas Lubrication in a High Λ Region", *JSME, International Journal*, 30, pp 836-842.
- Khonsari, M.M. and Booser, E., 2001, *Applied Tribology*, John Wiley & Sons Inc.
- Ku, C.-P. R., and Heshmat, H., 1992, "Compliant Foil Bearing Structural Stiffness Analysis: Part I – Theoretical Model Including Strip and Variable Bump Foil Geometry", *ASME J of Tribol.*, 114, pp. 394-400.

Maple 9.5, 2004, Maplesoft, Waterloo Maple Inc.

Matlab 6.1, R-12., 2001, The Mathworks Inc.

Patankar, S.V., *Numerical Heat Transfer and Fluid Flow*, 1980, Series in Computational Methods in Mechanics and Thermal Science, McGraw-Hill.

Peng, Z-C., 2003 “Thermohydrodynamic Analysis of Compressible Gas Flow in Compliant Foil Bearings”, *Thesis.*, Louisiana State University, Baton Rouge, L. A.

Peng, Z-C and Khonsari, M.M., 2004 “Hydrodynamic Analysis of compliant Foil Bearings with compressible Air Flow”, *ASME J of Tribology.*, 126, pp.542-546.

Peng, Z-C and Khonsari, M.M., 2004 “On the limiting load carrying capacity of foil bearings”, *ASME J of Tribology.*, 126, pp.817-818.

Radil, K., Howard, S. and Dykas, B. 2002 “The Role of Radial Clearance on the Performance of Foil Air Bearings”, *Tribology Transactions*, ASME/STLE Tribology Conference in Cancun, Mexico.

Rao, R.S.R., Vijayaraghavan, R., Siddananjappa, S., Vyasamurthy, A.K., 1996 “Foil Journal Bearings having straight foils useful for providing support for high speed rotors and process for fabricating said bearing”, United States Patent, No: 5536087.

Salehi, M., Heshmat, H., Walton II, J.F., Tomaszewski, M. J., “Test of a mesoscopic turbine simulator to speeds in excess of 700,000 rpm on foil bearings”, Paper GT2004-53870 , ASME Journal of Engineering for gas turbines and power. Accepted for publication.

Singhal, S., 2004 “A Simplified Thermohydrodynamic Instability Of The Plain Cylindrical Hydrodynamic Journal Bearings”, *Thesis.* Louisiana State University, Baton Rouge, L. A.

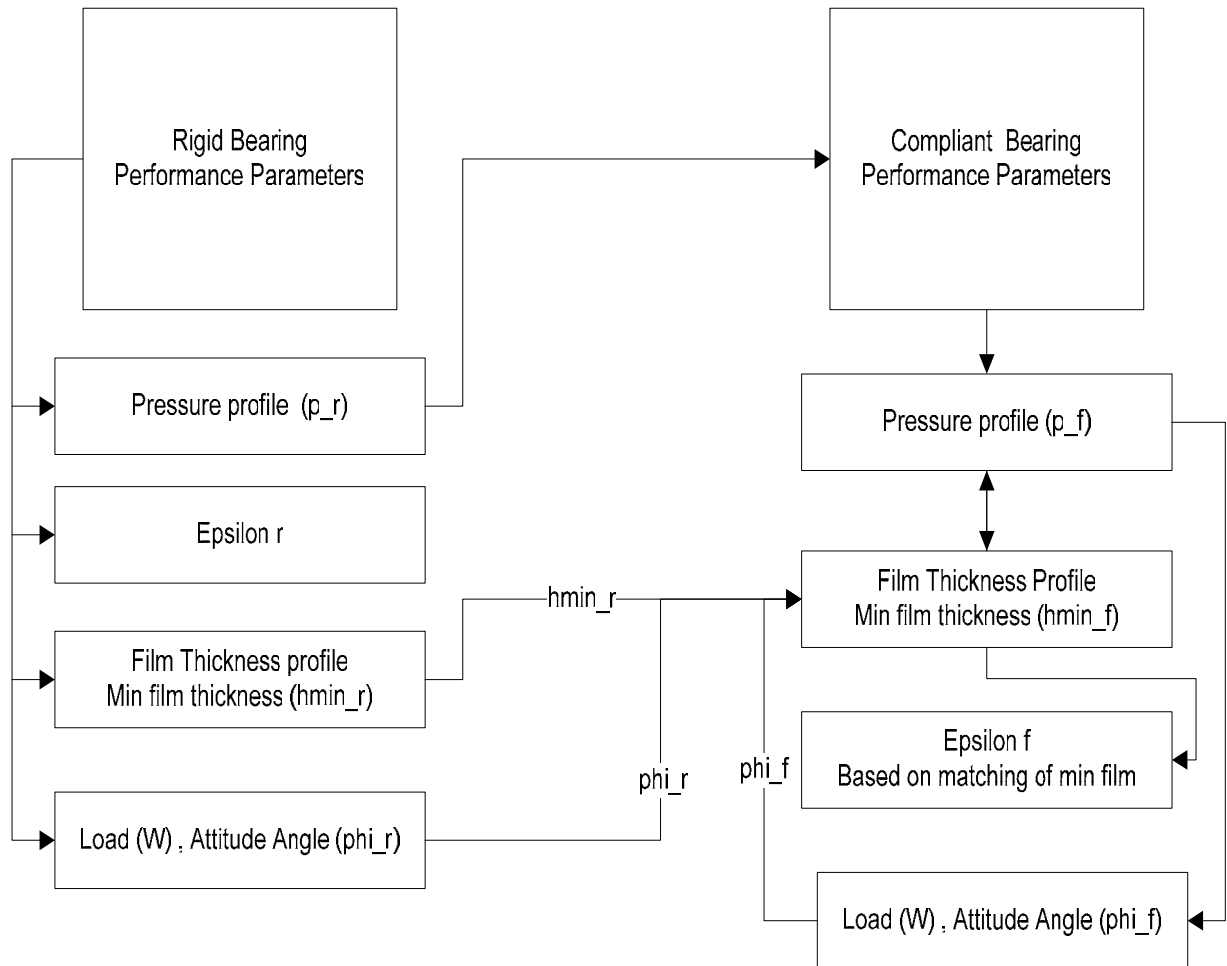
Singhal, S and Khonsari, M M. Proceedings of the Institution of Mechanical Engineers - Part J - Journal of Engineering Tribology, 2005, Vol. 219 Issue 3, p225-234.

Strom.T., Program Manager, December 1987, Advanced Gas Turbine (AGT) Technology Development Project-Final Report, NASA CR-180891.

Walowit, J.A., and Anno, J.N., 1975, *Modern Developments in Lubrication Mechanics*, Applied Science Publishers Ltd.

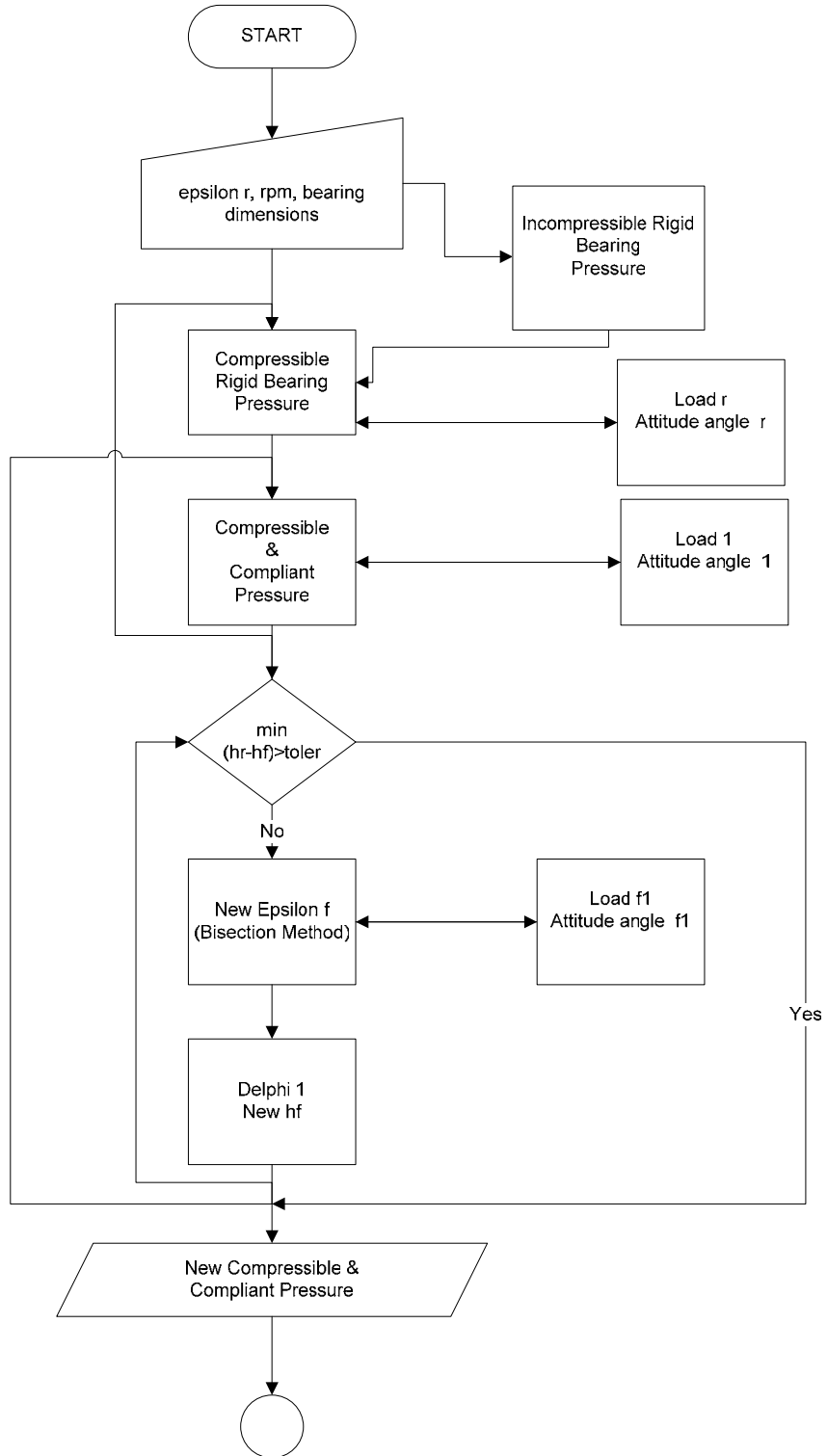
Appendix A

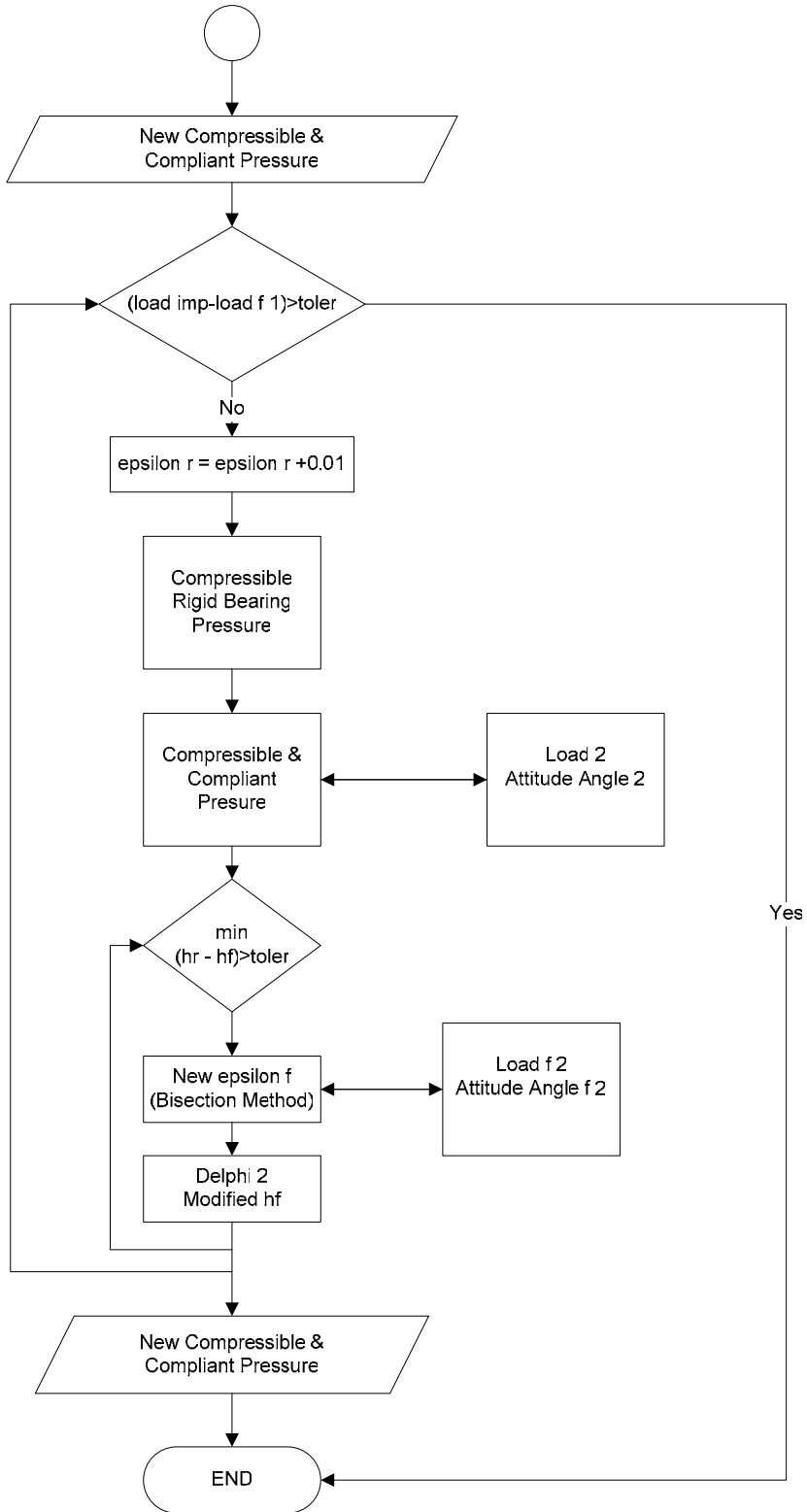
Flow Chart for Numerical Relation between Rigid and Compliant Journal Bearings



Appendix B

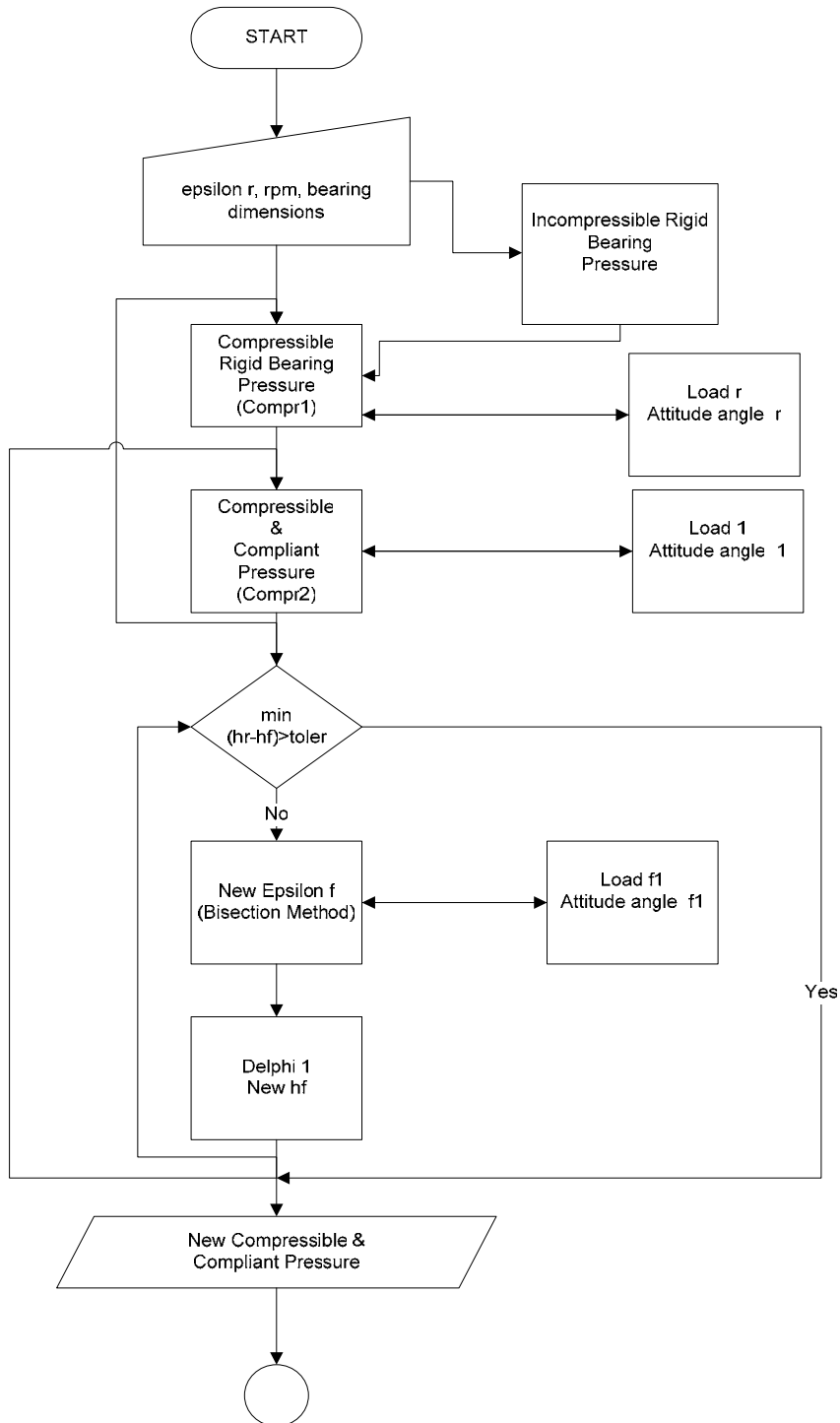
Flow Chart for Infinitely Long Approximation

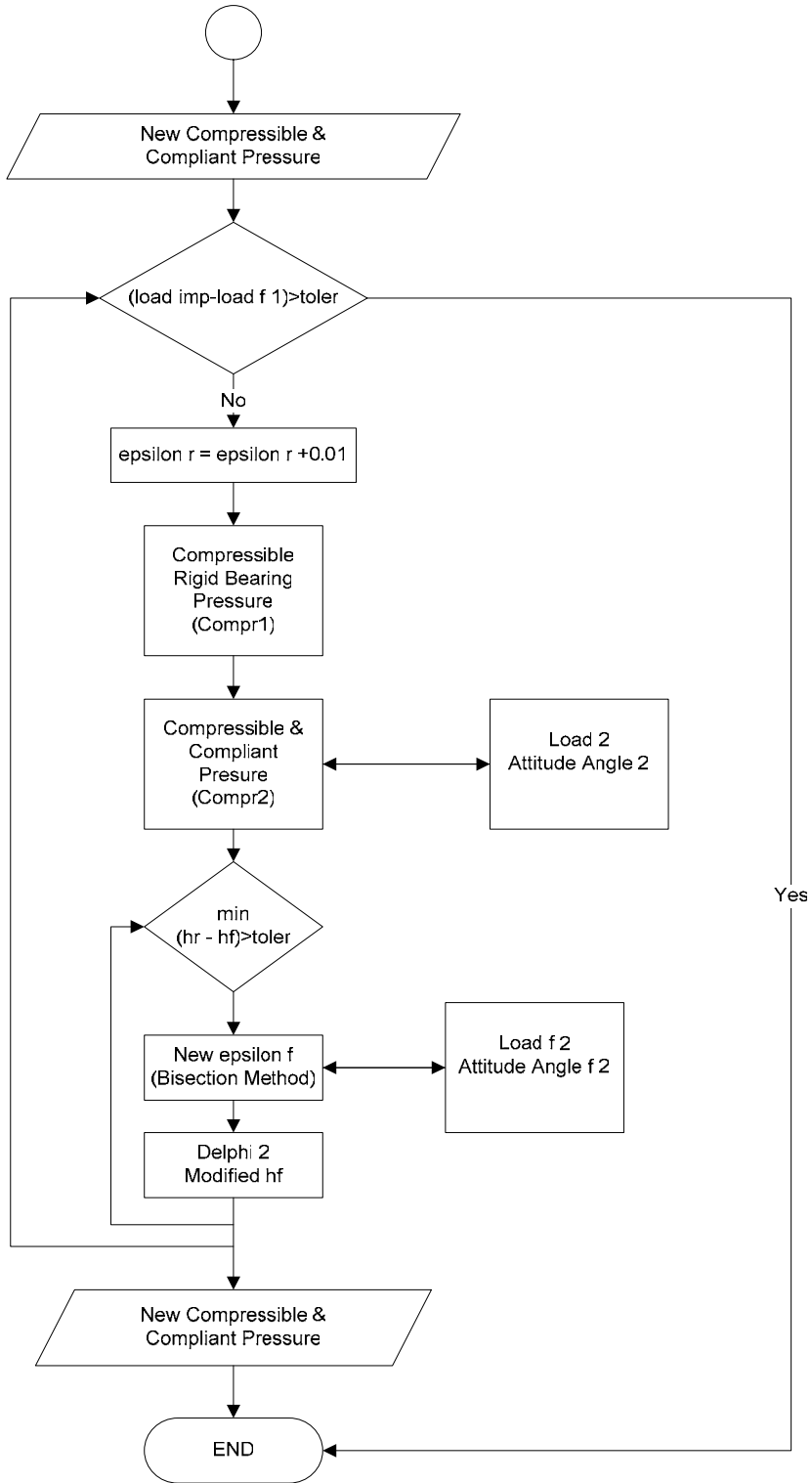




Appendix C

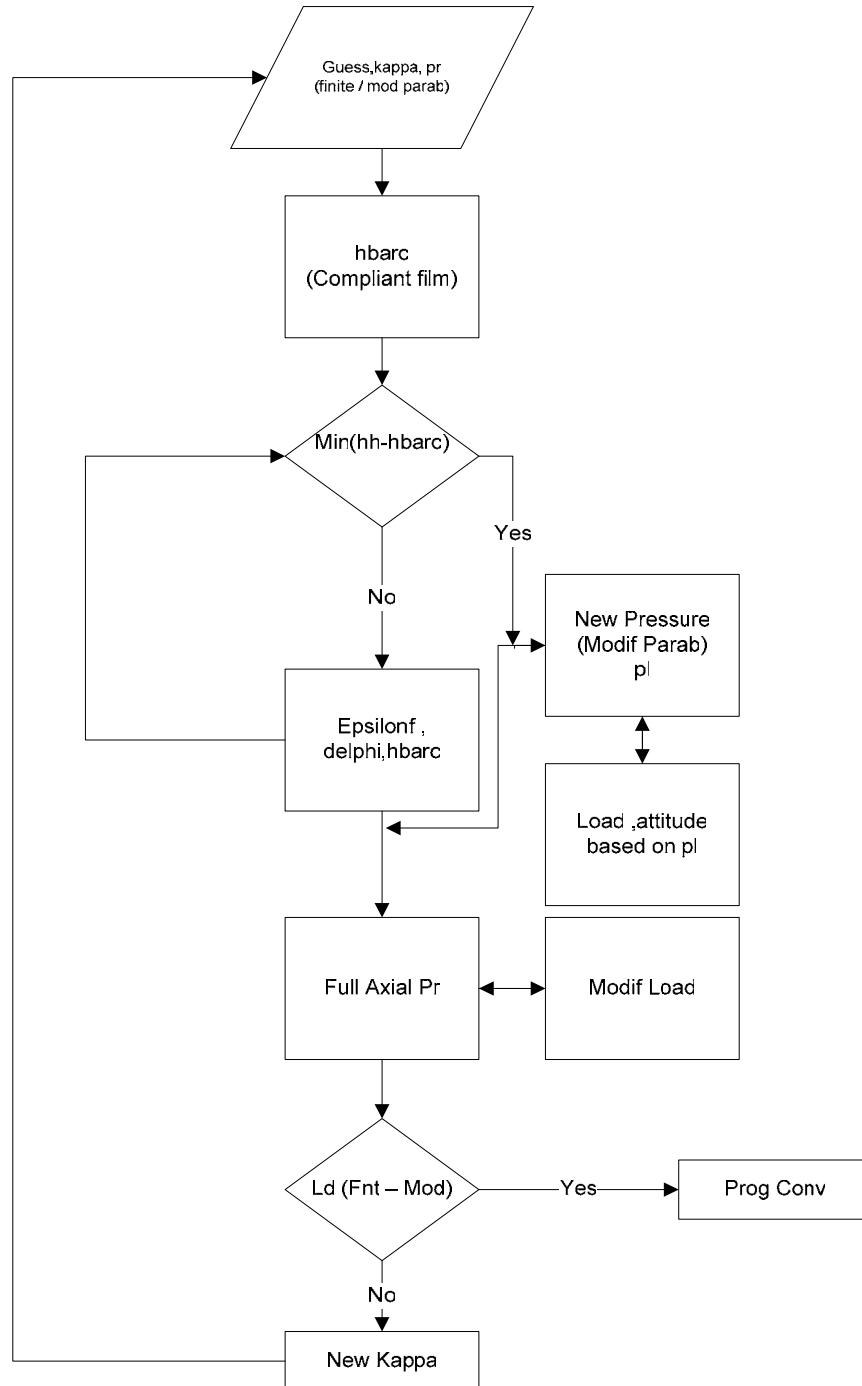
Flow Chart for Finite Approximation





Appendix D

Flow Chart for Modified Parabolic Approximation



Appendix E

Maple Program (Maple, 9.5, 2004) for Derivation of Modified Reynolds Equation

Part 1

Parabolic substitution for the general reynolds equation and then integrating twice with respect to y

```
> restart;
```

```
>
```

```
>
```

```
> a1:=Diff(Diff(pl,theta$1)*pl*h^3*(1-y^kappa)^2+Diff(pl,theta$1)*h^3*(1-y^kappa),theta$1);
```

$$a1 := \frac{\partial}{\partial \theta} \left(\left(\frac{\partial}{\partial \theta} pl \right) pl h^3 (1 - y^\kappa)^2 + \left(\frac{\partial}{\partial \theta} pl \right) h^3 (1 - y^\kappa) \right)$$

```
> a2:=Diff(Diff(pl,theta$1)*pl*h^3*Int(Int((1-y^kappa)^2,y),y)+Diff(pl,theta$1)*h^3*Int(Int((1-y^kappa),y),y),theta$1);
```

$$a2 := \frac{\partial}{\partial \theta} \left(\left(\frac{\partial}{\partial \theta} pl \right) pl h^3 \int \int (1 - y^\kappa)^2 dy dy + \left(\frac{\partial}{\partial \theta} pl \right) h^3 \int \int (1 - y^\kappa) dy dy \right)$$

```
> a3:=Diff(Diff(pl,theta$1)*pl*h^3*int(int((1-y^kappa)^2,y),y)+Diff(pl,theta$1)*h^3*int(int((1-y^kappa),y),y),theta$1);
```

$$a3 := \frac{\partial}{\partial \theta} \left(\left(\frac{\partial}{\partial \theta} pl \right) pl h^3 \left(- \frac{2 \left(\frac{y^{(1+\kappa)} y}{1+\kappa} - \frac{y^{(2+\kappa)}}{(1+\kappa)(2+\kappa)} \right)}{1+\kappa} + \frac{\frac{y^{(1+2\kappa)} y}{1+2\kappa} - \frac{y^{(2+2\kappa)}}{(1+2\kappa)(2+2\kappa)}}{1+2\kappa} + \frac{1}{2} y^2 \right) + \left(\frac{\partial}{\partial \theta} pl \right) h^3 \left(\frac{1}{2} y^2 - \frac{y^{(2+\kappa)}}{(1+\kappa)(2+\kappa)} \right) \right)$$

```
> b1:= (D/L)^2*Diff(pl^2*h^3*Diff((1-y^kappa),y$1)*(1-y^kappa)+pl*h^3*Diff((1-y^kappa),y$1),y$1);
```

```
>
```

```
>
```

$$b1 := \frac{D^2 \left(\frac{\partial}{\partial y} \left(pl^2 h^3 \left(\frac{\partial}{\partial y} (1-y^\kappa) \right) (1-y^\kappa) + pl h^3 \left(\frac{\partial}{\partial y} (1-y^\kappa) \right) \right) \right)}{L^2}$$

pl represents the center line pressure and h does not vary in the axial direction and both are constant along y.

> **b2:=(D/L)^2*Int(Int(Diff(pl^2*h^3*Diff((1-y^kappa),y\$1)*(1-y^kappa)+pl*h^3*Diff((1-y^kappa),y\$1),y\$1),y),y);**

$$b2 := \frac{D^2 \int \int \frac{\partial}{\partial y} \left(pl^2 h^3 \left(\frac{\partial}{\partial y} (1-y^\kappa) \right) (1-y^\kappa) + pl h^3 \left(\frac{\partial}{\partial y} (1-y^\kappa) \right) \right) dy dy}{L^2}$$

> **b3:=(D/L)^2*int(int(Diff(pl^2*h^3*Diff((1-y^kappa),y\$1)*(1-y^kappa)+pl*h^3*Diff((1-y^kappa),y\$1),y\$1),y),y);**

$$b3 := \frac{D^2 \left(\frac{1}{2} pl^2 h^3 (1-y^\kappa)^2 + h^3 pl (1-y^\kappa) \right)}{L^2}$$

> **c1:=lambda*((1-y^kappa)*Diff(h*pl,theta\$1)+Diff(h,theta\$1));**

$$c1 := \lambda \left((1-y^\kappa) \left(\frac{\partial}{\partial \theta} (h pl) \right) + \left(\frac{\partial}{\partial \theta} h \right) \right)$$

> **c2:=lambda*Int(Int(((1-y^kappa)*Diff(h*pl,theta\$1)+Diff(h,theta\$1)),y),y);**

$$c2 := \lambda \int \int (1-y^\kappa) \left(\frac{\partial}{\partial \theta} (h pl) \right) + \left(\frac{\partial}{\partial \theta} h \right) dy dy$$

> **c3:=lambda*int(int(((1-y^kappa)*Diff(h*pl,theta\$1)+Diff(h,theta\$1)),y),y);**

$$c3 := \lambda \left(\left(\frac{\partial}{\partial \theta} (h pl) \right) \left(\frac{1}{2} y^2 - \frac{y^{(2+\kappa)}}{(1+\kappa)(2+\kappa)} \right) + \frac{1}{2} \left(\frac{\partial}{\partial \theta} h \right) y^2 \right)$$

Final form of equation.

>

> $a_3+b_3=c_3+C_1y+C_2$;

$$\left(\frac{\partial}{\partial \theta} \left(\left(\frac{\partial}{\partial \theta} pl \right) pl h^3 \left(-\frac{2 \left(\frac{y^{(1+\kappa)} y}{1+\kappa} - \frac{y^{(2+\kappa)}}{(1+\kappa)(2+\kappa)} \right)}{1+\kappa} + \frac{\frac{y^{(1+2\kappa)} y}{1+2\kappa} - \frac{y^{(2+2\kappa)}}{(1+2\kappa)(2+2\kappa)}}{1+2\kappa} + \frac{1}{2} y^2 \right) \right. \right. \\ \left. \left. + \left(\frac{\partial}{\partial \theta} pl \right) h^3 \left(\frac{1}{2} y^2 - \frac{y^{(2+\kappa)}}{(1+\kappa)(2+\kappa)} \right) \right) \right) + \frac{D^2 \left(\frac{1}{2} pl^2 h^3 (1-y^\kappa)^2 + h^3 pl (1-y^\kappa) \right)}{L^2} = \lambda \left(\left(\frac{\partial}{\partial \theta} (h pl) \right) \left(\frac{1}{2} y^2 - \frac{y^{(2+\kappa)}}{(1+\kappa)(2+\kappa)} \right) + \frac{1}{2} \left(\frac{\partial}{\partial \theta} h \right) y^2 \right) + C_1 y + C_2$$

>

where C1 and C2 represent the constants of Integration to be evaluated.

>

Part B

```
> (Diff((Diff(pl, theta))*pl*h^3*(-2*(y^(1+kappa))*y/(1+kappa)-
y^(2+kappa)/((1+kappa)*(2+kappa)))/(1+kappa)+(y^(1+2*kappa))*y/(1
+2*kappa)-
y^(2+2*kappa)/((1+2*kappa)*(2+2*kappa)))/(1+2*kappa)+1/2*y^2)+(D
iff(pl, theta))*h^3*(1/2*y^2-y^(2+kappa)/((1+kappa)*(2+kappa))),
theta)+D^2*(1/2*pl^2*h^3*(1-y^kappa)^2+h^3*pl*(1-y^kappa))/L^2
= lambda*((Diff(h*pl, theta))*(1/2*y^2-
y^(2+kappa)/((1+kappa)*(2+kappa)))+1/2*(Diff(h,
theta))*y^2)+C1y+C2;
```

$$\left(\frac{\partial}{\partial \theta} \left(\left(\frac{\partial}{\partial \theta} pl \right) pl h^3 \left(-\frac{2 \left(\frac{y^{(1+\kappa)} y}{1+\kappa} - \frac{y^{(2+\kappa)}}{(1+\kappa)(2+\kappa)} \right)}{1+\kappa} + \frac{y^{(1+2\kappa)} y}{1+2\kappa} - \frac{y^{(2+2\kappa)}}{(1+2\kappa)(2+2\kappa)} + \frac{1}{2} y^2 \right) \right. \right. \\ \left. \left. + \left(\frac{\partial}{\partial \theta} pl \right) h^3 \left(\frac{1}{2} y^2 - \frac{y^{(2+\kappa)}}{(1+\kappa)(2+\kappa)} \right) \right) \right) + \frac{D^2 \left(\frac{1}{2} pl^2 h^3 (1-y^\kappa)^2 + h^3 pl (1-y^\kappa) \right)}{L^2} = \lambda \left(\left(\frac{\partial}{\partial \theta} (h pl) \right) \left(\frac{1}{2} y^2 - \frac{y^{(2+\kappa)}}{(1+\kappa)(2+\kappa)} \right) + \frac{1}{2} \left(\frac{\partial}{\partial \theta} h \right) y^2 \right) + C_1 y + C_2$$

The Boundary Conditions are evaluated:
The Resulting Equation is of the form

```
> Diff(Diff(pl,theta$1)*pl*h^3*(upsilon1-
y*psi1)+Diff(pl,theta$1)*h^3*(tau1-
y*beta1),theta$1)+(D/L)^2*(h^3*(pl^2)*(-
y^kappa+y^(2*kappa)+y/2)+pl*(1-y^kappa)+y-
1))=lambda*(Diff((pl*h),theta$1)*(tau1-
y*beta1)+Diff(h,theta$1)*(y^2/2-y/2));
```

$$\left(\frac{\partial}{\partial \theta} \left(\left(\frac{\partial}{\partial \theta} pl \right) pl h^3 (\upsilon_1 - y \psi_1) + \left(\frac{\partial}{\partial \theta} pl \right) h^3 (\tau_1 - y \beta_1) \right) \right) \\ + \frac{D^2 \left(h^3 pl^2 \left(-y^\kappa + y^{(2\kappa)} + \frac{1}{2} y \right) + pl(-y^\kappa + y) \right)}{L^2} = \lambda \left(\left(\frac{\partial}{\partial \theta} (h pl) \right) (\tau_1 - y \beta_1) \right. \\ \left. + \left(\frac{\partial}{\partial \theta} h \right) \left(\frac{1}{2} y^2 - \frac{1}{2} y \right) \right)$$

Integrating the above equation along y from 0 to 1

```
> Int(Diff(Diff(pl,theta$1)*pl*h^3*(upsilon1-
y*psi1)+Diff(pl,theta$1)*h^3*(tau1-
y*beta1),theta$1)+(D/L)^2*(h^3*(pl^2)*(-
y^kappa+y^(2*kappa)+y/2)+pl*(1-y^kappa)+y-
1))=lambda*(Diff((pl*h),theta$1)*(tau1-
y*beta1)+Diff(h,theta$1)*(y^2/2-y/2)),y=0...1);
```

$$\int_0^1 \left(\frac{\partial}{\partial \theta} \left(\left(\frac{\partial}{\partial \theta} pl \right) pl h^3 (\nu_1 - y \psi_1) + \left(\frac{\partial}{\partial \theta} pl \right) h^3 (\tau_1 - y \beta_1) \right) \right)$$

$$+ \frac{D^2 \left(h^3 pl^2 \left(-y^\kappa + y^{(2\kappa)} + \frac{1}{2} y \right) + pl(-y^\kappa + y) \right)}{L^2} = \lambda \left(\left(\frac{\partial}{\partial \theta} (h pl) \right) (\tau_1 - y \beta_1) \right)$$

$$+ \left(\frac{\partial}{\partial \theta} h \right) \left(\frac{1}{2} y^2 - \frac{1}{2} y \right) dy$$

The Final Equation is as follows:

```
>
Diff(Diff(pl,theta$1)*pl*h^3*chi1+Diff(pl,theta$1)*h^3*chi2,theta$1)+(D/L)^2*(h^3*(pl^2*chi3+pl*chi4))=lambda*(Diff(pl*h,theta$1)*chi2-1/12*(Diff(h,theta$1)));
```

$$\left(\frac{\partial}{\partial \theta} \left(\left(\frac{\partial}{\partial \theta} pl \right) pl h^3 \chi_1 + \left(\frac{\partial}{\partial \theta} pl \right) h^3 \chi_2 \right) \right) + \frac{D^2 h^3 (pl^2 \chi_3 + pl \chi_4)}{L^2} = \lambda \left(\left(\frac{\partial}{\partial \theta} (h pl) \right) \chi_2 - \frac{1}{12} \frac{\partial}{\partial \theta} h \right)$$

Where

```
> a:=(1-y^kappa)^2;
```

$$a := (1 - y^\kappa)^2$$

```
> upsilon:=simplify(int(a,y));
```

$$v := \frac{y^{(1+2\kappa)} + y^{(1+2\kappa)\kappa} + y + 3y\kappa + 2y\kappa^2 - 2y^{(1+\kappa)} - 4y^{(1+\kappa)\kappa}}{(1+2\kappa)(1+\kappa)}$$

```
> psi1:=simplify(eval(upsilon,'y=1'));
```

$$\psi_1 := \frac{2\kappa^2}{(1+2\kappa)(1+\kappa)}$$

```
> upsilon1:=simplify(int(upsilon,y));
```

$$v1 := \frac{2y^2\kappa^3 + 7y^2\kappa^2 + \kappa y^{(2+2\kappa)} - 8\kappa y^{(2+\kappa)} + 7y^2\kappa + 2y^{(2+2\kappa)} + 2y^2 - 4y^{(2+\kappa)}}{2(2+\kappa)(1+2\kappa)(1+\kappa)}$$

>
> **psi2:=eval(upsilon1,'y=1');**

$$\psi2 := \frac{2\kappa^3 + 7\kappa^2}{2(2+\kappa)(1+2\kappa)(1+\kappa)}$$

> **upsilon2:=simplify(eval(int(upsilon1,y),'y=1'));**

$$v2 := \frac{\kappa^2(95\kappa + 32\kappa^2 + 4\kappa^3 + 85)}{6(2+\kappa)(1+2\kappa)(1+\kappa)(3+2\kappa)(3+\kappa)}$$

> **b:=(1-y^kappa);**

$$b := 1 - y^\kappa$$

> **tau:=int(b,y);**

$$\tau := y - \frac{y^{(1+\kappa)}}{1+\kappa}$$

> **beta1:=simplify(eval(int(tau,y),'y=1'));**

$$\beta1 := \frac{\kappa(3+\kappa)}{2(1+\kappa)(2+\kappa)}$$

> **tau1:=int(tau,y);**

$$\tau1 := \frac{1}{2}y^2 - \frac{y^{(2+\kappa)}}{(1+\kappa)(2+\kappa)}$$

> **beta2:=simplify(eval(tau1,'y=1'));**

$$\beta2 := \frac{\kappa(3+\kappa)}{2(1+\kappa)(2+\kappa)}$$

>
> **tau2:=simplify(eval(int(tau1,y),'y=1'));**

$$\tau2 := \frac{\kappa(11 + 6\kappa + \kappa^2)}{6(1+\kappa)(2+\kappa)(3+\kappa)}$$

>
> **chi1:=simplify(eval(int(upsilon1-y*psi2,y),'y=1'));**

$$\chi1 := -\frac{(2\kappa^2 + 15\kappa + 19)\kappa^2}{12(3+\kappa)(3+2\kappa)(1+\kappa)(2+\kappa)}$$

```
>  
> chi2:=simplify(eval(int(tau1-y*beta1,y),'y=1'));
```

$$\chi^2 := -\frac{(\kappa+5)\kappa}{12(3+\kappa)(2+\kappa)}$$

```
>  
> chi3:=simplify(eval(int(-y^kappa+y^(2*kappa)/2+y/2-  
1/2,y),'y=1'));
```

$$\chi^3 := -\frac{3+9\kappa+2\kappa^2}{4(1+2\kappa)(1+\kappa)}$$

```
> chi4:=simplify(eval(int((1-y^kappa)+y-1,y),'y=1'));
```

$$\chi^4 := \frac{-1+\kappa}{2(1+\kappa)}$$

Vita

Amith Hanumappa Reddy hails from Bangalore city located in the southern part of India. The city is popularly known for its beautiful gardens, various centers catering to research and development in the field of engineering, medicine and science. He completed his high schooling from Sri Ramakrishna Vidyashala located in Mysore, India. Pre University at National College Jayanagar and received his Bachelor of Engineering degree in 1999 in the field of mechanical engineering from Rashtreeya Vidyalaya College of Engineering, Bangalore, India, which is ranked among the top ten colleges in India. After graduation he joined National Aerospace Laboratories as a project graduate trainee, a premier research and development establishment in the field of aerospace engineering. He then enrolled for the master's program at South Dakota State University, Brookings, South Dakota, and transferred after a semester to Louisiana State University A & M, Baton Rouge, Louisiana, at the Mechanical Engineering Department under the Center for Rotating Machinery (CeRoM) group in Jan 2002. At this group he was exposed to various research and industrial projects related to the field of tribology- (wear, friction, and bearing design and lubrication). He also carried out a co-operative education program at Entergy Waterford 3 Nuclear Power Station under the systems engineering group. His main interest areas are in the field of aerospace / automotive / mechanical engineering design and analysis, performance evaluation, reliability engineering and predictive maintenance and optimization. Some of his hobbies include adventure sports, classic motorcycle restoration projects, motorsports, college football and travel.